UNIVERSIDADE FEDERAL DE SANTA CATARINA
CENTRO TECNOLÓGICO - CTC
PROGRAMA DE PÓS-GRADUAÇÃO EM ENGENHARIA MECÂNICA

JOÃO PEDRO DUARTE DA SILVA

EXPERIMENTAL AND THEORETICAL ANALYSIS OF AN ELECTRO-HYDROSTATIC ACTUATOR FOR ULTRA DEEPWATER APPLICATIONS

FLORIANÓPOLIS
2019

João Pedro Duarte da Silva

EXPERIMENTAL AND THEORETICAL ANALYSIS OF AN ELECTRO-HYDROSTATIC ACTUATOR FOR ULTRA DEEPWATER APPLICATIONS

Dissertação submetida ao Programa de Pós Graduação em Engenharia Mecânica da Universidade Federal de Santa Catarina para a obtenção do título de Mestre em Engenharia Mecânica
Orientador: Prof. Dr. Victor Juliano De Negri
Coorientador: Dr. Alexandre Orth

Florianópolis
2019

Ficha de identificação da obra elaborada pelo autor,

através do Programa de Geração Automática da Biblioteca Universitária da UFSC.

da Silva, João Pedro Duarte
EXPERIMENTAL AND THEORETICAL ANALYSIS OF AN ELECTRO HYDROSTATIC ACTUATOR FOR ULTRA DEEPWATER APPLICATIONS / João Pedro Duarte da Silva ; orientador, Victor Juliano De Negri, coorientador, Alexandre Orth, 2019.
115 p.

Dissertação (mestrado) - Universidade Federal de Santa Catarina, Centro Tecnológico, Programa de Pós-Graduação em Engenharia Mecânica, Florianópolis, 2019.

Inclui referências.

1. Engenharia Mecânica. 2. Engenharia Mecânica. 3. Atuador eletro-hidrostático. 4. Sistemas de atuação de válvulas submarinas. 5. Testes experimentais. I. De Negri, Victor Juliano. II. Orth, Alexandre. III. Universidade Federal de Santa Catarina. Programa de Pós-Graduação em Engenharia Mecânica. IV. Título.

João Pedro Duarte da Silva

Experimental and Theoretical Analysis of an Electro-Hydrostatic Actuator for Ultra Deep Water Applications

O presente trabalho em nível de mestrado foi avaliado e aprovado por banca examinadora composta pelos seguintes membros:

Prof. Jonny Carlos da Silva, Dr.
Universidade Federal de Santa Catarina

Prof. Yesid Ernesto Asaff Mendoza, Dr.
Universidade Federal de Santa Catarina

Certificamos que esta é a **versão original e final** do trabalho de conclusão que foi julgado adequado para obtenção do título de mestre em Engenharia Mecânica.

_____

Prof. Dr. Andrey Ricardo da Silva
Coordenador em Exercício do Programa de Pós Graduação em Engenharia Mecânica

_____

Prof. Dr. Victor Juliano De Negri
Orientador

Florianópolis, 14 de novembro de 2019.

Dedico este trabalho à minha companheira Sabrina Teixeira Estevam, aos meus pais Elenesia Ana Duarte da Silva e Pedro da Silva e aos meus irmãos Bruno, Anna, Charlotte, Michelle e Charles.

AGRADECIMENTOS

Agradeço primeiramente as duas mulheres da minha vida, as quais com carinho, amor e dedicação foram meus alicerces durante toda essa jornada, minha mãe Elenesia Ana Duarte da Silva e minha companheira e melhor amiga Sabrina Teixeira Estevam. Muito obrigado também aos meus demais familiares por estarem sempre lá quando eu precisei de um abraço.

Aos meus amigos do LASHIP, com os quais sempre pude contar em momentos de dúvidas e que me proporcionaram o melhor ambiente possível durante minha estada.

Aos meus colegas, e também amigos, da Bosch Rexroth - das plantas de São Paulo, Brasil e de Lohr am Main, Alemanha – pela atenção e gentileza que fizeram da experiência de trabalharmos juntos algo instrutivo e agradável.

Ao meu orientador professor Victor Juliano De Negri pelos sábios conselhos, sinceridade e paciência.

Ao meu co-orientador Alexandre Orth e a empresa Bosch Rexroth que me forneceram a oportunidade de colaborar neste projeto.

Ao Programa de Pós-Graduação em Engenharia Mecânica pela infra-estrutura e professores de altíssimo nível, o que me proporcionou um ótimo ambiente para aquisição de conhecimento e debate de ideias.

Obrigado também a todas as pessoas que, de uma forma ou de outra, contribuiram para o meu crescimento profissional e/ou pessoal durante este periodo, em especial à Bruno Duarte da Silva, Richard de Medeiros Castro, Gabriel Linhares Baldo, Amadeu Plácido Neto, Eduardo Bruno Felipe, Juergen Schneider, Thomas Franz, Tim Strohmenger e Gottfried Hendrix.

Science is a way of thinking much more than it is a body of knowledge.
(Carl Sagan)

RESUMO

Ultimamente, em sistemas submarinos de produção de petróleo e gás, o uso de sistemas totalmente elétricos (*All-Electric Systems* - AES) aumentou devido às suas várias vantagens em comparação com suas contrapartes eletro-hidráulicas convencionais, como redução nos custos de instalação e operacionais, resposta rápida do sistema, redução no diâmetro de cabos umbilicais, alto nível de flexibilidade operacional e projeto sustentável. Neste contexto, um atuador eletro-hidrostático (*Electro-Hydrostatic Actuator* - EHA) - composto por um servomotor, uma transmissão hidrostática e um cilindro hidráulico com uma mola para efetuar a função de falha-segura – trata-se de uma solução que pode ser aplicada a sistemas de produção totalmente elétricos, preservando as melhores características de sistemas electro-hidráulicos convencionais, como confiabilidade, compacidade, robustez e densidade de energia em um projeto sustentável e de interface totalmente elétrica. Neste trabalho, um atuador de válvula submárina eletro-hidrostático - desenvolvido especialmente para operar com válvulas gaveta com diâmetro nominal de 2 polegadas em profundidades de até 3.000 metros - é modelado matematicamente, simulado numericamente e validado pelo confronto de seus resultados com os de experimentos em um protótipo. O modelo validado é então simulado, com um modelo de válvula gaveta, em vários cenários diferentes e avaliado em termos de funcionalidade e consumo energético. Os resultados obtidos através das simulações realizadas apresentam um sistema com comportamento robusto durante as operações nominais de abertura e fechamento da válvula gaveta, bem como durante as funções de falha segura, em todos os cenários avaliados. O EHA demonstra ter baixo consumo energético, com a possibilidade de se predefinir um consumo máximo de potência, o qual é controlado pela limitação da velocidade angular do seu servomotor. As influências da profundidade de instalação do equipamento e da pressão do poço no comportamento do sistema também são investigadas.

Palavras-chave: Atuador eletro-hidrostático. Sistemas de controle submarino. Sistemas de atuação de válvulas submarinas.

RESUMO EXPANDIDO

Introdução

Segundo relatórios recentes, a demanda mundial por energia deve crescer mais de 25% até 2040 (IEA, 2018). Até 2035, espera-se que as empresas de Exploração e Produção (E&P) precisem adicionar cerca de 43 milhões de barris por dia de nova produção de petróleo de projetos ainda não autorizados para atender à demanda, com a exploração *offshore* sendo responsável por cerca de 30% de toda a produção. Espera-se que cerca de metade do volume total produzido *offshore* provenha de recursos de águas profundas e ultraprofundas (McKinsey & Company, 2019).

Nesse contexto, a exploração de petróleo e gás em águas ultraprofundas tem enorme importância na matriz energética mundial. A título de exemplo, o plano de negócios e gestão 2019-2023 da empresa brasileira Petrobras (2019) menciona que se pretende aplicar 56% dos investimentos disponíveis para exploração e produção no campo do pré-sal, o qual se localiza em regiões de águas ultraprofundas.

Equipamentos destinados a aplicações em águas ultraprofundas, localizadas em profundidades entre 1830 e 3000 m, devem ser projetados para as altas pressões externas devido à coluna de água e, também, a dificuldade de se realizar manutenção em tais locais. Além dessas considerações, o equipamento deve ser projetado para operar com manutenção mínima durante toda a vida útil de um poço de produção, que pode ser de 25 anos ou mais (Orth, 2014).

A aplicação de atuadores eletro-hidrostáticos (EHA) em equipamentos submarinos, como Árvores de Natal Molhadas (ANM) e Manifoldes, conta com inúmeras vantagens, pois reúne as melhores características dos sistemas de produção eletro-hidráulicos convencionais como confiabilidade, compacidade e robustez com as vantagens proporcionadas por sistemas de produção totalmente elétricos como redução nos custos de instalação e operacionais, resposta rápida do sistema, redução no diâmetro de cabos umbilicais, alto nível de flexibilidade operacional e projeto sustentável.

O emprego de um EHA para movimentação de válvulas gaveta em ANMs já foi investigado anteriormente em Goularte (2018) - em uma parceria entre o Laboratório de Sistemas Hidráulicos e Pneumáticos (LASHIP) da Universidade Federal de Santa Catarina (UFSC) com a empresa Bosch Rexroth - onde o conjunto EHA / válvula gaveta foi modelado

e simulado, nos programas Matlab Simulink e Simster, e avaliado estática e dinamicamente em termos de funcionalidade, consumo e eficiência energética.

Neste trabalho, um protótipo de um atuador eletro-hidrostático (EHA) destinado à aplicações submarinas em águas ultraprofundas é testado experimentalmente, modelado matematicamente com as devidas simplificações em seu sistema eletro-hidrostático para proteção de propriedade intelectual, e simulado numericamente a fim de se obter uma representação matemática adequada e aplicá-la em simulações posteriores em um ambiente de trabalho simulado em diferentes cenários de profundidade, pressões de poço e restrições de potência consumida.

Objetivos

Esta pesquisa tem como objetivo avaliar o desempenho de um protótipo de atuador eletro-hidrostático (EHA) para operações em águas ultraprofundas em termos de funcionalidade e consumo de energia. Para atingir esse objetivo, um modelo matemático do EHA é desenvolvido, simulado e validado com os resultados experimentais de um protótipo. O modelo validado é então aplicado a operar um modelo matemático de válvula gaveta em simulações posteriores, onde o ambiente de trabalho do EHA é emulado em diferentes cenários operacionais, como pressões de poço e profundidades de instalação do equipamento.

Metodologia

São utilizadas as referências bibliográficas disponíveis para obtenção das informações que sustentam e introduzem o tema a ser dissertado. O modelo matemático foi desenvolvido integralmente no software Simster, disponibilizado pela Bosch Rexroth, e baseado nos modelos apresentados em Goularte (2018) e Orth e Hendrix (2018) com atualizações referentes a mapas de eficiência das bombas hidráulicas e no esquema do sistema eletro-hidrostático.

Através de um sistema de aquisição de dados adequado e um computador para controle e monitoramento do protótipo, foram obtidos dados experimentais suficientes para auxiliar na validação do modelo matemático desenvolvido. Contudo, o sistema de aquisição de dados utilizado não faz parte desta dissertação.

Após a validação, o modelo do EHA foi posteriormente aplicado para a operação de um outro modelo de uma válvula gaveta, baseado nos modelos apresentados em Mashiba (2011)

e Goularte (2018), em um ambiente simuladamente hiperbárico onde a influência da profundidade de instalação do equipamento, pressões de poço, e potência disponível para consumo foram investigadas no que diz respeito ao comportamento estático e dinâmico do sistema durante operações nominais e de falha-segura.

Resultados e Discussões

O modelo matemático apresentou comportamento aderente ao protótipo em termos de velocidades do atuador e motor elétrico, pressões das câmaras dos cilindros hidráulicos, corrente elétrica e consequentemente potência consumida.

Por possuir um cilindro hidráulico, exclusivo para a mola de retorno, para a exercer a função de falha-segura, o EHA apresenta a possibilidade de acumular a energia potencial da mola e libera-la somente em situações de emergência para fechamento da válvula. Com esta característica, o sistema poupa a potência que seria requerida para movimentação da mola durante operações nominais de abertura da válvula.

O conjunto EHA/válvula gaveta foi simulado em profundidades de 0, 1000, 2000 e 3000 metros, onde se observou uma maior força requerida para abertura da válvula a medida que a profundidade diminuía e, por conseguinte, uma maior demanda de potência no motor elétrico. Contudo, esta mesma característica não se repete durante o fechamento da válvula gaveta, comportamento este que ocorre devido à dissipação de energia em uma válvula de retenção operada por piloto que é utilizada no sistema para garantir que o EHA mantenha a posição, quando desejado, sem a necessidade de fornecer potência ao servomotor. Este efeito de dissipação de energia é elucidado através das equações matemáticas que descrevem o comportamento do sistema durante o fechamento da válvula gaveta.

A função de falha-segura, que deve garantir o fechamento da válvula gaveta em situações de emergência, foi simulada em quatro cenários diferentes – máxima e miníma profundidade e máxima e nula pressão de poço – onde o sistema demonstrou ser capaz de fechar a válvula gaveta em todos as situações simuladas, sendo que o cenário com máxima profundidade e nula pressão de poço apresentou o maior tempo necessário para fechamento da válvula, comportamento este explicado através do somatório das forças externas envolvidas no sistema.

A utilização de um controlador de potência consumida – o qual limita a velocidade angular do servomotor em função da potência máxima permitida – foi investigada, onde se limitou o consumo de potência do sistema para 100 Watts no cenário de maior demanda

energética (máxima pressão de poço e mínima profundidade), na qual o EHA demonstrou ser capaz movimentar a válvula gaveta com robustez satisfatória, apenas necessitando de mais tempo para a abertura da mesma, visto que a velocidade é limitada para que o sistema opere dentro dos limites estabelecidos de consumo energético.

Conclusão e Trabalhos Futuros

O modelo matemático desenvolvido apresentou boa aderência aos resultados experimentais adquiridos a partir do protótipo, permitindo, de maneira adequada, a avaliação do comportamento da EHA em um ambiente de trabalho simulado. Por meio dessas simulações e análises, as seguintes conclusões podem ser alcançadas.

Quanto maior a profundidade d'água, considerando a mesma pressão de poço, menor será a força requerida resultante que deverá ser superada pela EHA para abrir a válvula de gaveta e, consequentemente, menor será a potência requerida pelo motor elétrico para operar o sistema.

O sistema de execução da função de falha-segura do EHA demonstrou ser capaz de fechar totalmente a válvula gaveta em todos os quatro cenários simulados, nos quais o cenário sem pressão dentro da válvula e profundidade máxima demonstrou ser o mais crítico para a mola de fechamento. Em outras palavras, a pressão do poço ajuda o movimento de fechamento, enquanto a pressão hidrostática externa funciona de maneira oposta, no que diz respeito ao fechamento da válvula durante a falha-segura.

A válvula de retenção operada por piloto cumpre seu papel de manter o EHA parado quando o motor elétrico está em repouso, embora funcione como um dissipador de energia durante a operação de fechamento da válvula de gaveta, quando as forças mecânicas resultantes ajudam o movimento de retorno, o que é o estado padrão durante a operação de fechamento da válvula gaveta. Aumentar a relação de áreas do piloto da válvula de retenção não influencia significativamente esse comportamento. Em um estudo em que se pretende regenerar a energia fornecida pela válvula durante o movimento de fechamento, a utilização da válvula de retenção operada por piloto, na configuração atual, deve ser revisada.

O controle de limitação de potência mostrou-se uma boa estratégia quando se destina a economizar o consumo máximo de potência do EHA, aumentando o tempo para abrir a válvula de gaveta. Entretanto, a eficiência global do sistema tende a diminuir em velocidades menores, como pode ser estimado pelos mapas de eficiência das bombas hidráulicas do sistema.

Logo, uma limitação no consumo máximo de potência para abrir a válvula exigiria, por consequência, a renúncia de uma quantidade resultante de energia que seria perdida devido à diminuição da eficiência do sistema. Por fim, esta pesquisa apresentou os pontos fortes e fracos do protótipo estudado para aplicações em equipamentos submarinos nos cenários investigados e finalmente, os modelos apresentados podem ser utilizados para estudos e análises posteriores.

Como sugestão de pesquisas futuras, menciona-se o estudo da aplicação de EHAs para operar válvulas de outros tamanhos e / ou diferentes tipos; a realização de testes, no protótipo, com uma válvula real em ambiente hiperbárico, onde se poderá emular experimentalmente todos os cenários simulados nesta pesquisa; a análise da viabilidade de um projeto que aproveite a energia mecânica disponibilizada pela válvula gaveta durante o movimento de retorno e a realização de testes de resistência no protótipo e análise do desempenho do sistema à medida que o número de ciclos realizados aumenta.

Palavras-chave: Atuador eletro-hidrostático. Sistemas de controle submarino. Sistemas de atuação de válvulas submarinas.

ABSTRACT

Recently, in subsea oil & gas production systems, the use of All-Electric Systems (AES) has increased due to their several advantages in comparison with the conventional electro-hydraulic counterparts, such as installation and operational costs reduction, fast system response, reduction of umbilical cables diameter, high level of operational flexibility and environment-friendly design. In this context, an Electro-Hydrostatic Actuator (EHA) – a system comprised of a servomotor, a hydrostatic transmission and a hydraulic cylinder with a fail-safe spring – is a solution that can be applied in AES while preserving the best characteristics of conventional electro-hydraulic systems, such as reliability, compactness, robustness and power density in an environmental friendly and power-by-wire connectivity design. In this research, a subsea valve EHA – particularly devised to operate with 2 inches gauge gate valves at water depths of up to 3,000 meters – is mathematically modeled, numerically simulated and validated by the confrontation of its results with those of experiments in a prototype. The validated model is then simulated with a gate valve model in several different scenarios and evaluated in terms of functionality and power consumption. The obtained results through the carried out simulations present a system with robust behavior during the opening and closing operations of the gate valve as well as during the fail-safe functions in all simulated scenarios. The EHA demonstrates to have low power consumption, with the possibility of predefine a maximum power consumption, which is controlled by limiting the electric motor angular velocity. The influence of the equipment installation water depth and wellbore pressure in the system behavior are investigated as well.

Keywords: Electro-hydrostatic actuator. Subsea control systems. Subsea valve actuator.

LISTA DE FIGURAS

LIST OF TABLES

LIST OF ABBREVIATIONS

AES - All-Electric Systems

AMV - Annulus Master Valve

API - American Petroleum Institute

AWV - Annulus Wing Valve

BLDC - Brushless Direct Current

BOP - Blowout Preventer

CAPEX - Capital Expenditure

CIU - Chemical Injection Unit

COV - Cross Over Valve

EHA - Electro Hydrostatic Actuator

FPSO - Floating Production, Storage and Offloading

HMI - Human Machine Interface

HPU - Hydraulic Power Unit

HXT - Horizontal Christmas Trees

ISO - International Organization for Standardization

LASHIP - Laboratório De Sistemas Hidráulicos E Pneumáticos

MCS - Master Control Station

MCS - Master Control Station

MTBF - Mean Time Between Failure

MV - Master Valve

OPEX - Operational Expenditure

PLEM - Pipeline End Manifold

PLET - Pipeline End Termination

PMV - Production Master Valve

PVT - Performance Verification Testing

PWV - Production Wing Valve

ROV - Remotely Operated Vehicle

RWP - Rated Working Pressure

SCM - Subsea Control Module

SCSSV - Surface Controlled Subsea Safety Valve

SDU - Subsea Distribution Unit

SPS - Subsea Power Supply

SV - Swab Valves

SVA - Subsea Valve Actuator

VXT - Vertical Christmas Tree

WCT - Wet Christmas Tree

WV - Wing Valve

XT - Xmas Trees

LIST OF SYSMBOLS

GREEK ALPHABET

$\dot{\theta}_p$	Pump angular velocity.	[rad/s]
$\ddot{\theta}_p$	Pump angular acceleration	[rad/s^2]
$\dot{\theta}_{SM}$	Angular velocity of the electric motor	[rad/s]
μ	friction coefficient between the gate valve and its seats	[-]
Δp	Pressure differential	[Pa]
Δp_{cv}	Pressure differential through check valve	[Pa]
Δp_{max}	Pressure drop per control edge	[Pa]
Δp_p	Pressure differential through the pump	[Pa]
ρ_{pf}	Specific mass of the production fluid	[kg/m^3]
ρ_{SW}	Specific mass of the sea water	[kg/m^3]
ρ_{hf}	Specific mass of the hydraulic fluid	[kg/m^3]
ω_{fb}	Angular velocity feedback	[rad/s]
ω_{max}	Maximum angular velocity	[rad/s]
ω_{ref}	Angular velocity reference	[rad/s]
ω_{ref_lim}	Angular velocity reference limit	[rad/s]
η_g	Global efficiency	[%]
η_m	Mechanical Efficiency	[%]
η_v	Volumetric efficiency	[%]

LATIN ALPHABET

AG	Distance between the water surface and the platform	[m]
A_{cyl1}	Effective area of the main cylinder	m^2
A_{cyl2}	Effective area of the spring cylinder	m^2
$A_{VG}(x)$	Opening area of the valve	[m^2]
A_{VG0}	Maximum area of action of the pressure differential through the gate valve	[m^2]
B_1	Main cylinder viscous friction coefficient	[N.s/m]
B_2	Spring cylinder viscous friction coefficient	[N.s/m]
b_{SM}	Electro motor viscous friction coefficient	[Nms/rad]
D	Oil pipe diameter	[m]
d_{cyl1}	Main cylinder piston diameter	[m]
d_{cyl2}	Spring cylinder piston diameter	[m]
d_{ID}	Seat inner diameter	[m]
d_{OD}	Seat outer diameter	[m]
D_p	Pump displacement	[m^3/rad]
d_{rod}	Cylinder rod diameter	[m]
d_{stem}	Gate valve stem diameter	[m]
f	friction coefficient of the oil pipe	[-]
Fat_{co1}	Main cylinder coulomb friction	[N]
Fat_{co2}	Spring cylinder coulomb friction	[N]
Fat_{est1}	Main cylinder static friction	[N]
Fat_{est2}	Spring cylinder static friction	[N]
F_{cyl1}	Main cylinder hydraulic force	[N]
F_{cyl2}	Spring cylinder hydraulic force	[N]
F_{drag}	Friction force between the gate and seats of the valve	[N]
F_{enc}	Enclosure force acting on the actuator rod	[N]
F_{fric}	Friction forces	[N]
F_{seal}	Friction force due to the contact between the seals and the stem in the bonnet	[N]
F_{sp}	Safe spring force	[N]

F_{spo}	Spring pre-load force	[N]
F_v	Force acting on the stem due to the gate valve internal pressure	[N]
g	Gravity acceleration	[m/s^2]
$G_{qv/p}$	Flow rate – pressure gradient	[m^3/(Pa.s)]
h	Opening percentage of the gate valve	[%]
i_{SM}	Electric motor electrical current	[A]
J_p	Pump moment of inertia	[kg.m^2]
J_{SM}	Electric motor moment of inertia	[kg.m^2]
K	Flow rate resistance coefficient of the gate valve	[-]
KV_{leak}	Internal leakage coefficient of the hydraulic pump	[m^3/s.Pa$^{0.5}$]
K_e	Electric motor back electromotive force constant	[Nm/A]
K_{sp}	Safe spring elastic coefficient	[N/m]
K_t	Electric motor torque constant	[Nm/A]
Kv_{cv}	Check valve flow rate gain	[m^3/(Pa$^{0.5}$.s)]
L	Length of the production oil pipe	[m]
LDA	Water depth of installation of the equipment	[m]
L_{SM}	Electrical inductance of the electric motor	[H]
m_1	Main cylinder mass	[kg]
m_2	Spring cylinder piston mass	[kg]
p_{0pcv}	Opening pressure of the pilot operated check valve	[Pa]
p_A	Pressure in the main cylinder chamber A	[Pa]
p_{Apcv}	Pressure in port A of the pilot operated check valve	[Pa]
p_B	Pressure in the main cylinder chamber B	[Pa]
p_{Bpcv}	Pressure in port B of the pilot operated check valve	[Pa]
pb_{pcv}	Pilot check valve effective spring rate	[Pa]
p_C	Pressure in the spring cylinder chamber C	[Pa]
p_d	Pressure downstream the gate valve flow rate direction	[Pa]
P_e	Electrical power	[W]
p_{enc}	Electro hydrostatic actuator reservoir pressure	[Pa]
P_m	Mechanical power	[W]
p_o	Opening pressure	[Pa]
P_r	Required power	[W]

p_{sep}	Pressure on the surface oil separator	[Pa]
P_u	Useful power	[W]
p_{WELL}	Well bore pressure	[Pa]
px_{pcv}	Pilot pressure of the pilot operated check valve	[Pa]
qv_{leak}	Pump internal leakage flow rate	[m^3/s]
qv_{tp}	Pump theoretical flow rate	[m^3/s]
qv	Flow rate	[m^3/s]
qv_{max}	Flow rate at maximum pressure drop	[m^3/s]
R_{pcv}	Pilot area ratio of the pilot operated check valve	[-]
R_{SM}	Electrical resistance	[Ω]
R_T	Gear transmission ratio	[-]
$T1$	Delay Time	[s]
T_f	Pump friction torque	[Nm]
T_{load}	Load torque required by the gear transmission	[Nm]
T_{tp}	Pump theoretical torque	[Nm]
U_{in}	Voltage input	[V]
u_{pcv}	Opening ratio of the pilot operated check valve	[-]
U_{SM}	Voltage	[V]
v_{oil}	Production fluid velocity	[m/s]
v_t	Friction transitional velocity	[m/s]
x	Position of the actuator/gate valve	[m]
x_{co}	Crack open/close position, position in which the bore of the gate starts to communicate with the gate valve bore.	[m]
X_{fb}	Position feedback	[m]
X_{ref}	Position reference	[m]
x_{sp}	Spring cylinder piston position	[m]
x_{tot}	Maximum gate valve stroke	[m]

SUMÁRIO

1 INTRODUCTION

1.1 CONTEXTUALIZATION

As being reported recently, the world demand for energy is set to grow by more than 25 % until 2040 (IEA, 2018). By 2035, Exploration and Production (E&P) companies are expected to need adding about 43 million barrels per day of new crude production from unsanctioned projects to meet demand, with offshore exploitation been responsible for about 30% of the new crude production. About half of the total offshore volume is expected to come from deepwater and ultra-deepwater resources (McKinsey & Company, 2019).

In this context, the Oil & Gas exploitation in deep and ultra-deep waters has enormous importance on world's energetic matrix. For instance, the business plan and management 2019-2023 of the Brazilian company Petrobras (2019) mentions that it intends to invest 56% of the Investments in Exploration and Production on the pre-salt field.

Equipment intended to be applied in ultra-deep waters, which are located in depths between 1830 to 3000 m, must be designed for the high external pressures due to the column of water and the difficulty to perform maintenance in such places. Beyond these considerations, the equipment must operate with minimum maintenance during a well location's entire service life, which can be 25 years or more (Orth, 2014).

The application of electro-hydrostatic actuators (EHA) in subsea equipment, such as Xmas Trees (XT) and Manifolds, has several advantages, as it brings together the best characteristics of conventional electro-hydraulic production systems, such as reliability, compactness, and robustness, with the advantages offered by all-electric systems (AES) such as reduced installation and operating costs, rapid system response, reduced umbilical cable diameter, high level of operational flexibility and sustainable design (Goularte, 2018).

The use of an EHA for the actuation of gate valves in XTs has been previously investigated in Goularte (2018) - in a partnership between the Laboratory of Hydraulic and Pneumatic Systems (LASHIP) of the Federal University of Santa Catarina (UFSC) and the company Bosch Rexroth - where the EHA / gate valve assembly has been modeled and simulated in the Matlab Simulink and Simster software, and statically and dynamically evaluated in terms of functionality, power consumption and energy efficiency.

In this research, a prototype of an electro-hydrostatic actuator (EHA) for applications in depths up to 3000 meters is experimentally tested, mathematically modeled in a layout with the appropriated simplifications to protect intellectual property, and numerically simulated in order to obtain an appropriated mathematical representation and apply it in subsequent simulations in a simulated work environment in different depth scenarios, well pressures and power constraints.

1.2 OBJECTIVES

This research aims to evaluate the performance of an electro-hydrostatic actuator (EHA) prototype for ultra-deepwater operations in terms of functionality and power consumption. To achieve this goal, a mathematical model of EHA and the forces involved was developed, simulated, and validated with the prototype experimental results. The validated model was then applied to operate a gate valve mathematical model and also evaluated in other simulations where its working environment is emulated with different operating scenarios such as well pressures and depths.

1.2.1 Specific Objectives

These research specific objectives are:

- Updating of the EHA mathematical model presented in previous researches, namely Orth and Hendrix (2018) and Goularte (2018), with the prototype design and its components experimental data;
- Execution of the experimental tests with the prototype;
- Validation of the mathematical model comparing experimental and simulation results;
- Use of the validated mathematical model in further simulations where working environmental conditions are emulated and evaluate it in terms of functionality and power consumption;

2 LITERATURE REVIEW

2.1 SUBSEA PRODUCTION SYSTEM

According to Bai and Bai (2010), a subsea production system is composed of one or more completed subsea wells, production wellheads, production trees, flow lines, submarine equipment and control facilities to operate the wells. There can be several variations in terms of complexity, such as from a single satellite well with a single flow line connected to a fixed platform to several wells grouped around a manifold, which transfers the fluid to a floating installation or directly to on-shore installations.

On Figure 2.1, a typical subsea production system including a Floating Production, Storage, and Offloading (FPSO) is presented. Onboard the vessel, the Master Control Station (MCS), Subsea Power Supply (SPS) and other equipment, such as a Chemical Injection Unit (CIU) are placed. Umbilical cables connect the FPSO with the Subsea Distribution Unit (SDU) are installed, transferring hydraulic and electrical power, chemicals and communication signals to the subsea installation. The SDU, in its turn, manages the split and distribution of the umbilical to the Xmas Trees (XTs).

Figure 2.1 - Typical Subsea Production System.

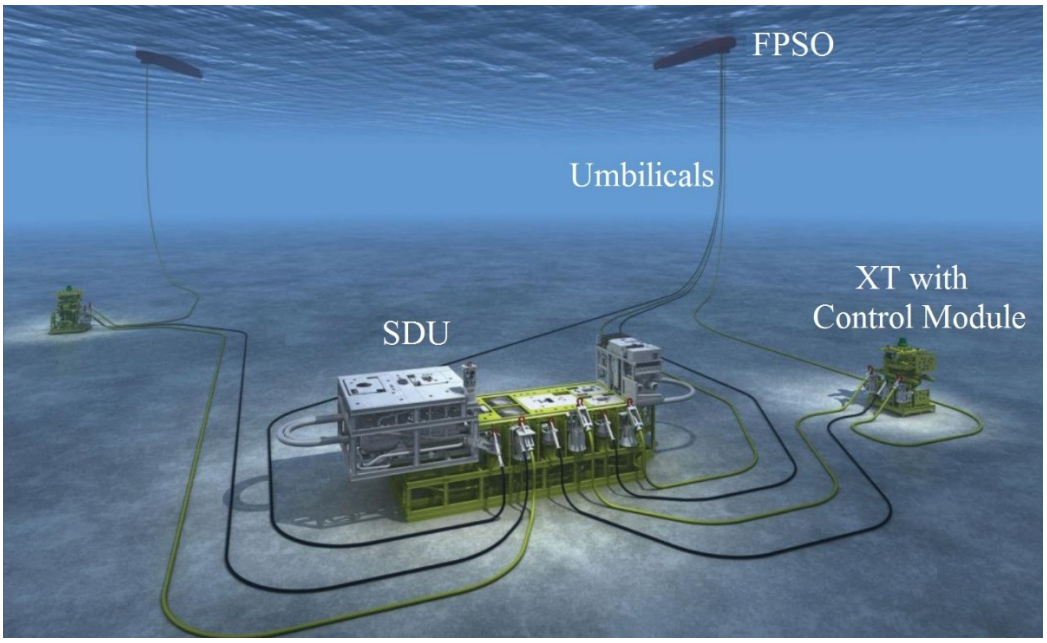

Source: Modified from Zalavadiya, 2018.

Among the equipment used in the underwater production, it can be highlighted the Wet Christmas Tree (WCT), Jumpers, Manifold, Pipeline End Termination, PLEM (Pipeline End Manifold), Flowlines, Risers and FPSO (Floating Production Storage and Offloading (Bai and Bai, 2010) (Morais, 2013). These are individually described in the following sections.

2.1.1 Subsea Control Module (SCM)

The SCM is an independently retrievable unit responsible for providing well control functions during the production phase of subsea oil and gas production, such as actuation system and condition monitoring (Oilfield Wiki, 2017) (Bai and Bai, 2010). Figure 2.2 illustrates the typical components of an SCM.

Figure 2.2 - Typical SCM Components

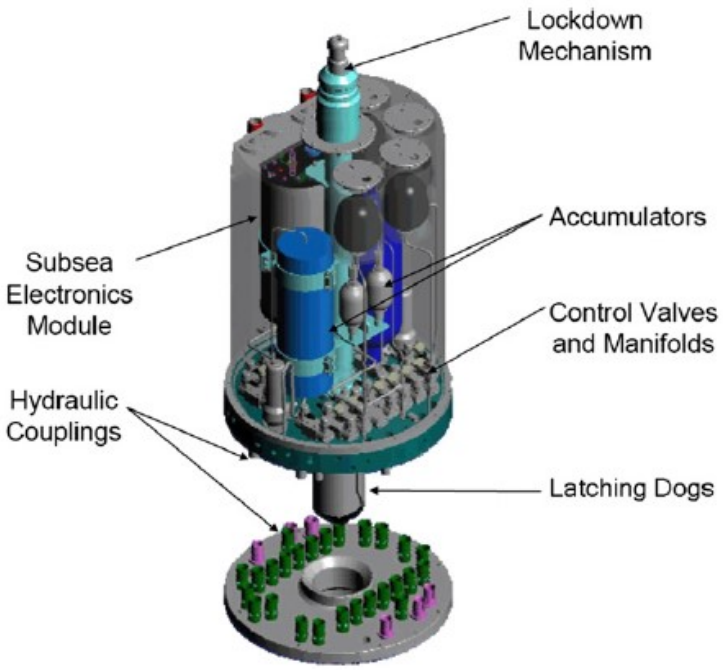

Source: Oilfield Wiki, 2017.

Typical functions controlled and monitored by a SCM are:

- Actuation of fail-safe return production tree actuators and downhole safety valves;
- Actuation of flow control choke valves, shutoff valves, manifold diverter and shutoff valves, chemical injection valves and others;

- Actuation and monitoring of surface-controlled reservoir analysis and monitoring systems, sliding sleeve, choke valves;
- Monitoring of downhole pressure, temperature, and flow rates;
- Monitoring of sand probes and production tree and manifold pressures, temperatures, and choke positions.

2.1.2 Subsea Christmas Tree (XT)

The Christmas tree, also called Xmas tree (XT), is responsible for closing a well and controlling fluid flow during production or injection (SPE, 2014). A XT is a housing with bores fitted with valves, pipes, and connections placed on top of a wellbore. The valves are operated by electrical or hydraulic signals or manually by a diver or Remotely Operated Vehicle (ROV) (Bai and Bai, 2010) (Torbergsen et al., 2012). It is designed to withstand the high pressures and temperatures of the well and the high hydrostatic pressures and low temperatures of the marine environment (Morais, 2013). The valves allow the well to be closed externally, if necessary. The primary function of an XT is to act as a barrier between the reservoir and the environment, but other typical functions requirements include:

- Direct the fluid produced from the well to the flowline (called production tree) or to canalize the injection of water or gas into the formation (called injection tree);
- Fluid flow rate regulation through a choke (when necessary);
- Condition monitoring at the tree level, such as well pressure, annulus pressure, temperature, sand detection, and others;
- Safely stop the flow of fluid produced or injected employing valves actuated by a control system;
- Protection fluids injection into the well or the flowline, such as inhibitors for corrosion or hydrate prevention.

The size and configuration of an XT are not the same from one offshore field to another since it needs to be designed for the individual reservoir conditions and the possible solutions

available (Berven, 2013) (Fikri, 2016). Valves commonly present in an XT system are (Plácido, 2018) (ISO 10417, 2005):

- Surface Controlled Subsea Safety Valve (SCSSV): It is a directly actuated on/off valve controlled by the surface, which closes in emergencies preventing the flow of hydrocarbons or fluid up the tubing;
- Master Valves (MV): On/off valves with the function of completely closing/opening their respective bore tubing of the well. The production master valve (PMV) opens/closes the production tubing, while the annulus master valve (AMV) latches the injection flow, and it usually remains closed during production. These keep in a redundant structure to improve reliability/availability. The production master valve is commonly the valve next to the SCSSV in the production flow, and the annulus master valve is the first valve in its piping.
- Wing Valves (WV): These are continuously controllable valves with the function of controlling the flow of its bore. These are located between the master valves and the external outlets. These valves are the first to be shut when the well must be closed.
- Swab Valves (SV): Valves used during workover processes, which provide a controllable and safe re-entry into the well structure when the workover equipment needs to be installed on top of the well and are only opened when the workover equipment is attached correctly and sealed.
- Cross Over Valve (COV): This valve allows the communication between the annulus and production bores. It can be used to bleed up a pressure rise, for instance.

Most valves used in a Christmas tree are fail-safe, that means that in the event of system failure, the valves return to a safe-state to mitigate hazards. In average, a subsea tree contains eight valves. Typically, they are all gate valve types but also can be ball valves. The subsea tree is attached on top of the wellhead housing through a support interface piece called tubing hanger (Plácido Neto, 2018).

There are two primary conceptions of Xmas Trees, the vertical (VXT) and the horizontal (HXT) which are illustrated in Figure 2.3. The VXT and HXT main characteristics are discussed in the sections below.

Figure 2.3 – Illustrative Vertical (a) vs Horizontal (b) Xmas Tree.

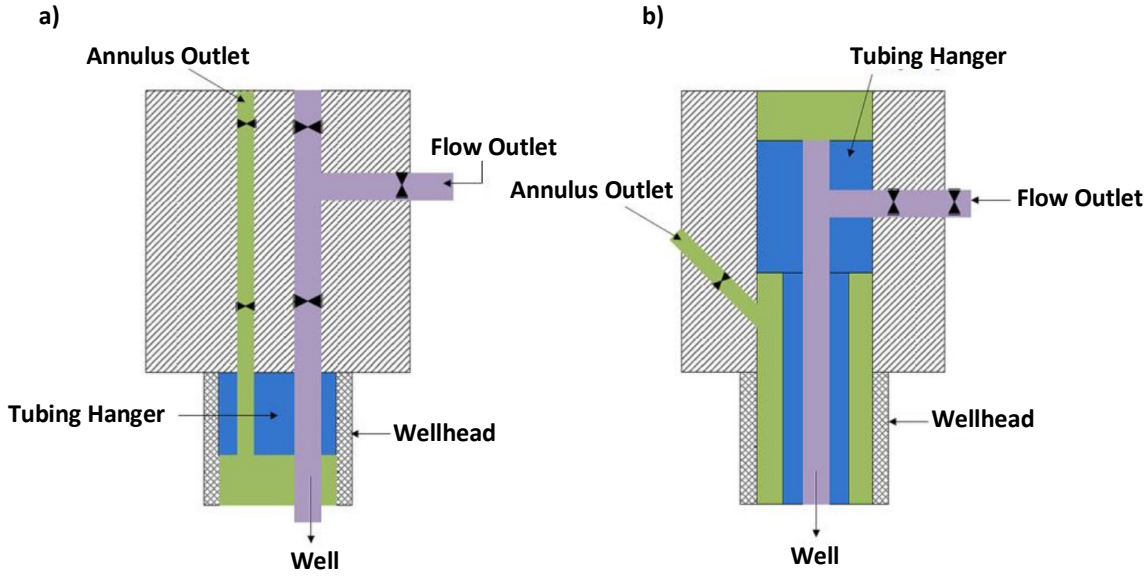

Source: Modified from Fikri, 2016.

2.1.2.1 Vertical Xmas Tree (VXT)

In the VXT, also called dual-bore Xmas Tree, the production and annulus master valves keep positioned above the tubing hanger, which in this kind of tree is dual-bore and laid down before the XT (Fikri, 2016). The production and annulus bore pass vertically through the tree body. This characteristic has an impact on the capacity for workover operations that can be conducted with the XT still in-place. The production and annulus wing valves, PWV and AWV, are located after the point at which the production and annulus lines cross into the horizontal plane. Production and annulus swab valves that allow for well workover and intervention are included in the system through a T-joint located in between the master and wing valves of the Xmas tree production and annulus lines (Bai and Bai, 2010) (Berven, 2013). A schematic VXT valve arrangement is presented in Figure 2.4.

Figure 2.4 - VXT main elements.

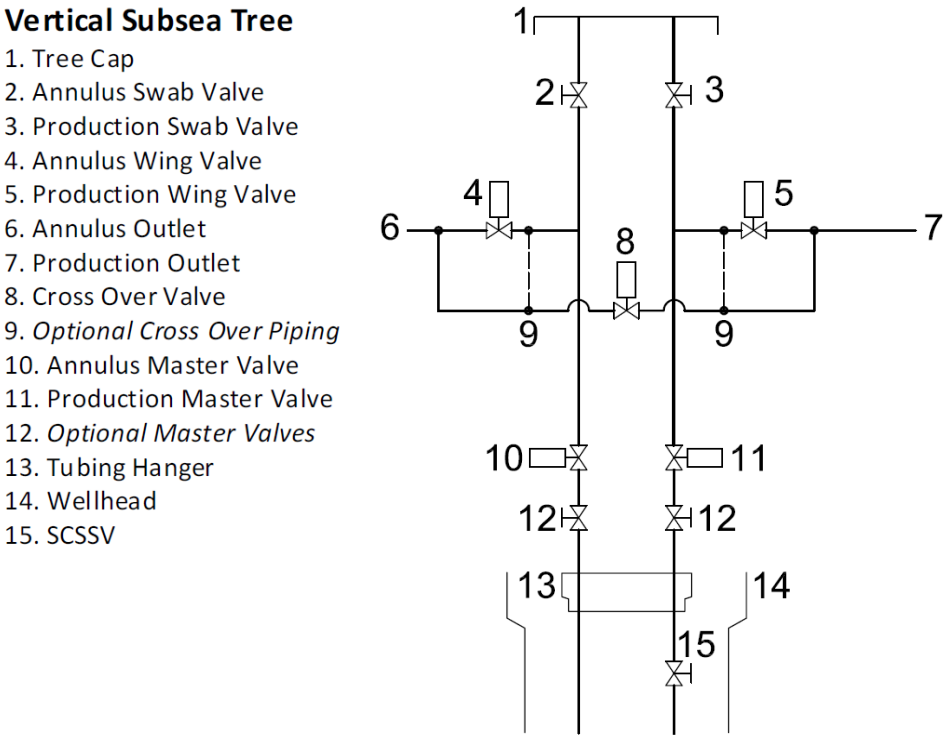

Source: ISO 13628-4, 2011.

VXTs are widely applied in subsea fields due to their flexibility of installation and operation. Due to the tubing hanger be positioned in the wellhead, this tree can be recovered without having to recover the downhole completion (Bai and Bai, 2010).

2.1.2.2 Horizontal Xmas Tree (HXT)

HXTs can be distinguished from the VXTs by observing that the production and annulus master valves are located on the side of the tubing hanger (Berven, 2013) and opposing to the VXT, which is dual-bore, the horizontal Xmas tree and the tubing hanger are mono-bore (Fikri, 2016). Figure 2.5 presents three examples of HXTs configurations and its main components.

Figure 2.5 - Examples of HXTs and its main elements.

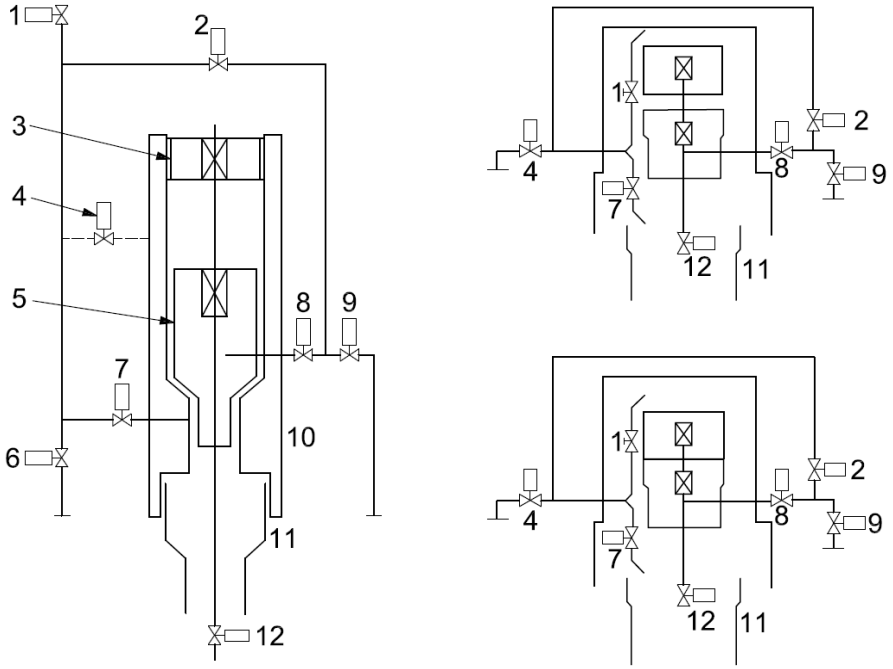

Source: ISO 13628-4, 2011

HXTs are a more recent technology and have incremental innovations compared to the traditional trees. Its architecture allows the production column to be withdrawn from the interior of the well for repairs without the necessity of removing the XT from the wellhead, because the valves are mounted on the lateral sides, allowing simple well intervention and tubing recovery. This concept is especially beneficial for wells that need a high number of interventions. Swab valves are not used in the HXT since they have electrical submersible pumps applications. The crucial HXT feature is that the tubing hanger is installed in the tree body instead of the wellhead. This arrangement requires the tree to be installed onto the wellhead before completion of the well (Bai and Bai, 2010) (Morais, 2013).

2.1.3 Manifold

The subsea manifold (Figure 2.6) is a flow-routing subsea hardware (subsea flow router), composed of pipes and valves, which connects between subsea trees and flow lines. Its purpose is to optimize the subsea layout arrangement and reduce the number of risers connected to the platform. The manifold is one of the most essential equipment in subsea operation, due to its multiple functions, such as centralizing and controlling production fluid from several XTs (Oilfield Wiki, 2017).

Figure 2.6 - Four subsea trees tied to one central manifold.

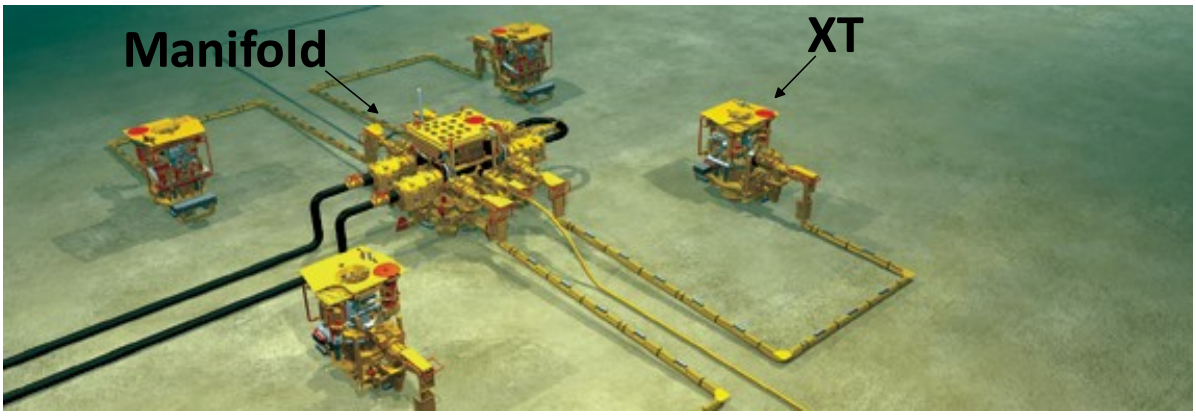

Source: Modified from Oilfield Wiki, 2017.

Other manifold functions are the injection of water, gas or chemicals into the reservoir employing an injection manifold, and the injection of gas into the production well utilizing the gas lift manifold. The numerous types of manifolds range from a simple pipeline end manifold (PLEM/PLET) to large structures such as a subsea process system (Morais, 2013) (FishSafe, 2009).

2.1.3.1 PLEM (Pipeline End Manifold)

The PLEM has the function of distributing the flow of two or more leads to a duct or vice versa. In function, this closely resembles the manifold, except for the monitoring and control of the flow (Bai and Bai, 2010) (FishSafe, 2009).

2.1.3.2 PLET (Pipeline End Termination)

PLET is an equipment that allows the submarine interconnection between the flowline and flexible ducts (risers). It consists basically of an isolation valve, set of tubes, hydraulic connectors, a panel for remote valve operation and a structure to support its components (Bai and Bai, 2010) (FishSafe, 2009).

2.1.4 Umbilical Systems

The communication between the topside and the subsea equipment (XTs, Manifold, and others) is carried out through umbilical cables (Figure 2.7), which are an arrangement of pipes and/or electric conductors grouped in a shielded enclosure that is assembled from the host station to the subsea production equipment (Oliveira, 2016).

Figure 2.7 - Umbilical cable cross section example.

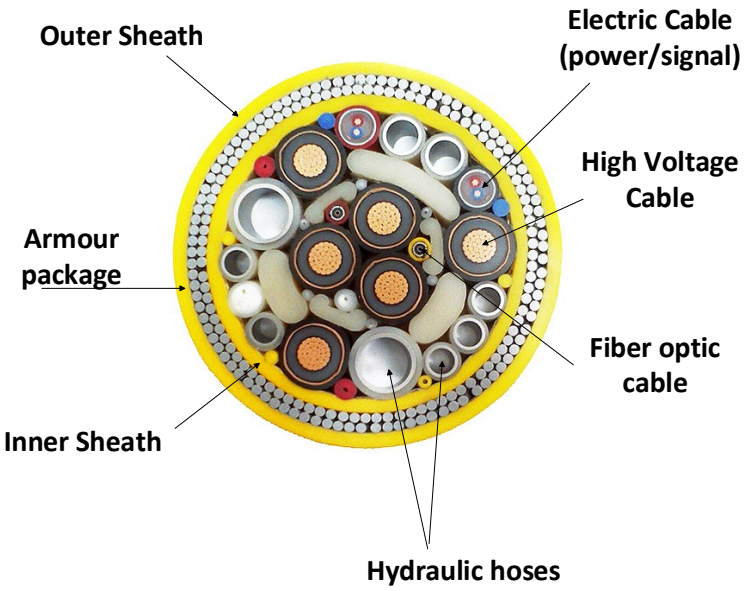

Source: Modified from OilField Wiki, 2017.

Umbilical functions include electrical monitoring signals and optical signals, hydraulic controls on Xmas trees and manifolds, injecting chemicals into the wells, controlling temperatures and pressures, among other functions (Morais, 2013) (ISO 13628-6:2009).

2.2 XMAS TREE SUBSEA ACTUATION SYSTEMS

According to Berven (2013), the subsea actuation system is the element responsible for performing several vital control functions in a subsea production system, such as the control of the flow through the following XT piping systems:

- Production line through the use of production master and wing valves;
- Water and/or gas injection lines;
- Annulus line through the use of annulus master and wing valves;
- Annulus injection line;
- Service lines such as chemical fluid injection;
- Isolation through use of cross-over valves or down-hole safety valves.

The XT piping systems, and consequently valve's internal diameter, are commonly constructed of piping with the following nominal sizes:

Table 2.1: Overview of XT piping internal diameters by system.

Valve Function	**Valve Nominal diameter [in]**
Production Valve	5" - 7"
Annulus Valves	2"
Chemical Injection Valve	3/8" - 1"
Isolation Valve	1/2" - 1"
Blowback Valve	1/2" - 1"

Source: Berven, 2013.

The design structure of these systems can be considered as composed of three essential elements: the valve, the bonnet, and the actuator. There are several types of valves and actuators available in the market, thus making a large number of possible combinations between these components. The actuators can be of the electromechanical or hydraulic type and are

responsible for the closing and opening function of the production valves, the valves are commonly the gate or ball type whereas the bonnet is the structural coupling between the valve and the actuator (Goularte, 2018).

Figure 2.8 shows a traditional valve/actuator assembly. A gate valve, a bonnet and a hydraulic actuator with a pressure compensator, safe return spring and ROV bucket for manual operation compose the system.

Figure 2.8 - Subsea Actuation System example

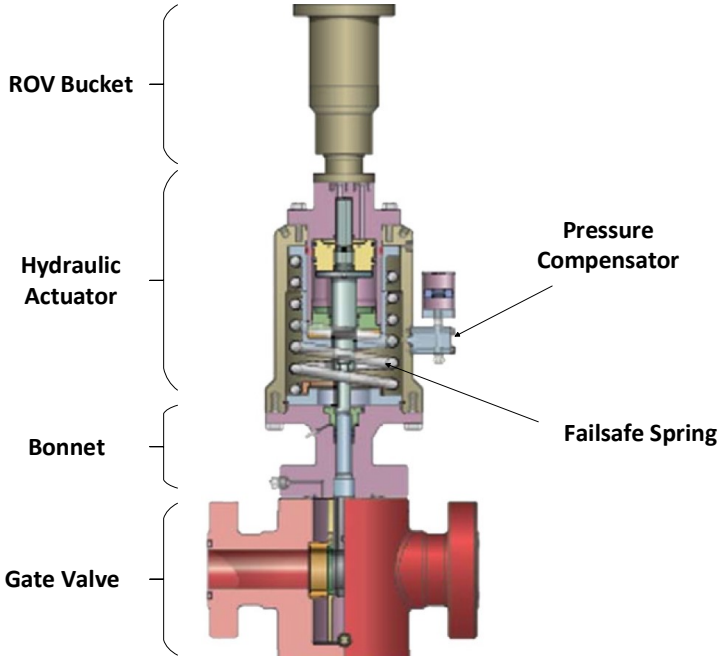

Source: Adapted from Bai and Bai, 2010.

Gate valves are widely used in XTs, manifolds, and blowout preventer (BOP) due its long history of application in the sector and high reliability due it has been through extensive development with proven field use and design improvements. Likewise, one of the main characteristics of such valves is the minimum obstruction to the flow passage when fully opened, resulting in a small pressure drop in the production line and consequently an economic loss of power.

2.3 SUBSEA CONTROL SYSTEMS

The primary purpose of the control system is open and close the valves present in the subsea equipment, such as Christmas trees, manifolds, and chokes installed in jumpers (Bai and Bai, 2010) (Goularte, 2018). The five principal types of control systems used in subsea control are:

- Direct hydraulics;
- Piloted hydraulics;
- Direct electro-hydraulics;
- Multiplexed electro-hydraulics;
- All-electric.

The direct hydraulics, piloted hydraulics, and direct electro-hydraulic subsea control strategies are not commonly applied in deep and ultra-deepwater due to their slow response when working with long distances between the platform and the subsea equipment (Goularte, 2018). In the next sub-sections, a brief explanation of the multiplexed electro-hydraulic and all-electric control systems is presented. For more information about subsea control systems, see Bai and Bai, 2010.

2.3.1 Multiplexed Electro-Hydraulic Control System

The multiplexed electro-hydraulic control strategy, depicted in Figure 2.9, is the most widely used approach for deep waters. It replaces the multiple control lines of other hydraulic control systems with a single communication and adds a local subsea control module (SCM) in the seabed. The communication between the master control station (MCS) and the SCM is performed through the subsea electronics module (SEM). A single SCM can locally control the flow in the cylinders much faster and with less power loss in the umbilical (Bai and Bai, 2010).

The local controller makes the system flexible, expansible and enables its employment in deep waters (Goularte, 2018). To perform a subsea valve opening, the operator sets the MCS to request the subsea valve actuator (SVA) movement, sending a coded message from the MCS to the SEM, which interprets the message and energize the appropriated solenoid, allowing hydraulic fluid to flow into the SVA. To perform the closing movement, the solenoid is de-energized, allowing the safe spring to push the actuator to its returned position, sending the

hydraulic fluid to the sea (as shown in Figure 2.9) or to a return line back to the platform (Bai and Bai, 2010) (Mashiba, 2011).

Figure 2.9 - Multiplexed Electro-hydraulic Control System.

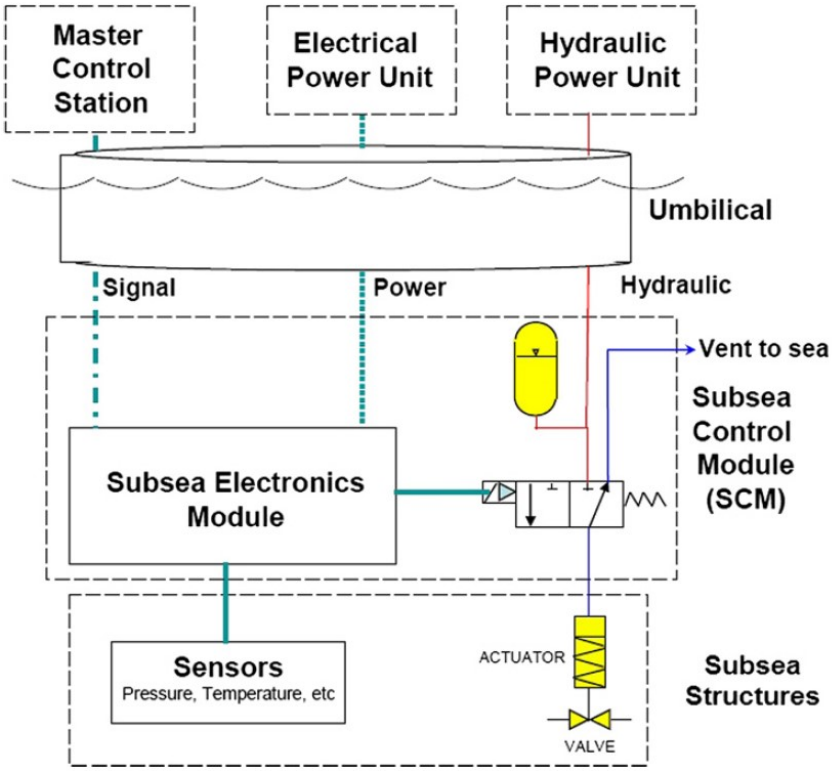

Source: Bai and Bai, 2010.

The main advantages of this control strategy are a system short-time response, no distance limitations, reduction in umbilical size comparing with the other hydraulic solutions, seabed status monitoring available and high level of operational flexibility. However, in the other hand, this control system requires a high level of complexity, increase of surface and subsea components, requires electrical connectors, high level of fluid cleanness and periodic fluid recharging since it commonly does release the hydraulic fluid to the ocean (Bai and Bai, 2010).

2.3.2 Subsea All-Electric Control System

According to Berven (2013), all-electric production control systems are distinguished from hydraulic and electro-hydraulic production control systems by its prime mover working principle. The prime movers and the control and umbilical power lines deliver electrical power throughout the production system. Separated signal cables or integrated signal on power cables transfer the system data and control commands back and forth from the field systems to the surface facility HMI (Human Machine Interface) at the MCS (Master Control Station). Electrical cables replace the hydraulic power supply unit and pipes. The production systems also require injection lines to supply chemicals, so some hydraulic units and supply lines will still be required in the system. Figure 2.10 illustrates an all-electric control system structure.

Figure 2.10 - All-electric control system scheme.

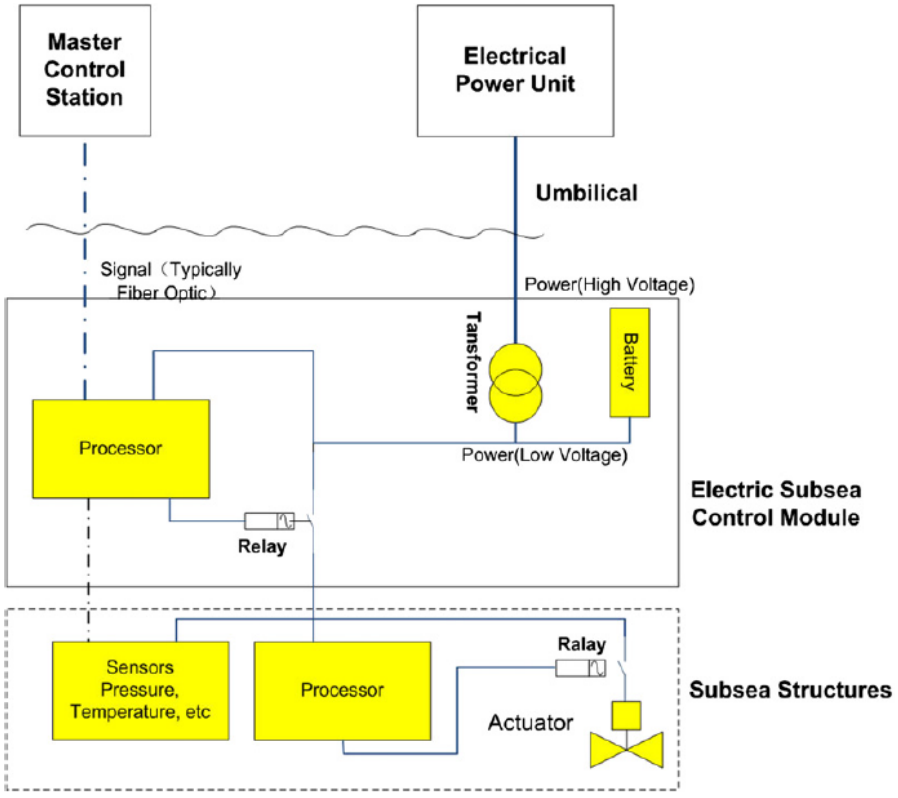

Source: Bai and Bai, 2010.

The actuators in the production control system are driven by electrical motors, which transfer the electrical energy prevenient of the umbilical into mechanical energy in the form of angular movement. A gearbox transmission, in its turn, is used to convert the angular movement

into linear in order to operate the subsea production valve, as illustrated in Figure 2.11 (Berven, 2013).

Figure 2.11 - Valve/Electro mechanic actuator assembly.

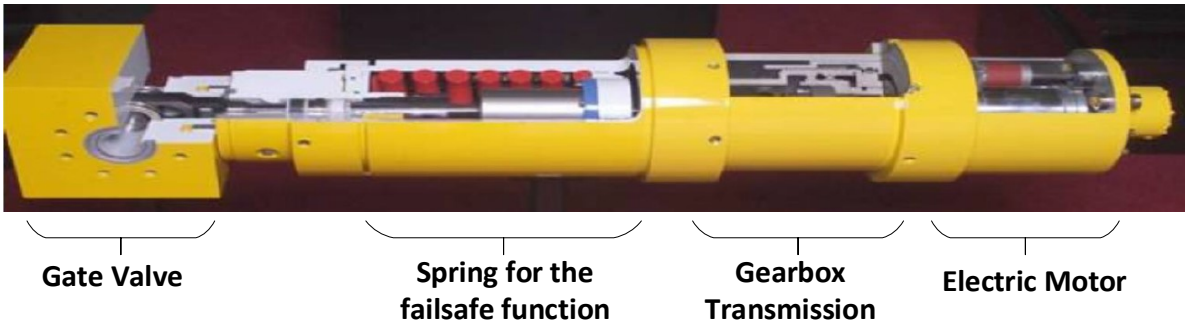

Source: Modified from Berven, 2013.

One of the main advantages of all-electric systems (AES) is the operational expenditure (OPEX) reduction due to its flexibility in installation and maintenance stages of the equipment, real-time system response and reduction on umbilical diameter. From the environmental perspective, these systems are less harmful than the conventional hydraulic counterparts are since it does not release hydraulic fluid to the ocean (Bai and Bai, 2010) (Goularte, 2018) (Berven, 2013).

Besides, the overall weight of an all-electric subsea production system will be smaller than a traditional electro-hydraulic design due to the elimination of hydraulic lines in umbilicals, which lead to a significant decrease in distribution system weight per unit length. There is also the possibility of using an alternative chemical injection method that could eliminate chemical injection tubing. Figure 2.12 illustrates an illustrative comparison between traditional electro-hydraulic umbilical cables (a), all-electrical umbilical with chemical injection lines (b) and all-electric umbilical with only electrical lines (c) (Berven, 2013).

Figure 2.12 - Illustrative comparison between the cross sections of traditional electro-hydraulic and all-electric umbilical cables.

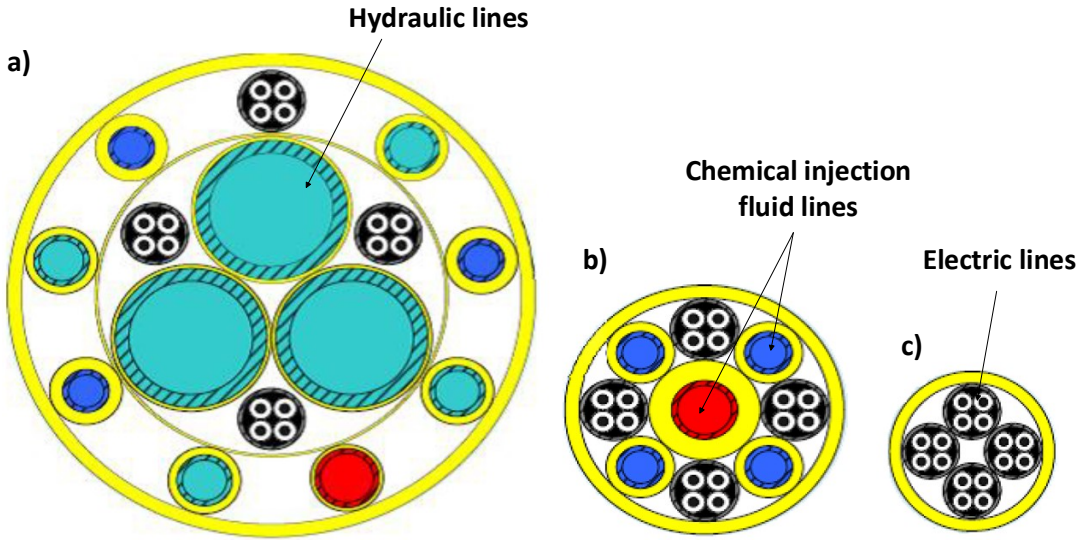

Source: Berven, 2013.

Nevertheless, actuators used in all-electric systems have some disadvantages when compared with conventional hydraulic actuators, such as the need of a mechanism to ensure the permanence of the production valve open position when the electric actuator is in stand-by. This necessity, allied to the friction losses and a lower power density of electromechanical systems, leads to a potentially problematic increase in weight and volume (Abicht, 2017) (Zalavadiya, 2018). Mashiba (2010), states that for reasons of reliability, this kind of actuator is rarely applied in the well safety equipment, being its current application restricted to processing subsea equipment.

2.4 ELECTRO-HYDROSTATIC VALVE ACTUATOR FOR ALL-ELECTRIC CONTROL SYSTEMS

Orth and Hendrix (2018) and Goularte et al. (2018) present an electro-hydrostatic actuator (EHA) solution to be applied in the all-electric production control system. This concept aims to ally the performance of hydraulic actuators in terms of safety, power density and efficiency with the simple electric interface, installation and operational costs reduction, real-time system response and environment benefits of all-electric systems. Figure 2.13 illustrates an all-electric control system using one EHA to operate the production valve.

Figure 2.13 - All-electric production control system with an electro-hydrostatic actuator.

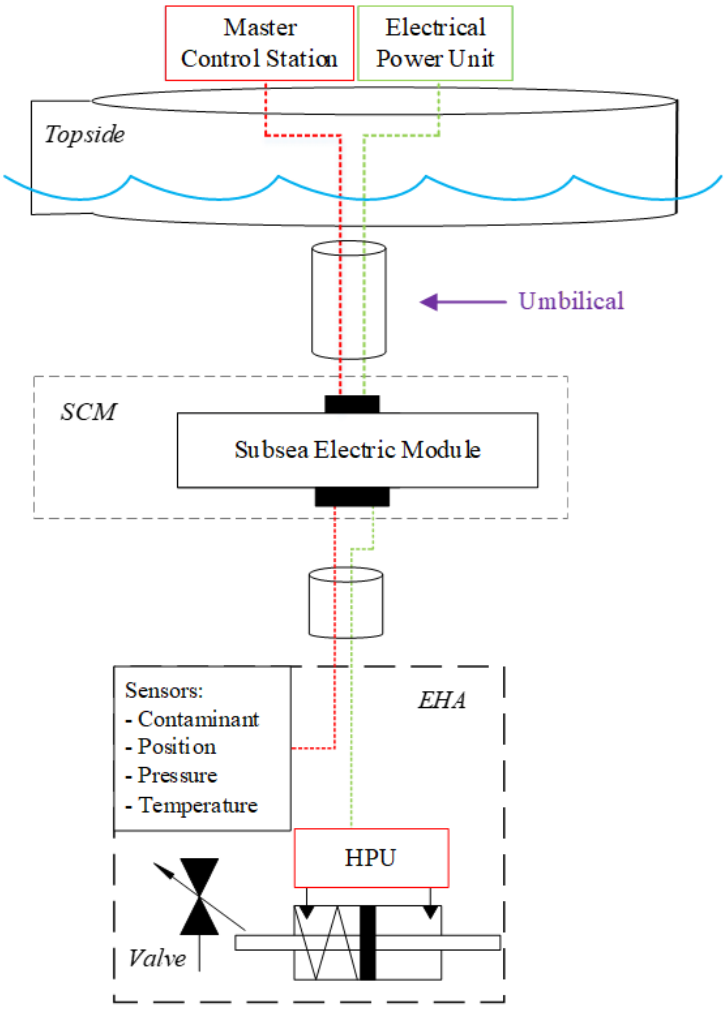

Source: Adapted from Goularte *et al.*, 2018.

As stated by Weber *et al.* (2016), electro-hydrostatic actuators (EHA) combine many of the inherent advantages of hydraulic drive technology, i.e., reliability, robustness, large forces, high transmissions, proper overload protection, easy gear change, ease of use, low maintenance effort, compact design and easy 'plug and play' connectivity. Gannon (2017), mentions that this is already a mature technology in aircraft applications due to its many advantages and since the power is generated only upon reception of electric input command, these systems are also referred as 'power-by-wire' type actuation systems.

The EHA studied in this research is a prototype developed by Bosch Rexroth AG based on their patent WO/2016/023712. It consists of a servomotor with fixed displacement pumps which convert electrical power into hydraulic in order to operate a hydraulic double rod hydraulic cylinder. The patent diagram is illustrated in Figure 2.14.

Figure 2.14 - The patented concept of the electro-hydrostatic subsea valve actuator.

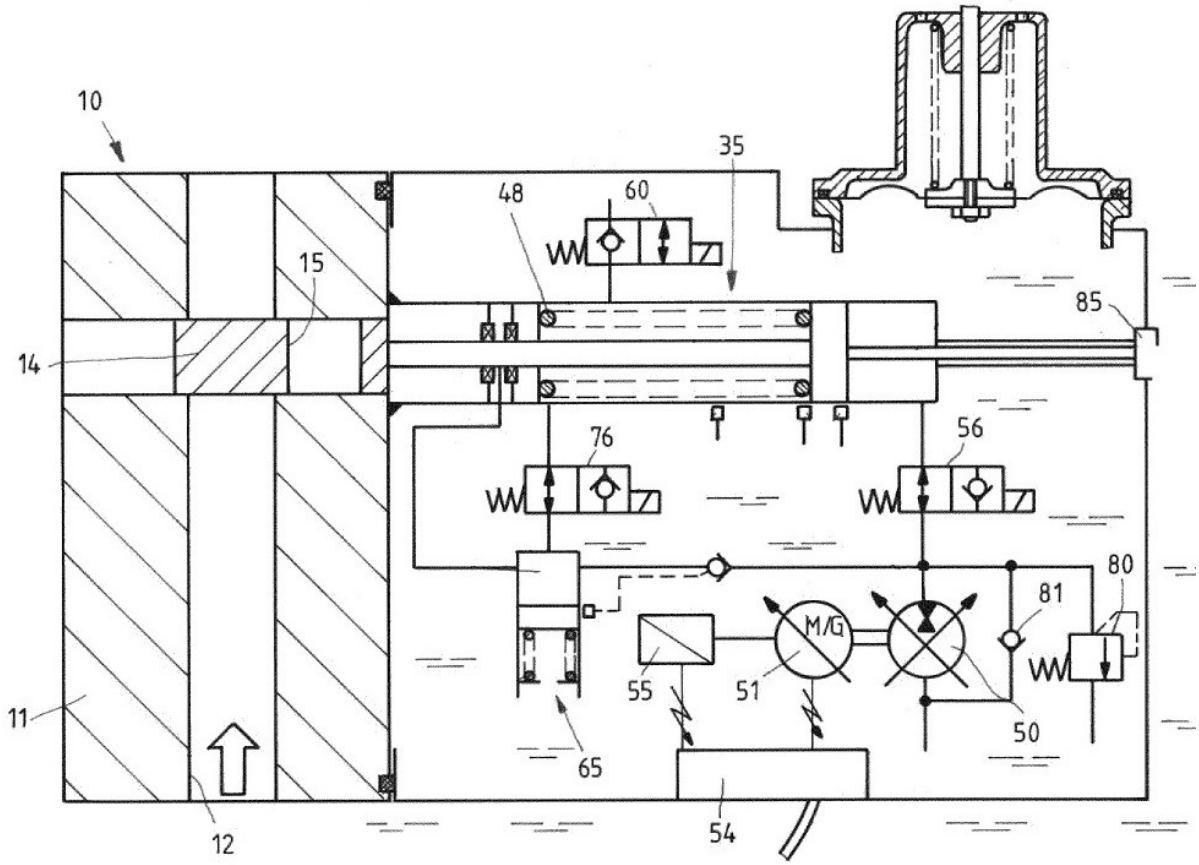

Source: Modified from patent WO/2016/023712.

The main components present in Figure 2.17 are: gate valve (10), valve housing (11), valve bore (12), gate (14), bore of the gate (15), electro-hydraulic system, hydraulic cylinder (35), compression spring (48), hydraulic pump (50), electric motor (51), electric control unit (54), angular velocity sensor (55), on-off directional seat valve (56, 60 and 76), hydraulic accumulator (65), relief valve (80), check valve (81) and manual interface for ROV operations (85). On the following chapter, the system's design functionalities and characteristics, as well as its requirements, are detailed.

3 SUBSEA VALVE ACTUATOR PROTOTYPE

In this chapter, a detailed explanation of both hydraulic and electrical components of the subsea valve actuator (SVA) prototype and its working principle – with the appropriate simplification – is given. This system components and/or characteristics has already been investigated through previous researches namely Körtgen (2014), Orth *et al.* (2016), Placido Neto (2016, 2018), Geßner (2017), Goularte (2018) and Zalavadiya (2018) which were a background for the present work.

3.1 MODULAR DESIGN

The subsea valve actuator (SVA) prototype studied in this research is an electro-hydrostatic actuator (EHA) particularly devised to operate with 2 inches gauge gate valves at depths of up to 3.000 meters. Its composition can be delineated as divided into modules as illustrated in Figure 3.1 and described next.

Figure 3.1 - SVA design and external interfaces.

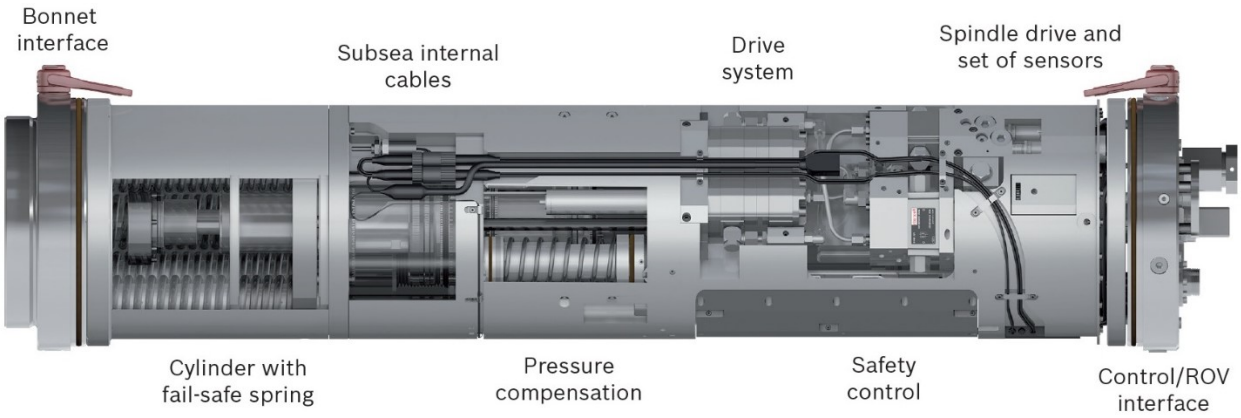

Source: Bosch Rexroth AG, 2018.

As shown in Figure 3.1, the SVA prominent modules are:

- Bonnet interface: Mechanical standardized interface which connects the SVA to the gate valve;

- Cylinder with fail-safe spring: A four-chamber cylinder with a spring module to perform the fail-safe function;
- Drive system: A redundant Hydraulic Power Unit (HPU);
- Pressure compensation: System which ensures that the SVA internal pressure is compensated with the subsea environmental pressure;
- Safety control module: A also redundant assembly of on/off valves which open in emergency depressurizing the hydraulic system and releasing the safety spring to return the actuator;
- Spindle drive and ROV interface: A mechanical interface which allows the driving of the SVA by a Remotely Operated Vehicle (ROV).

The hydraulic diagram of the SVA system prototype is presented below in Figure 3.2 with the appropriated simplifications and modifications in order to protect intellectual property.

Figure 3.2 - Schematic diagram of the subsea valve actuator prototype.

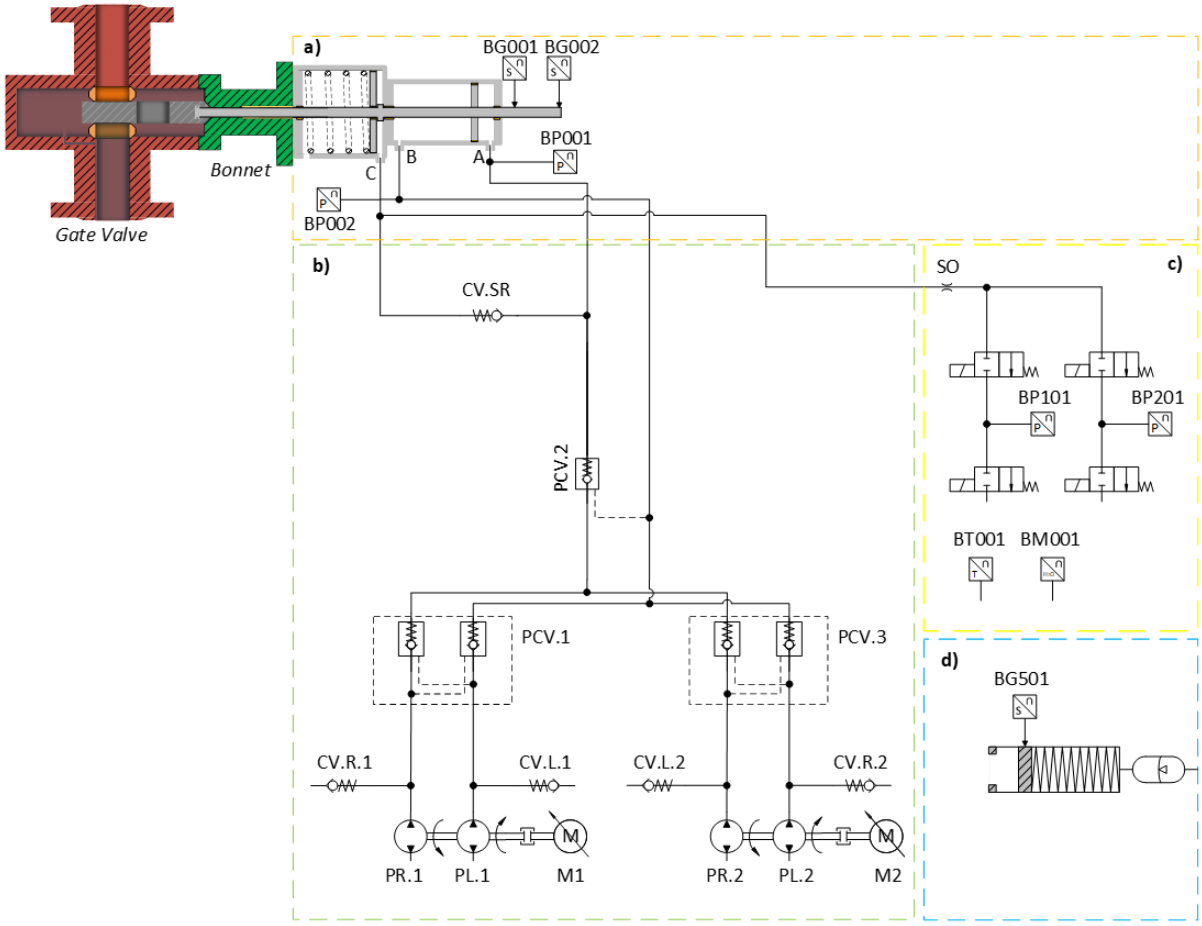

Source: Author.

The four blocks illustrated in Figure 3.2 are:

a) Cylinder module with fail-safe spring;
b) Drive system;
c) Safety control module;
d) Pressure compensation system;

The sensors included in the system are:

- BG001 and BG002: Redundant position sensors of the actuator's rod;
- BP001 and BP002: Respectively the pressure sensors of the main cylinder chambers A and B;
- BP101 and BP201: Sensors to monitor the pressure between the safety valves. If one assembling of valves is opened, these sensors allow the condition monitoring of the reservoir and spring cylinder chamber C pressures.
- BG501: Position sensor of the pressure compensator position, which allows the verification of the hydraulic system oil volume and consequently the detection of hydraulic fluid leakage;
- BM001: Detection of water contamination;
- BT001: Sensor for monitoring of the hydraulic fluid temperature;

3.2 SYSTEM FUNCTIONALITIES

An explanation of the system functionalities and characteristics is carried out in the following sections.

3.2.1 Pressure Compensation

The subsea valve actuator compensation system (Figure 3.2d) contains a preloaded spring, which ensures that the internal enclosure pressure will be higher than the environmental pressure (air or seawater). Figure 3.3 shows a representative illustration of the compensation mechanism.

Figure 3.3 - Schematic representation of compensator piston.

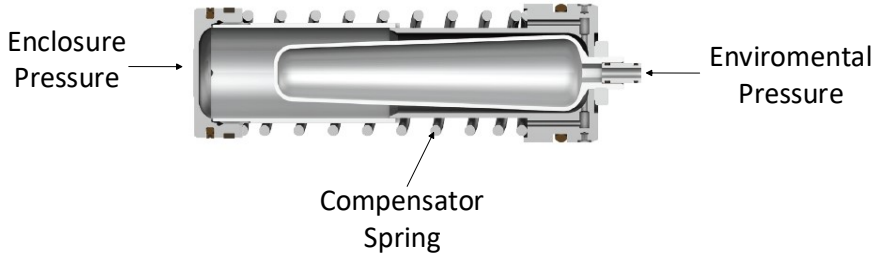

Source: Bosch Rexroth AG, 2018.

The additional pressure provided by the spring, which can variate from 0.5 to 2 bar, has the purpose of avoiding any inlet contamination from the environment such as seawater, sand, or organic materials. Besides, the sensors BM001 (water detection) and BT001(temperature) are used to monitor the quality of the hydraulic oil while the position encoder BG501 is used in the pressure compensation system to detect any possible leakage to the outside.

3.2.2 Fail-Safe Spring Clamping

In the studied EHA system, the spring is meant to be compressed once and remain in place until an emergency situation where the ON-OFF safety valves are opened, allowing the depressurization of the chambers A and C of the hydraulic cylinders (Figure 3.2a), releasing the spring to push the actuator to its returned position and consequently closing the valve. This characteristic allows the system to save the energy that would be necessary to compress the spring in standard operations.

During the spring clamping operation, the safety valves (Figure 3.2c) are closed, and then one of the electric motors is actioned – to facilitate the clarification, the motor M1 is chosen from now on –. The motor drives its hydraulic pumps through gear transmission. The pump PR.1 supplies hydraulic fluid to the chamber C of the spring cylinder while the other cylinder chamber is opened to the reservoir. If the pressure required to move the spring be enough to move the actuator's load, both main and spring cylinder will move together as a tandem cylinder, and the pump PR.1 will supply hydraulic fluid for both chambers A and C. However, in typical operation, the pressure required to move the actuator's load is much higher than the

required pressure to clamp the springs due to the spring cylinder bigger diameter. Therefore, the piston of the spring cylinder moves alone, compressing the spring, while the pump PL.1 sucks fluid from the reservoir through the valve check valve CV.L.1. Figure 3.4 represents a clamping spring operation, the high-pressure lines are represented in red, low pressure in blue, and the arrows indicate the flow rate direction.

Figure 3.4 - Representation of the clamping cylinder operation.

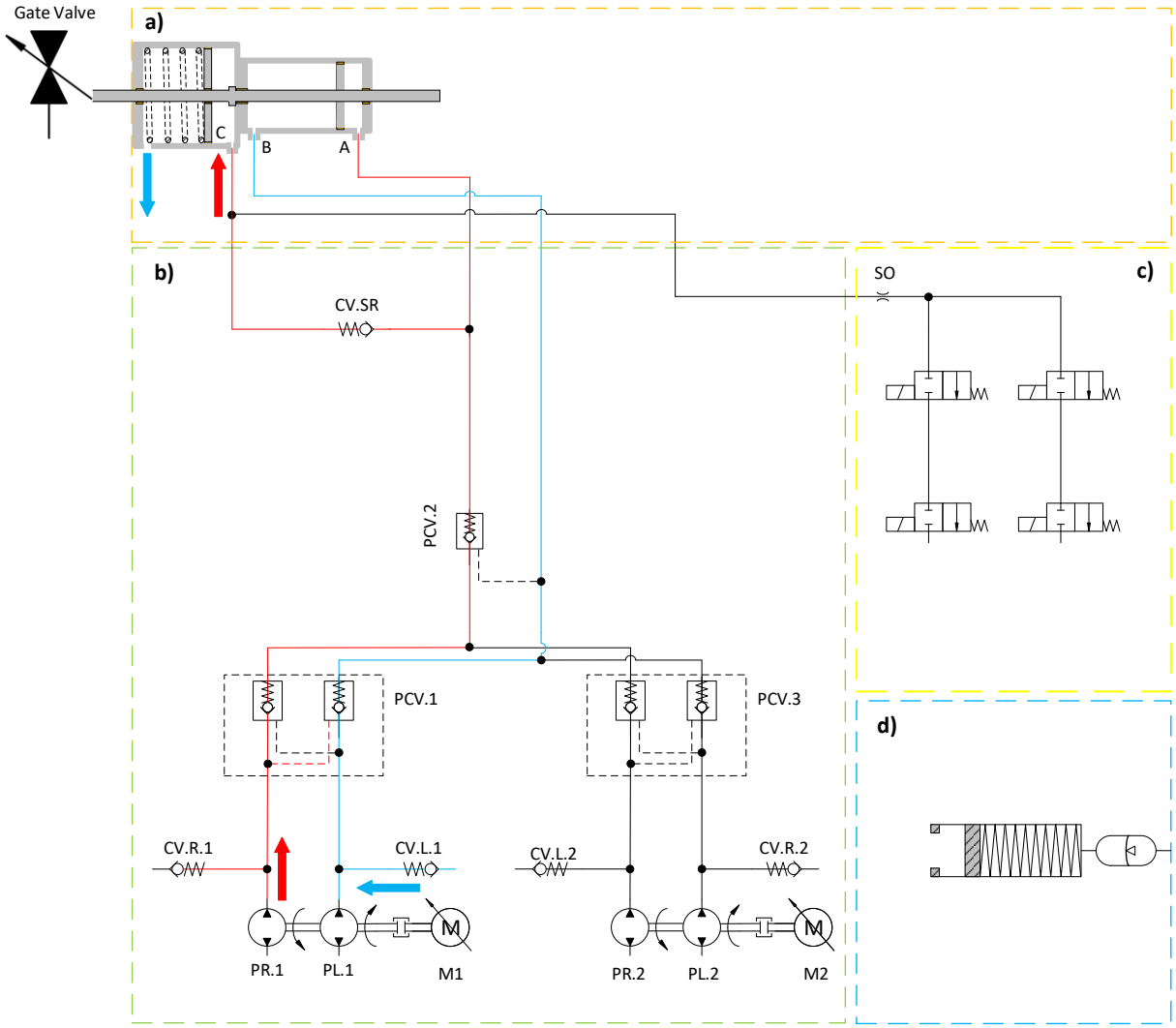

Source: Author.

3.2.3 Standard Operation

In standard operation condition, the spring cylinder chamber C remains locked by the safety valves, saving then, the energy that would be necessary to move the spring.

During the standard forward movement, the pump PR.1 (or PR.2), directs the fluid from the reservoir to the main cylinder chamber A passing through the pilot check valve PCV.1 (or PCV.3), and the pilot check valve PCV.2. The fluid of the chamber B is sucked by the pump PL.1 (or PL.2) passing through the valve PCV.1 (or PCV.3).

The check valves CV.R.1, CV.L.1, CV.R.2 and CV.L.2 work to supply fluid to the lines in situations where the pressure decreases below the reservoir's. The pilot check valves PCV.1, PCV.2 and PCV.3 lock the cylinder chambers when the electric motors are off, thus ensuring the remaining of the actuator position without the need of any additional power.

On the standard returning movement, the electric motor moves in the opposite way. The system's operation is similar, with just a mirroring on the operating valves. Figure 3.5 represents the system standard operations.

Figure 3.5 - Representation of the standard operational forward (a) and returning (b) movements of the SVA.

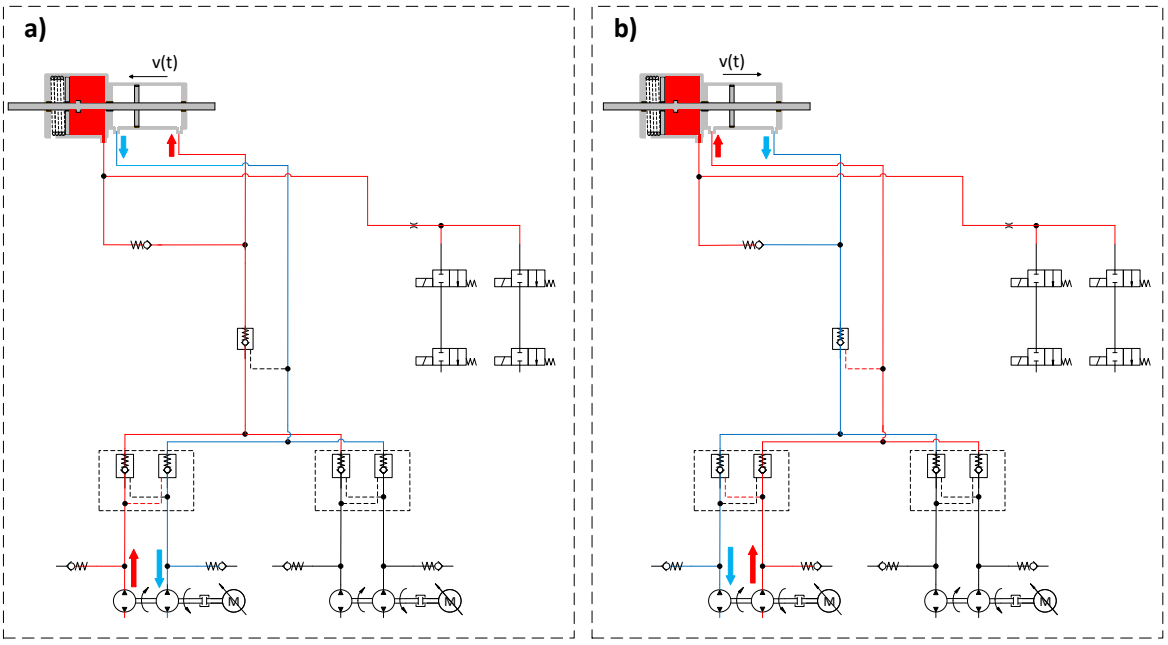

Source: Author.

As can be observed in Figure 3.5, during standard operations, the fluid on the spring cylinder chamber C remains confined by the action of the safety ON-OFF valves and the check valve CV.SR allows the flow rate just for filling the chamber.

3.2.4 Fail-Safe Function

On the fail-safe function, the safety valves are opened, and then all cylinder's chambers are depressurized releasing the safety spring to pull the actuator to its safe position as illustrated in Figure 3.6. In this function, all lines are depressurized. The color blue represents the low-pressure lines, in red are pressurized by the spring action, and the orange color represents the fluid sucked by the cylinder.

Figure 3.6 - Schematic representation of the safe-return operational function.

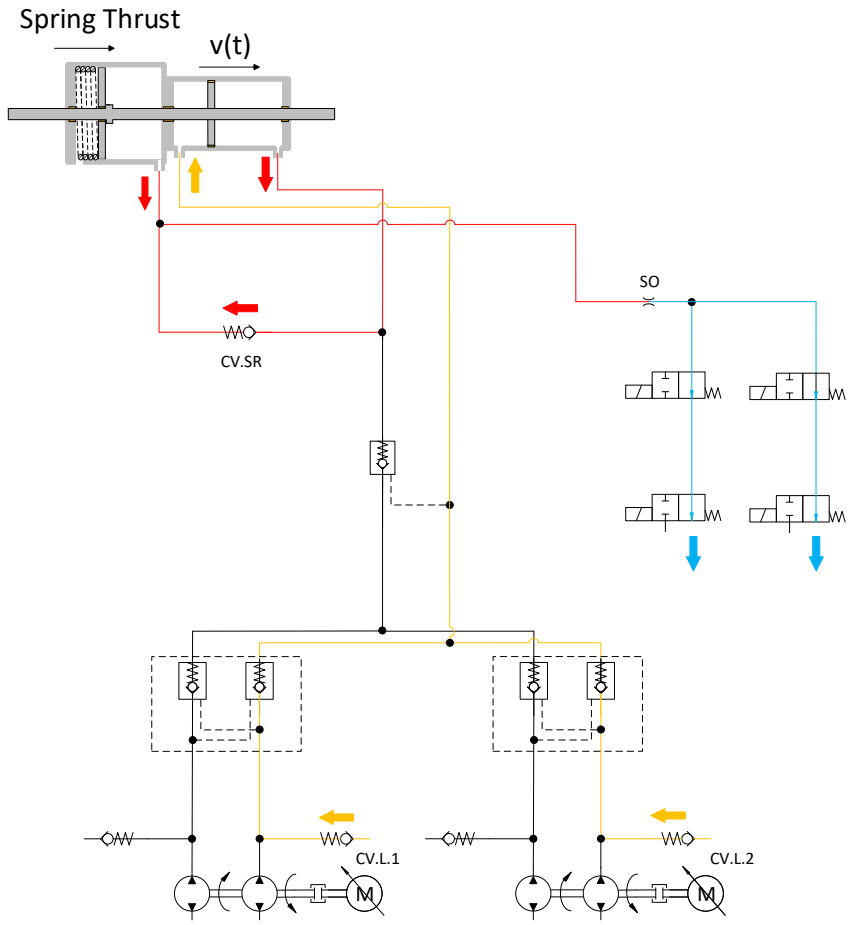

Source: Author.

As shown in Figure 3.6, during the safe-return function, the hydraulic fluid present in chambers A and C is pulled out through the safety block while chamber B is supplied by the check valves CV.L.1 and CV.L.2 Note that it is just needed one of the two parallel lines of the safety block to perform the safety function. The orifice SO pressure drop is responsible for guarantee a smooth return of the actuator.

3.3 SUBSEA VALVE ACTUATOR REQUIREMENTS

For submarine equipment installed in deep and ultra-deepwater, due to the difficulties of access, and consequently to the very high costs of intervention, it is necessary to guarantee a high mean time between failure (MTBF) for its components. This is because it is desirable to increase the availability of the system and reduce operating costs (OPEX) and possible loss of profit (Mashiba, 2010). For this reason, the qualification tests performed on subsea equipment are much more rigorous and extensive than the qualification tests applicable to surface equipment. Among the applicable standards specifications for subsea valve actuators, the performance requirements below can be highlighted (ISO 13628-4:2010) (ISO 10423:2009).

- The actuator force must be sufficient to execute the opening and closing of the subsea valve in its most severe conditions without exceeding 90 % of the hydraulic operating pressure. This requirement is used for all hydraulic actuators since they are designed for operating in a specific rated working pressure (RWP), which is provided by the surface hydraulic power unit (HPU). Once in the studied actuator design, the HPU keeps inside the SVA. This requirement could be reformulated from “90 % of the hydraulic operating pressure” to “90 % of the maximum hydraulic force”);
- The fail-safe system must be capable of move the valve/actuator to its safe position in the following scenarios:
  1. From 1 bar absolute to the maximum working pressure in the valve bore: In this case, the studied actuator is designed to operate gate valves with well pressures up to 10.000 psi (690 bar), then the safe return system must be capable of returning the valve to its totally closed position in all possible well manometric pressure ranges from 0 to 690 bar;
  2. Differential pressure across the valve bore sealing mechanism equal to the rated bore pressure at the time of operation: In standard operation conditions, the pressure differential across the valve is less than the well pressure because of the hydrostatic

pressure above the valve due to the column of fluid. Although, this is a conservative requirement, which aims to guarantee the performance of the fail-safe system in all possible scenarios;

3. External pressure on the valve/actuator assembly at the maximum water depth using seawater specific gravity of 1.03 (ISO 13628-4:2011 7.10.2.3.3 c): As it will be explained in the following chapters, the external hydrostatic pressure produces a force in the forward direction on the actuator, which must be overcome in the fail-safe operation;
4. No hydraulic assistance in the closing (opening) direction of the actuator other than hydrostatic pressure due to the operating depth: The fail-safe return device must be designed to be a passive system in order to guarantee its functionality independent of external influence;
5. A minimum additional pressure of 100 psi (6.9 bar) above the external hydrostatic pressure at maximum operating depth acting at the counter direction of the safe closing (opening) movement during the fail-safe function.

As stated by Ali *et al.* (1996), the standard backpressure of 100 psi (6.9 bar) required in the last item above (item 5) is applied for subsea hydraulic actuators in order to guarantee that this pressure will overcome the “Air Gap” (AG), which is the distance between the water surface and the HPU in the platform as illustrated in Figure 3.7.

Figure 3.7 - Illustrative image of an all hydraulic subsea valve actuation system

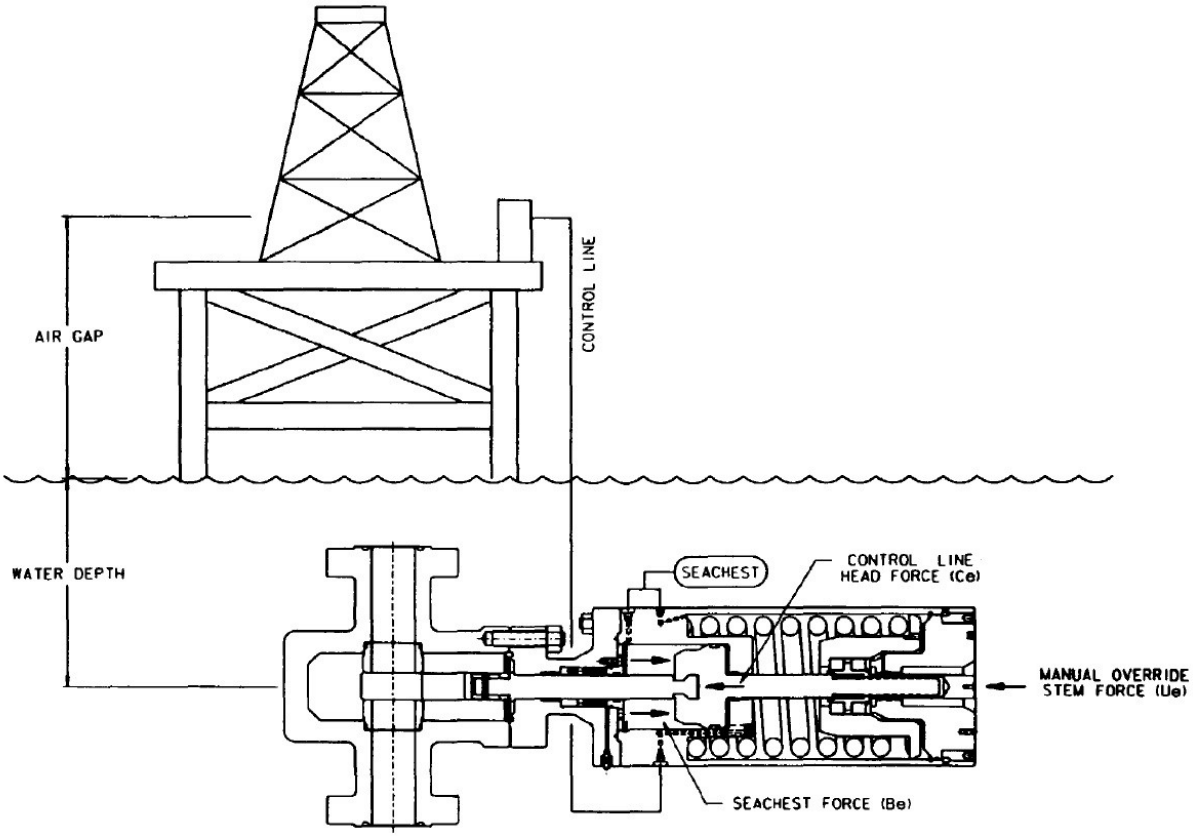

Source: Ali *et al*., 1996.

Because of, in the studied system, the hydraulic power unit (HPU) is an integral part of the EHA and, consequently, the hydraulic fluid does not need to go back from the subsea actuation system to the HPU reservoir at the platform, there would be no necessity to maintain this requirement for the studied actuator.

The following chapter presents how the EHA mathematical model has been developed as well as the gate valve model, which was used in the simulations to emulate a working load profile to the EHA after its validation process.

4 MATHEMATICAL MODEL

In this chapter, the main features of the EHA and gate valve mathematical models are characterized. Previous researches - namely Goularte (2018), Mashiba (2011) and Orth *et al.* (2018) – were used as primary references to the development of such models, where the software SIMSTER version 6.1 available by Bosch Rexroth (Bosch Rexroth US, 2014) was used as a modeling and simulation platform (see Appendix A).

4.1 MAIN FORCES OF THE SUBSEA VALVE ACTUATOR SYSTEM

As described in the previous chapters, the proposed SVA prototype is a subsystem designed to open and close 2 inches gauge gate valves of subsea trees and manifolds in depths up to 3000 meters. In order to do a better design of this system mathematical model, it is necessary to know, in the best possible way, all the forces involved in the process. Figure 4.1 illustrates the SVA cylinder and gate valve assembly and its main acting forces.

Figure 4.1 – Schematic overview of the forces involved in the Gate Valve/Actuator assembly.

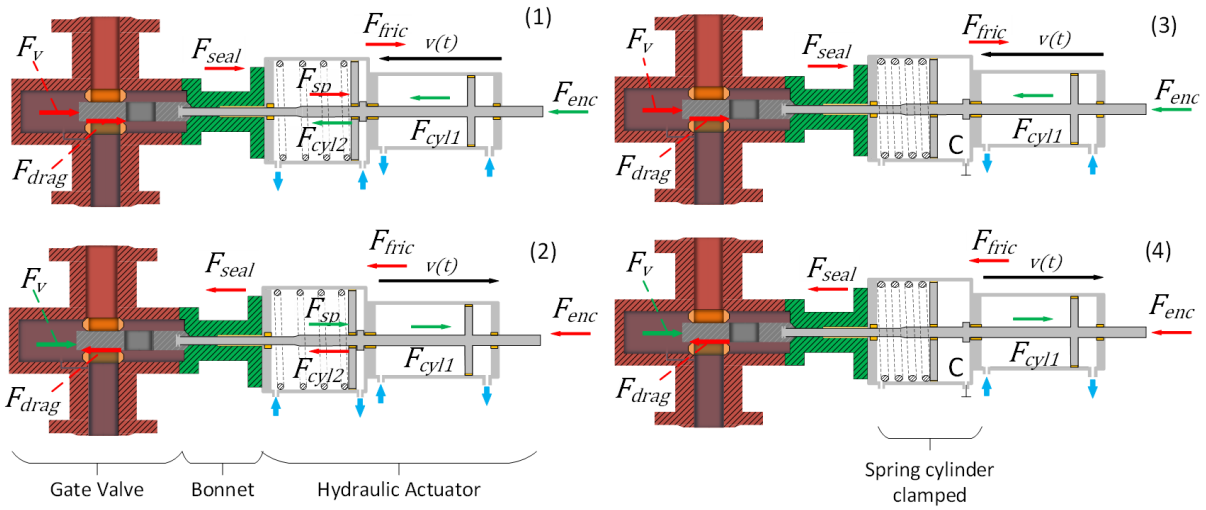

Source: Author.

Figure 4.1 (1) and (2) represent the main forces acting on the gate valve/actuator assembly during the opening and closing movement, if the ON-OFF safety valves are opened, allowing the flow rate between the spring cylinder chambers and the reservoir. In Figure 4.1 (3) and (4),

the safety valves are closed, blocking the flow rate between chamber C and reservoir, which eliminates the spring cylinder forces from the drive system perspective. Green arrows are the forces acting in the same direction of the movement, red arrows act in the opposite direction and blue arrows represent the flow rate direction. The forces mentioned in Figure 4.1 acting on the studied gate valve/actuator assembly are:

- Forces present on the actuator:
  - F_{enc} [N]: Enclosure force;
  - F_{cyl1} [N]:Main cylinder hydraulic force;
  - F_{cyl2} [N]:Spring cylinder hydraulic force;
  - F_{sp} [N]:Safe spring force;
  - F_{fric} [N]: Friction forces.

- Forces present on the Gate Valve and Bonnet:
  - F_v [N]:Force acting on the stem due to the valve internal pressure;
  - F_{drag} [N]:Friction force between the gate and seats of the valve;
  - F_{seal} [N]:Friction force due to the contact between the seals and the stem in the bonnet.

The forces mentioned above are better explained in the following sections.

4.1.1 Enclosure Force (F_{enc})

The hydraulic cylinder is submitted to the reservoir enclosure compensated pressure, which is equal to the subsea hydrostatic pressure plus an additional safety pressure (0.5 – 2bar). This enclosure pressure acts in the entire actuator surfaces minus the stem area. This interaction results in a force in the forward direction as described by

$$F_{enc} = p_{enc}.\frac{\pi}{4}.{d_{stem}}^2 \quad (1),$$

where p_{enc} [Pa] is the SVA enclosure pressure and d_{stem} [m] the gate valve stem diameter.

4.1.2 Hydraulic cylinder Forces

As described previously and can be observed in Figure 4.2, the studied actuator consists of two hydraulic cylinders, which can be divided in main cylinder and spring cylinder. The spring cylinder – together with its ON-OFF safety valves – is the element responsible for the safe-return function while the main cylinder has the purpose of moving the gate valve during standard operations.

On the spring cylinder, the connection between piston and rod allows the free movement of its piston in the actuator forward direction, which concedes to the system the possibility of close the chamber C with the ON-OFF safety valves and storage the spring's potential energy to perform the fail-safe function in emergencies. The forces acting in each cylinder are clarified in the following subsections.

Figure 4.2 – Four chambers hydraulic cylinder.

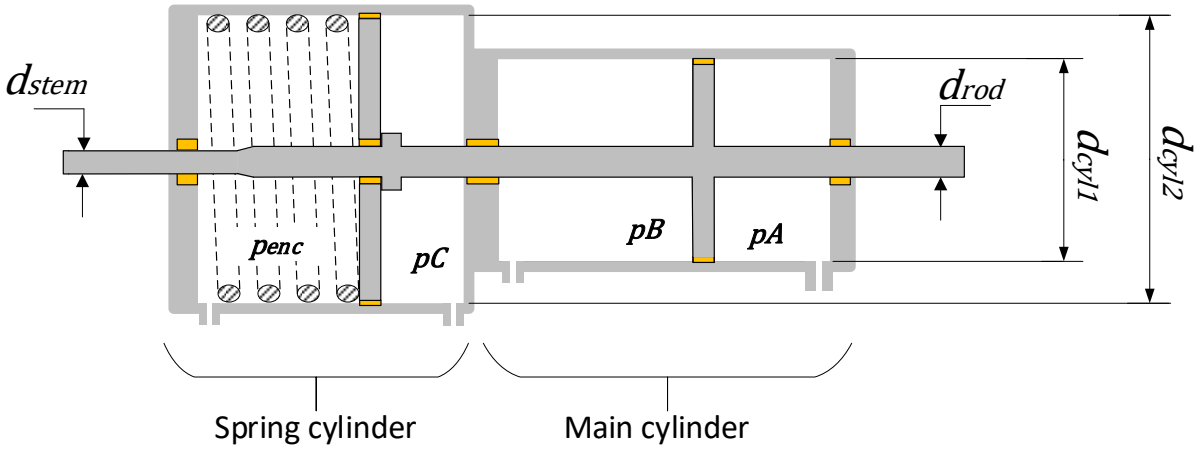

Source: Author

4.1.2.1 Main cylinder hydraulic force (F_{cyl1})

The main cylinder hydraulic force is dependent on its internal area and the pressure differential provided by the hydraulic power unit as can be observed by

$$F_{cyl1} = (p_A - p_B).\frac{\pi}{4}.({d_{cyl1}}^2 - {d_{rod}}^2) \quad (2),$$

where p_A and p_B [Pa] are, respectively, the pressures in the cylinder chamber A and B, d_{cyl1} [m] the main cylinder piston diameter and d_{rod} [m] the rod diameter.

4.1.2.2 Spring cylinder hydraulic force (F_{cyl2})

The spring cylinder hydraulic force is also a function of its internal area and pressure differential. Meanwhile, the chamber which contains the spring is connected to the reservoir, such that this force can be expressed by

$$F_{cyl2} = (p_C - p_{enc}).\frac{\pi}{4}.({d_{cyl2}}^2 - {d_{rod}}^2) \quad (3),$$

where: p_C [Pa] is the pressure in the cylinder chamber C and d_{cyl2} [m] the spring cylinder piston diameter.

4.1.2.3 Friction Forces Acting on the Cylinders (F_{fric})

Friction is one of the most critical aspects of hydraulic cylinders dynamic behavior. As reported by Yanada et al. (2014), friction may cause control errors, limit cycles, and poor performance of the system. Valdiero (2005) mentions that friction is a multifaceted nonlinear phenomenon that exhibits several nonlinear characteristics which are generally dependent on speed, temperature, the direction of movement, lubrication, and wear between surfaces, position and even the history of the movement. Conforming to Suisse (2005), due to dynamic seals used in hydraulic systems, the friction is mostly dependent on the applied pressure and seal installation forces.

On the hydraulic cylinders mathematical model, the resultant friction force represents the sum of all individual friction forces acting in the contacts between the cylinders seals with its piston and rod. This friction behavior on the Simster software is modeled as composed of four distinct forces, which are:

- Static friction (stiction): Occurs at zero speed and opposes to the movement with the same force (or torque) magnitude until a maximum value (Valdiero, 2005);

- Coulomb friction: Constant force opposed to the movement which occurs just in speeds different from zero and assumes that the friction does not depend on the magnitude of the speed (Costa *et al*., 2015);
- Viscous friction: Force opposed to the movement linearly proportional to the velocity (Valdiero, 2005);
- Stribeck friction: A non-linear friction behavior, which occurs in low-velocity operational sections, which produces a smooth transition from static to dynamic friction (Costa *et al*., 2015).

Another parameter implemented in the Simster friction mathematical model is the transitional velocity (v_t), which is the velocity where the friction state changes from mixed friction (all mentioned forces) to 'viscous plus coulomb' friction. The system resultant friction behavior is then the combination of these different parameters, as illustrated in Figure 4.3.

Figure 4.3 – Representation of the Simster friction model characteristics.

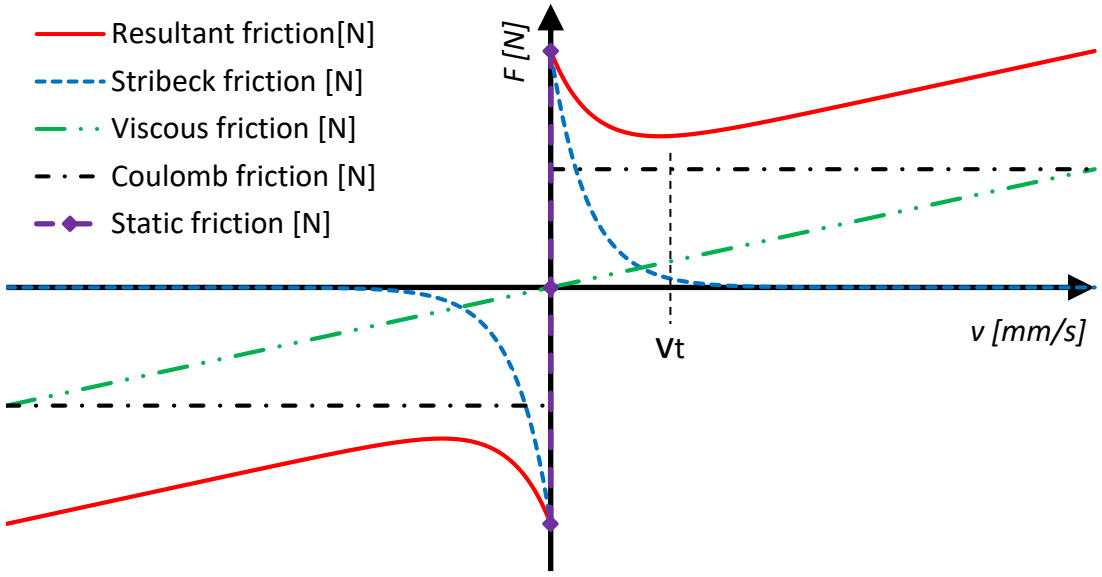

Source: Adapted from the Simster Library.

The resultant friction force curve, shown in Figure 4.3, is consistent with the commonly applied curves to represent steady-state-based models used to represent the friction forces behavior in hydraulic cylinders, namely Costa *et al*. (2015) and Valdiero (2005).

4.1.3 Fail-Safe Spring Force (F_{sp})

During regular operation, the spring force shall not be observed by the system, since the spring shall remain compressed and be released just in emergencies. However, for the compression operation and in emergencies the spring force observed by the hydraulic system is expressed by

$$F_{sp} = F_{spo} + K_{sp}.x_{sp} \quad (4),$$

where F_{spo} [N] is the spring pre-load force, K_{sp} [N/m] the spring elastic coefficient and x_{sp} [m] the spring cylinder piston position.

4.1.4 Drag Force (F_{drag}): Friction force between the gate and seats of the valve

The drag force is the main component of all friction forces of the valve-actuator assembly, being the result of the working pressure action of the valve on the sealing diameter of the gate against the downstream seat. For this force model development, the same model presented by Goularte (2018) was used, with just small peculiarities. This force is directly proportional to the pressure differential established between upstream and downstream of the valve as can be observed on

$$F_{drag}(x) = (A_{VG0} - A_{VG}(x)).(p_{WELL} - p_d(x)).\mu \quad (5),$$

where A_{VG0} [m^2] is the maximum area of action of the pressure differential through the gate valve, $A_{VG}(x)$ [m^2] the opening area of the valve, p_{WELL} [Pa] the wellbore pressure; $p_d(x)$ [Pa] the pressure downstream the flow rate direction and μ [dimensionless] the friction coefficient between the gate valve and its seats.

According to Wang and Kalsi (1991), the active pressure area of a gate valve depends on the effective sealing diameter "d_s" which is an imaginary diameter that seals the upstream high pressure from leaking into the downstream seat inside diameter. The sealing diameter, on the other hand, depends on many factors such as disc stiffness, seat edges, and uneven seat contact. However, Wang and Kalsi (1991) states that the sealing diameter can be adequately estimated through

$$d_s = \frac{1}{2}.(d_{ID} + d_{OD})$$ (6), used when the seat is considered narrow,

or

$$d_s = d_{ID} + \frac{1}{3}.(d_{OD} - d_{ID})$$ (7), used to when the seat is considered wide,

where d_{ID} [m] is the seat inner diameter and d_{OD} [m] the seat outer diameter.

For gate valve mathematical model, for conservative reasons, it was chosen to be used the equation 6 to estimate the effective sealing diameter, which will result in a higher normal force and consequently a more critical situation.

Then, with the sealing diameter "d_s", the "A_{VG0}" can be calculated with

$$A_{VG0} = \frac{\pi}{4}.{d_s}^2$$ (8).

The opening area of the valve, in its turn, is a function of the valve position and its diameter and can be calculated through

$$A_{VG}(x) = R^2.\left\{cos^{-1}\left[1 - \frac{h(x)}{25} + \frac{h(x)}{5000}\right] - sin\left(cos^{-1}\left[1 - \frac{h(x)}{25} + \frac{h(x)}{5000}\right]\right)\right\}$$ (9),

and

$$\mathrm{h}(x) = \begin{cases} 0, & if\ 0 \le x < x_{co} \\ \frac{x - x_{co}}{x_{tot} - x_{co}}.100\%, & if\ x_{co} \le x \le x_{tot} \end{cases}$$ (10),

where $h(x)$ [%] is the opening percentage of the valve, x [m] the position of the gate valve, x_{co} [m] the crack open/close position and x_{tot} [m] the maximum valve stroke. Figure 4.4 illustrates the relation between the valve position and its opening passage area.

Figure 4.4 – Representation of a gate valve passage area through the gate's position.

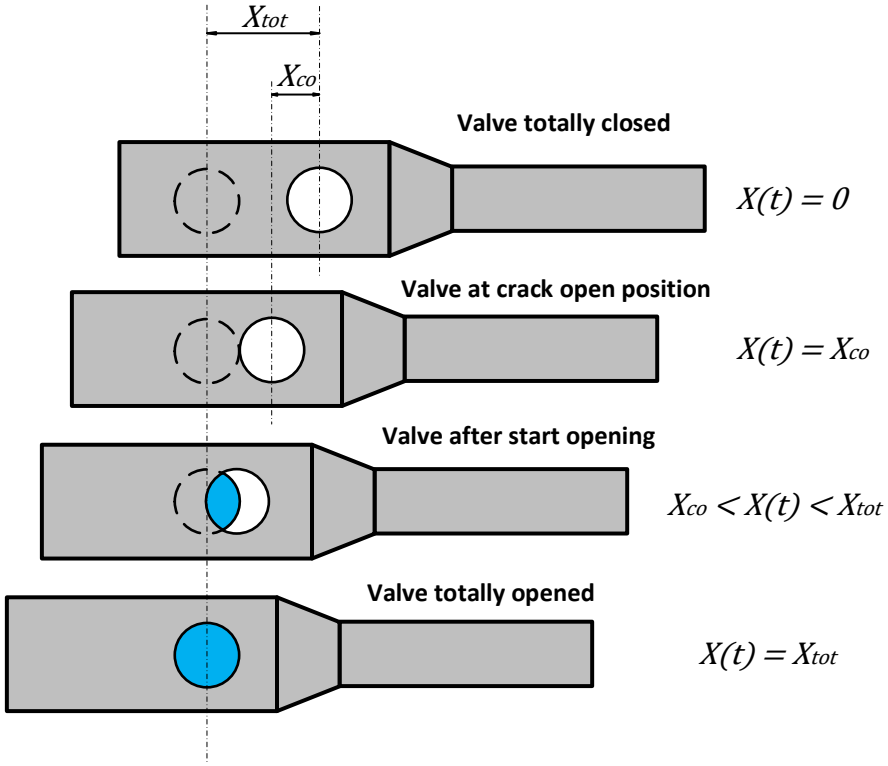

Source: Author.

The pressure at the downstream of the gate valve flow rate direction ($p_d(x)$), which is used to calculate the pressure drop against the gate, has two different behaviors, one before and other after the crack position, as can be seen in

$$p_d(x) = \begin{cases} p_{sep} + \rho_{pf}.g.(LDA+AG), if\ 0<x<x_{co} \\ p_{WELL} - K_{(x)}.\rho_{pf}.\frac{v_{oil(x)}{}^2}{2}, if\ x_{co}<x<x_{tot} \end{cases} \quad (11),$$

where p_{sep} [Pa] is the pressure on the surface oil separator, ρ_{pf} [kg/m^3] the specific mass of the production fluid, g [m/s^2] the gravity acceleration, LDA [m] the height of water column above valve, AG [m] the distance between the water surface and the surface separator, also called air gap, $K(x)$ [dimensionless] the flow rate resistance coefficient and $v_{oil}(x)$ [m/s] the production fluid velocity.

While open, the pressure downstream the valve is dependent on the valve's flow rate resistance coefficient "$K(x)$", which as stated in Mashiba (2010), can be estimated according to

$$K_{(x)} = 1984.e^{-0,735.h(x)^{0,545}} + 0,1 \quad (12).$$

Applying the Bernoulli's equation to the gate valve flow rate, the oil velocity can be expressed by

$$v_{oil}(x) = \begin{cases} 0, & if\ 0<x<x_{co} \\ \sqrt{\frac{2.(p_{WELL} - p_{sep}) - \rho_{pf}.g.(LDA+AG)}{\rho_{pf}.(1 + K_{(x)} + f_{(x)}.\frac{L}{D})}}, & if\ x_{co}<x<x_{tot} \end{cases} \quad (13),$$

where $f(x)$ [dimensionless] is the friction coefficient, L [m] the length of the oil pipe and D [m] the production fluid pipe diameter.

The friction coefficient "$f(x)$", in its turn, can be found through the Colebrook-White equation as in

$$\frac{1}{\sqrt{f_{(x)}}} = -2.log\left(\frac{\varepsilon}{3,7.D} + \frac{2,51}{v_{oil(x)}.D.\sqrt{f_{(x)}}}\right) \quad (14).$$

4.1.5 Friction force between bonnet seals and stem (F_{seal})

According to Mashida (2010), the bonnet sealing is composed of two unidirectional elements mounted in opposite directions in order to ensure the bidirectionality of the system as a whole. This sealing is responsible for completely isolating the valve body cavity, which is subjected to the well pressure, from the actuator spring chamber, subjected to the hydrostatic pressure of the compensation system.

Although, the friction between the seals and the SVA stem in the bonnet is a minimal force when compared to the other forces involved in the gate valve. For this reason, this force commonly has less importance in design calculations (Ali, 1996). Therefore, for the gate valve modeling in this research, the sealing force was considered a constant friction force.

4.1.6 Force acting on the stem due to the valve internal pressure (F_y)

Opposing the F_{enc}, this force is caused by the gate valve internal pressure acting in the stem area instead of the reservoir pressure.

As mentioned by Mashiba (2010) and Goularte (2018), the sealing used in gate valves are mounted in a way that allows the well pressure to inlet in the valve housing. Thus, it can be considered that the gate valve internal pressure is the same as in the wellbore. The "F_y" is then an expulsion force acting on the gate which is dependent on the well pressure and the stem area as stated in

$$F_y = \frac{\pi}{4} . {d_{stem}}^2 . p_{WELL} \quad (15).$$

4.2 ELECTRO-HYDRAULIC SYSTEM COMPONENTS

This subsection introduces the modeling of the components present in the electro-hydrostatic actuator system. These models are contained in the Simster software library, available by Bosch Rexroth, a partner in this research. The system modeled on Simster is simplified as not having any redundancies, as illustrated in Figure 4.5.

Figure 4.5 - Hydraulic diagram of the EHA modeled on Simster.

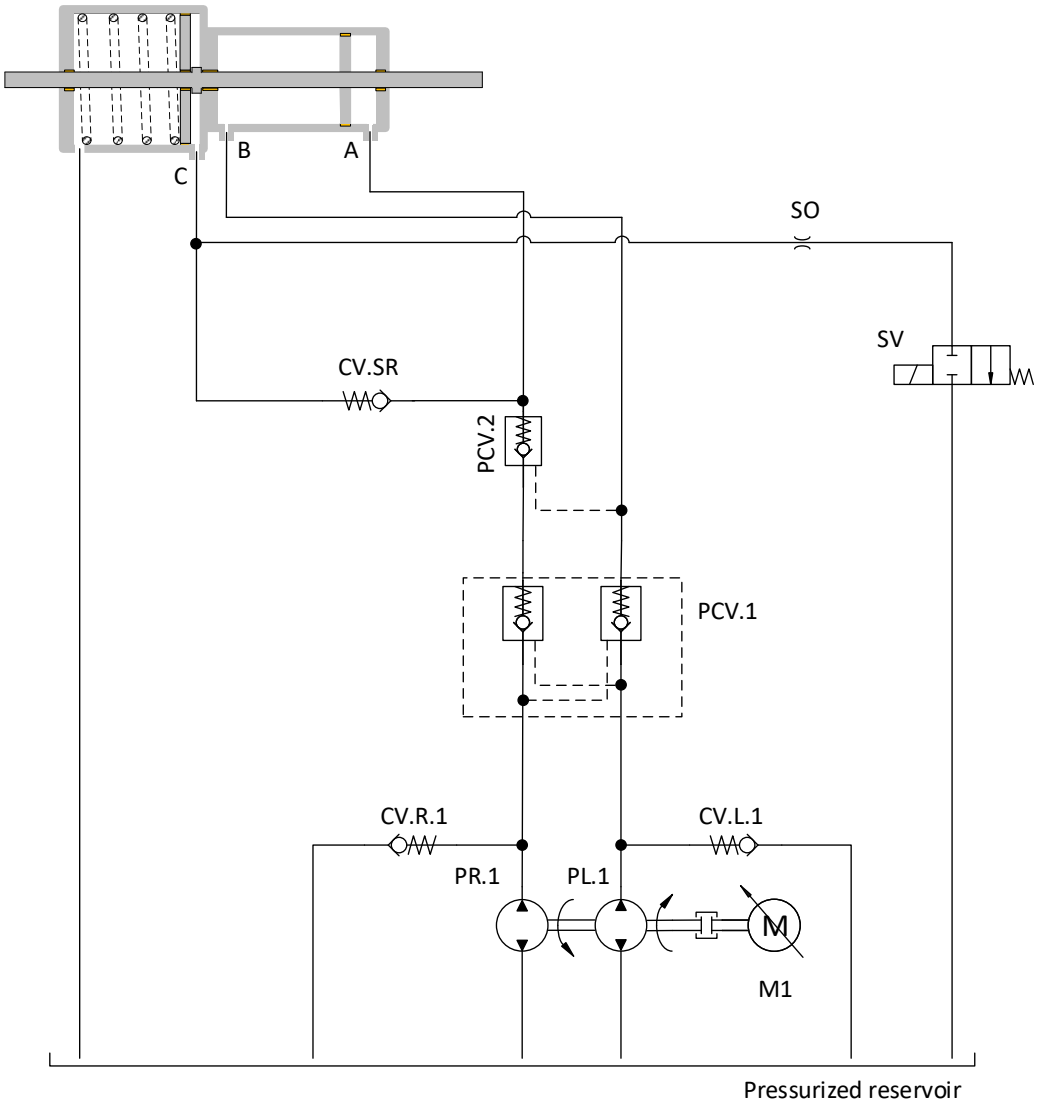

Source: Author

4.2.1 Hydraulic Cylinder

The four-chamber hydraulic cylinder modeling on the Simster software is made using two different cylinder models with an elastic linear contact model that allows the free movement of the spring cylinder in the forward direction as can be observed in Figure 4.6.

Figure 4.6 - Hydraulic cylinder model.

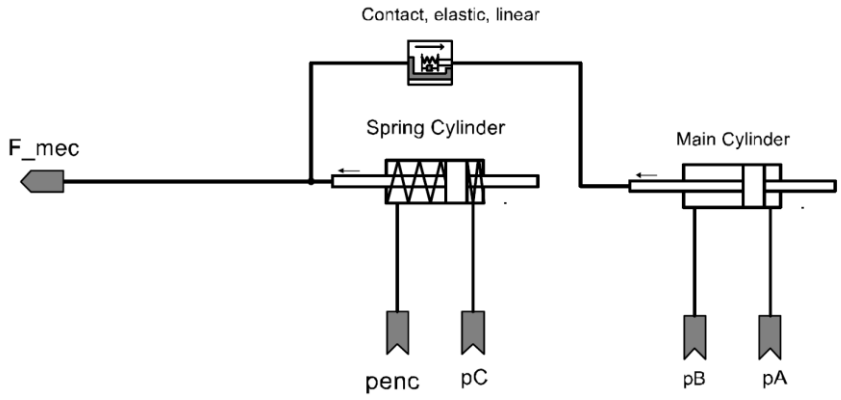

Source: Author.

The cylinder constructive parameters are presented in Table 4.1.

Table 4.1: Simster model hydraulic cylinder constructive parameters.

Parameter	Symbol	Value	Unit
Main cylinder piston diameter	d_{cyl1}	d_1	m
Rod diameter	d_{rod}	d_2	m
Main cylinder mass	m_1	M_1	kg
Main cylinder static friction	Fat_{est1}	F_1	N
Main cylinder Coulomb friction	Fat_{co1}	F_2	N
Main cylinder viscous coefficient	B_1	b_1	N.s/m
Actuator stroke	x_{tot}	x_1	m
Spring cylinder piston diameter	d_{cyl2}	d_3	m
Spring cylinder piston mass	m_2	M_2	kg
Spring preload force	F_{spo}	F_3	N
Spring elastic constant	K_{sp}	K_1	N/m
Spring cylinder static friction	Fat_{est2}	F_4	N
Spring cylinder running friction	Fat_{co2}	F_5	N
Spring cylinder viscous coefficient	B_2	b_2	N.s/m

Source: Author.

4.2.2 Check valve

Check valves are unidirectional valves customarily used to control the fluid flow orientation, allowing free flow in one direction and blocking in the opposite. The valve remains closed against flow until the pressure at its inlet creates sufficient force to overcome the spring force (Linsingen & De Negri, 2011). Figure 4.7 shows a schematic and a functional drawing of the check valve used in the system.

Figure 4.7 - Schematic and functional drawing of a check valve.

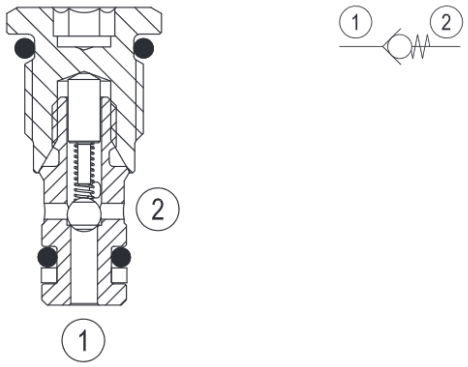

Source: Bosch Rexroth AG (2017).

The check valve Simster model behavior is modeled as a first-order function divided into three phases, as described below:

A. Phase 1 - Valve closed: The check valve remains closed as long as its pressure differential (Δp_{cv}) is smaller than its opening pressure (p_o);
B. Phase 2 - This region is modeled as a linear area. The valve is opening, and the ball moves out of the seat and acts against the spring. This phase lasts until the valve is totally opened. The parameter for describing the linear relation between the pressure difference and the flow rate is the Gradient Flow-pressure ($G_{qv/p}$), which is the angular coefficient of the flow rate versus pressure drop curve in this region;
C. Phase 3 - Valve fully opened: Once the check valve is fully opened, the behavior is modeled using the orifice equation. This behavior begins once the linear curve of phase 2 encounter the orifice behavior curve. The two parameters Pressure drop per control

edge (Δp_{max}) and Flow rate at pressure drop Δp (qv_{max}) are available for the parameterization of the check valve flow rate gain (Kv_{cv}).

Mathematically, the flow rate of the check valve Simster model can be calculated through

$$qv_{cv}(\Delta p) = \begin{cases} 0 & ,for\ \Delta p < p_o \\ G_{qv/p}.\Delta p & ,for\ p_o \leq \Delta p < (\frac{Kv_{cv}}{G_{qv/p}})^2 \\ Kv_{cv}.\sqrt{\Delta p} & ,for\ \Delta p \geq (\frac{Kv_{cv}}{G_{qv/p}})^2 \end{cases} \quad (16),$$

and

$$Kv_{cv} = \frac{qv_n}{\sqrt{\Delta p_n}} \quad (17).$$

The characteristic parameters of the check valve used in the prototype are presented in Table 4.2.

Table 4.2: Simster check valve model parameters

Parameter	Symbol	Value	Unit
Opening pressure	p_o	0.01	bar
Gradient Flow-pressure	$G_{qv/p}$	20	L/min/bar
Pressure drop per control edge	Δp_{max}	7	bar
Flow rate at pressure drop	qv_{max}	18	L/min
Delay time	T_l	10	ms

Source: Bosch Rexroth AG (2017).

Figure 4.8 (a) shows the Bosch Rexroth available datasheet curve of pressure versus flow rate of the applied check valve from where the parameters in Table 4.2 were extracted and Figure 4.8 (b) shows the same curve of its Simster model used in the simulations.

Figure 4.8 - Operational curves of the datasheet (a) and simulation model (b) of the used check valve.

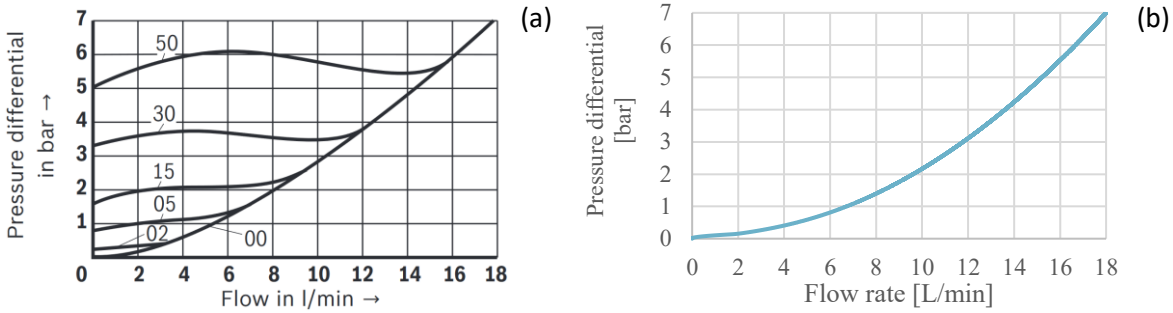

Source: (a) Bosch Rexroth AG (2017) and (b) Author.

4.2.3 Pilot Operated Check valve

The pilot operated check valve, illustrated in Figure 4.9, performs the same function of the simple check valve with the addition of a pilot which allows a reverse flow rate when triggered (Linsingen & De Negri., 2011). Figure 4.9 shows a schematic and a functional drawing of the pilot operated check valve used in the system.

Figure 4.9 - Schematic and functional drawing of a pilot operated check valve.

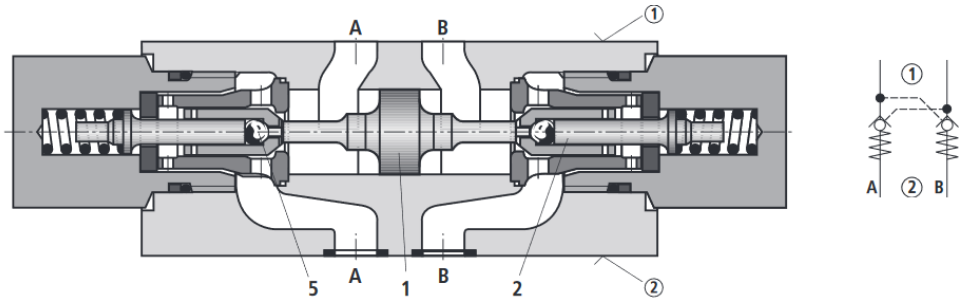

Source: Bosch Rexroth AG (2010).

The Simster pilot operated check valve sub-model – icon is shown in Figure 4.10 (a) - was used elaborate the valves PCV 1 and PVC 2 modeling. The parameters required by the model were obtained through the characteristic curve of these valves shown in Figure 4.10 (b). Valve PCV 1 is modeled according to curve 1, while PCV 2 is according to curve 2.

Figure 4.10 - Pilot operated check valve sub-model (a) and its qv-Δp characteristic curves (b).

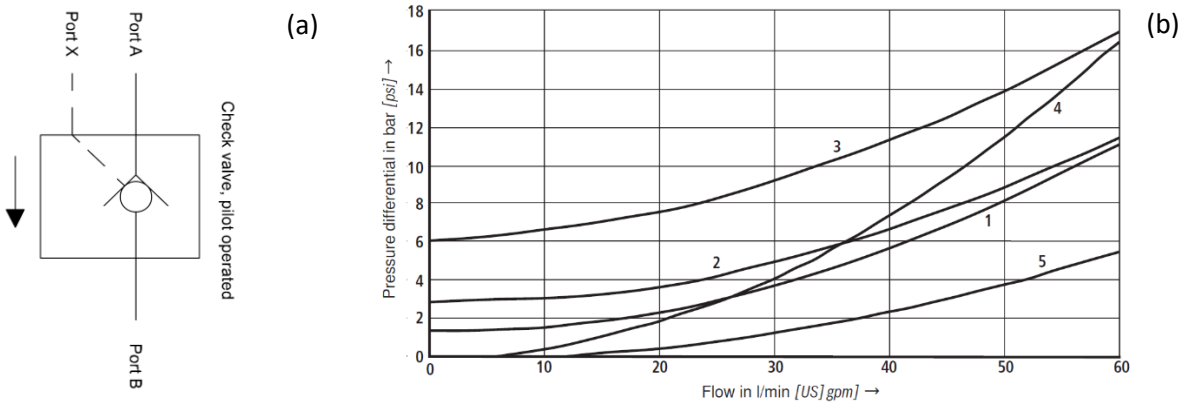

Shorce: (a) Simster and (b) Bosch Rexroth AG (2010).

The Simster sub-model of the pilot operated check valve works as a first-order system based primarily on two equations, a pressures sum balance and a flow equation, the first is employed to define the valve dimensionless opening ratio - ranges from 0 to 1 - and the second characterizes its flow rate. The opening ratio of the valve is calculated through

$For\ p_{A}{}^{pcv} \geq p_{B}{}^{pcv}$

$$u_{pcv} = \begin{cases} 0,\ p_{A}{}^{pcv} < p_{0}{}^{pcv} \\ \frac{(p_{A}{}^{pcv} - p_{B}{}^{pcv} - p_{0}{}^{pcv})}{dp_{pcv}},\ p_{0}{}^{pcv} \leq p_{A}{}^{pcv} \leq (p_{B}{}^{pcv} + p_{0}{}^{pcv} + dp_{pcv}) \\ 1,\ p_{A}{}^{pcv} > (p_{B}{}^{pcv} + p_{0}{}^{pcv} + dp_{pcv}) \end{cases} \quad (18),$$

$For\ p_{A}{}^{pcv} < p_{B}{}^{pcv}$

$$u_{pcv} = \begin{cases} 0, p_{x}{}^{pcv} < \left(\frac{p_{B}{}^{pcv} + p_{0}{}^{pcv} - p_{A}{}^{pcv}}{R_{pcv}} + p_{A}{}^{pcv}\right) \\ \frac{[(p_{x}{}^{pcv} - p_{A}{}^{pcv}).R_{pcv} + p_{A}{}^{pcv} - p_{B}{}^{pcv} - p_{0}{}^{pcv}]}{dp_{pcv}}, \left(\frac{p_{B}{}^{pcv} + p_{0}{}^{pcv} - p_{A}{}^{pcv}}{R_{pcv}} + p_{A}{}^{pcv}\right) \leq p_{x}{}^{pcv} \leq \left(\frac{dp_{pcv} + p_{B}{}^{pcv} + p_{0}{}^{pcv} + p_{A}{}^{pcv}.(R_{pcv} - 1)}{R_{pcv}}\right) \\ 1, p_{x}{}^{pcv} > \left(\frac{dp_{pcv} + p_{B}{}^{pcv} + p_{0}{}^{pcv} + p_{A}{}^{pcv}.(R_{pcv} - 1)}{R_{pcv}}\right) \end{cases}$$

(19),

where u_{pcv} [dimensionless] is the opening ratio of the valve, $p_{A}{}^{pcv}$, $p_{B}{}^{pcv}$ and $p_{x}{}^{pcv}$ [Pa] are respectively the pressures in port A, B and x of the valve, $p_{0}{}^{pcv}$ [Pa] the opening pressure

(referring to spring preload), R_{pcv} [dimensionless] the pilot area ratio and dp_{pcv} [bar] the valve effective spring rate.

The valve effective spring rate "dp_{pcv}", in its turn, is a parameter dependent on the flow rate at a defined pressure drop "qv_{max}" [m^3/s] and the flow rate – pressure gradient "$G_{qv/p}$" as expressed by

$$dp = \frac{qv_{max}}{G_{qv/p}} \quad (20),$$

and then, the pilot operated check valve flow rate can be calculated through

$$qv_{pcv} = sgn(p_{A^{pcv}} - p_{B^{pcv}}).u_{pcv}.\frac{qv_{max}}{\sqrt{\Delta p_{max}}}.\sqrt{|p_{A^{pcv}} - p_{B^{pcv}}|} \quad (21),$$

The adopted parameters for the Simster piloted operated check valve models are present in table 4.3.

Table 4.3: Simster pilot operated check valve model parameters.

Parameter	Symbol	PCV 1 Value	PCV 2 Value	Unit
Opening pressure	$p_0 pcv$	1.5	3	bar
Pressure drop per control edge	Δp_{max}	2.3	3.6	bar
Flow rate at pressure drop	qv_{max}	20	20	L/min
Gradient Flow-pressure	$G_{qv/p}$	100	100	L/min/bar
Delay time	$T1$	10	10	ms
Area Ratio Ax/Aa	R_{pcv}	12.5	12.5	-

Source: Bosch Rexroth AG (2010).

The resultant flow rate – pressure drop characteristic curve of the pilot check valve models can be seen in Figure 4.11, where the "A to B" represents the free flow direction and "B to A" – opening ratio equal to one – is the reverse flow rate.

Figure 4.11 - Flow rate – pressure drop characteristic curves of the pilot operated check valve.

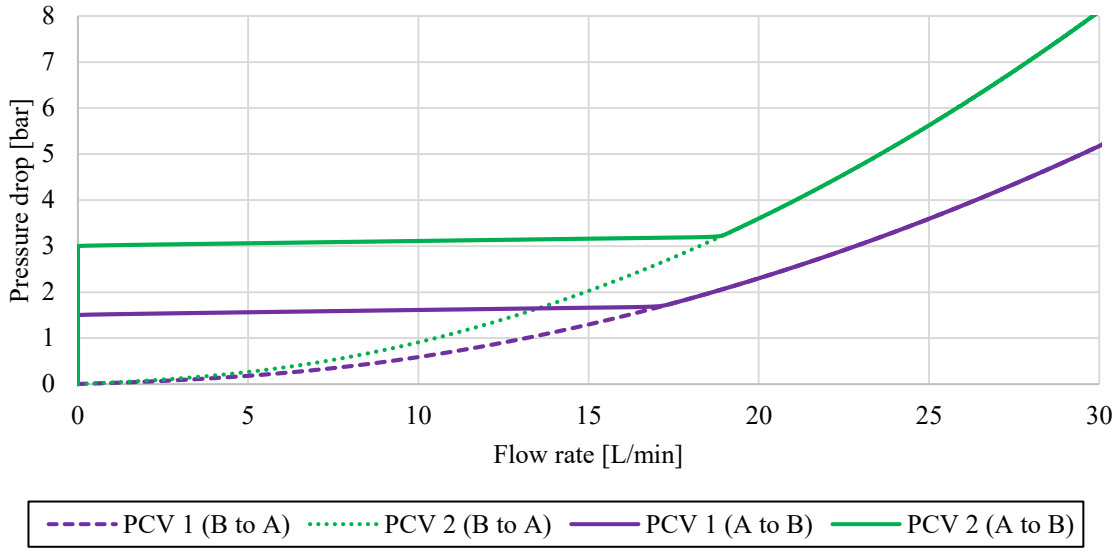

Source: Author

4.2.4 Hydraulic Pumps

As stated by Linsingen (2013), hydraulic pumps are the components responsible for converting rotational mechanical energy into hydraulic energy in a primary conversion unit, the hydraulic energy is then transmitted by hydraulic lines to a secondary conversion unit where it is converted back into mechanical energy.

Hydraulic pumps commonly have volumetric losses due to its internal leakage, which occurs because of the existence of clearances between moving parts, pressure differences, angular speed, and also cavitation and aeration (Linsingen, 2013). Internal leakage tends to increase in proportion to the increase in the pressure difference imposed on the pump, but only at lower rotations the dependence of the volumetric efficiency with the rotation becomes apparent, since the flow generated by the pump at low rotations is lower, but its internal losses resulting from the pressure difference continue to be equal to the losses generated in higher rotations (Lana, 2005). Therefore, the volumetric efficiency (η_v) of a hydraulic pump can be expressed as

$$\eta_v = \frac{qv_{tp} - qv_{leak}}{qv_{tp}} \quad (22),$$

where qv_{tp} [m^3/s] is the pump theoretical flow rate and qv_{leak} [m^3/s] the pump internal leakage flow rate.

The pump theoretical flow rate is expressed by

$$qv_{tp} = D_p.\dot{\theta}p \quad (23),$$

in which D_p [m^3/rad] is the pump displacement and $\dot{\theta}p$ [rad/s] the pump angular velocity.

As an assumption for the pump modeling, the internal clearances were considered as an orifice, where the flow rate (qv_{leak}) is a function of the pump pressure differential as can be observed in

$$qv_{leak} = Kv_{leak}.\sqrt{\Delta p_p} \quad (24),$$

where Kv_{leak} [$m^3/s.Pa^{0.5}$] is the internal leakage coefficient and Δp_p [Pa] the pressure differential through the pump.

In hydraulic pumps, the most significant mechanical losses occur to the internal friction between its moving parts. The friction torque can be branched into torque due to mechanical friction, the torque due to viscous fluid friction and torque due to the friction generated by the pump seals (Lana, 2005). The sum of these three torques can be expressed as a friction torque so that the torque required by the pump (T_p) can be calculated by

$$T_p = J_p.\ddot{\theta}p + T_{tp} + T_f \quad (25),$$

where J_p [$kg.m^2$] is the pump moment of inertia, $\ddot{\theta}_p$ [rad/s^2] the pump angular acceleration, T_{tp} [Nm] the pump theoretical torque and T_f [Nm] the Pump friction torque.

The pump theoretical torque is calculated through

$$T_{tp} = D_p.\Delta p_p \quad (26).$$

The ratio, in steady state, between the theoretical and effective required torque by the hydraulic pump is named mechanical efficiency (η_m), expressed by

$$\eta_m = \frac{T_{tp}}{T_{tp} + T_f} \quad (27).$$

As the pressure differential through the pump increases, the leakage between its internal clearances also lubricates the contact between the moving parts, which helps to decrease the friction. Then, the pump mechanical efficiency tends to increase as the pressure differential grows.

The product between volumetric and mechanical efficiency is the pump global efficiency (η_g) which is also the ratio between the useful power (P_u) provided by the pump and its required power (P_r) as demonstrated in Equation 28.

$$\eta_g = \eta_v . \eta_m = \frac{P_u}{P_r} \quad (28).$$

In order to obtain a more representative mathematical model of the hydraulic power unit, the results presented by Zalavadiya (2018) – where an electric motor, transmission and pumps assembly, of the same kind as in the studied prototype, was tested under several velocities and pressure ranges, and its results presented in form of volumetric and mechanical efficiency – were modeled in the form of internal leakage coefficient and mechanical efficiency.

The internal flow rate coefficient (Kv_{leak}) [$m^3/s/Pa^{0.5}$] of the internal gear pump was then modeled according to a curve that better represented the found results. The resultant function is dependent on the pressure differential against the same as presented in

$$Kv_{leak} = A_{\eta v} . \Delta p_p + B_{\eta v} \quad (29).$$

For the mechanical efficiency (η_m) [dimensionless], both pump and gear transmission mechanical losses coefficient were simplified as just one component which the mechanical efficiency is dependent of the pump pressure differential as stated in

$$\eta_m = A_{\eta m} . {\Delta p_p}^2 + B_{\eta m} . \Delta p_p + C_{\eta m} \quad (30).$$

The resultant Simster gear transmission – pump sub-model structure is presented in Figure 4.12.

Figure 4.12 - Simster model of the gear and pump assembly

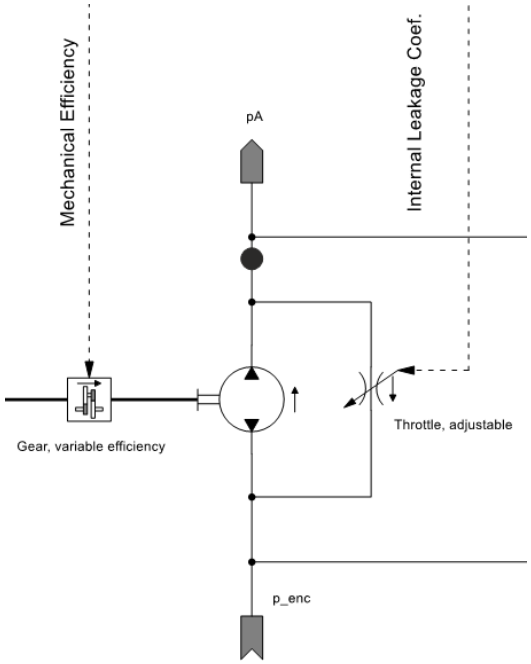

Source: Author.

With the developed model, the conditions of the same test as described in Zalavadiya (2018) were performed on Simster simulations. The comparison between the simulation and experimental results can be observed in Figures 4.13 and 4.14, where the abscissae axis represents the ratio of the pump angular velocity by the maximum tested velocity ($\omega_p/\omega_p max$), the ordinates axis are respectively the volumetric and global efficiency and each curve is operational differential pressure imposed to the pump, also represented as a ratio.

Figure 4.13 - Comparison between Simster simulation and experimental results: Volumetric efficiency of the external gear pump under different ranges of angular velocities and pressures.

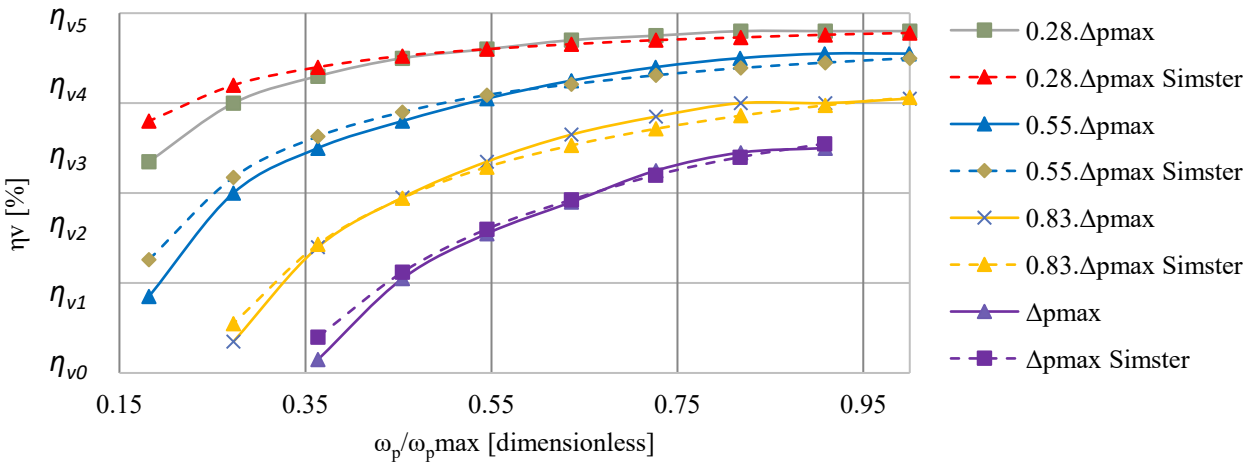

Source: Author.

Figure 4.14 - Comparison between Simster simulation and experimental results: Global efficiency of the external gear pump under different ranges of angular velocities and pressures.

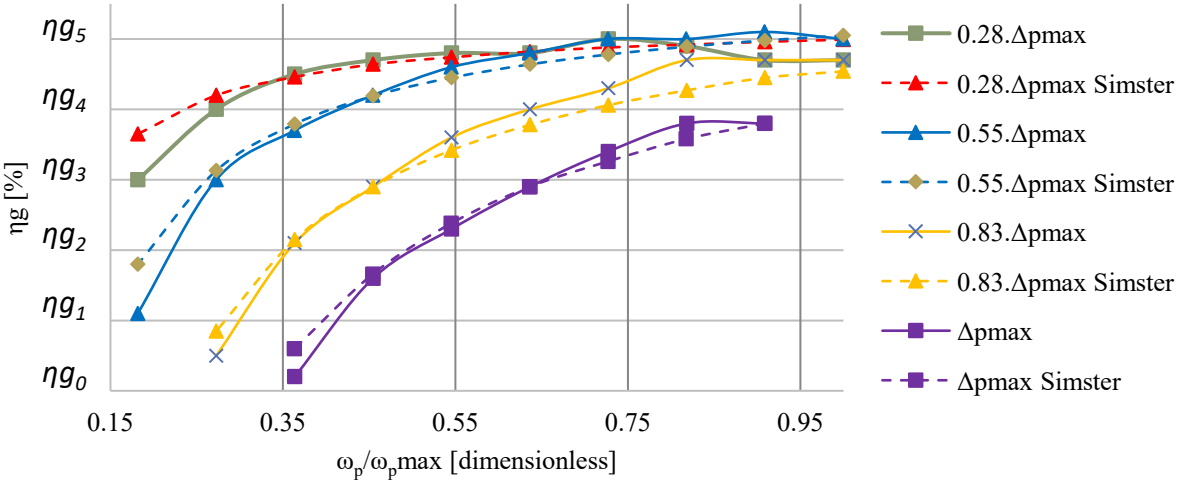

Source: Author.

As can be observed in Figures 4.13 and 4.14, the gear transmission and pumps assembly mathematical model showed good adherence to the experimental results presented in Zalavadiya (2018). The other adopted parameters for the Simster gear transmission and hydraulic pumps sub-models are present in table 4.5.

Table 4.4: Simster gear transmission and hydraulic pumps sub-model parameters.

Parameter	Symbol	Value	Unit
Displacement	D_p	V_1	cm^3/rot
Moment of Inertia	J_p	J_1	$Kg.m^2$
Transmission Ratio	R_T	$n_2 : n_1$	-

Source: Author.

4.2.5 Reservoir

In the EHA, all the hydraulic components are submerged in the reservoir, which is pressurized by a pressure compensation mechanism as represented in Figure 4.15.

Figure 4.15 - Compensation system representation.

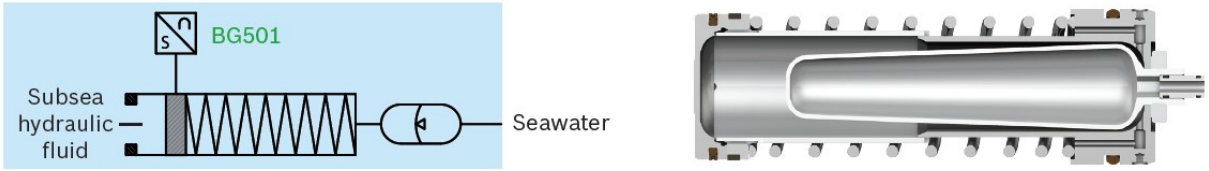

Source: Bosch Rexroth.

On the simulations, the reservoir was modeled as a source of constant pressure "p_{enc}" which is a function of the water depth "LDA" as in

$$p_{enc} = \rho_{SW}.g.LDA + p_{rs0} \quad (31),$$

where ρ_{SW} [kg/m^3] is the sea water specific density, g [m/s^2] the gravity acceleration, LDA [m] the water depth of installation of the equipment and p_{rs0} [Pa] the additional reservoir pressure provided by the compensator spring.

The reservoir parameters can be seen in Table 4.6.

Table 4.5: Compensated reservoir parameters.

Parameter	Symbol	Value	Unit
Sea water specific density	ρ_{SW}	1030	kg/m^3
Gravity acceleration	g	9.81	m/s^2
Additional reservoir pressure	p_{rs0}	$2x10^5$	Pa

Source: Author

4.2.6 Electric Motor

The electric motor used in the EHA is a brushless DC motor (BLDC motor), same as used in Goularte (2018) and Zalavadiya (2018), also defined as an electronically commuted motor which does not have brushes. This technology offers many advantages in comparison with brushed DC motors, such as increased speed vs. torque efficiency, longer life (as no brushes are used), noiseless operation, and increased efficiency in converting electrical power to mechanical power (HANSELMAN, 2011) (TEXAS INSTRUMENTS, 2011).

As presented by Goularte (2018) and Zalavadiya (2018), the angular velocity of the motor can be controlled by the variation of the supplied electric voltage (U_{SM}), described by

$$U_{SM} = K_e.\dot{\theta}_{SM} + R_{SM}.i_{SM} + L_{SM}.\frac{di_{SM}}{dt} \quad (32),$$

where K_e [V.s/rad] is the back electromotive force constant, $\dot{\theta}_{SM}$ [rad/s] the angular velocity of the electric motor, R_{SM} [Ω] the electrical resistance, i_{SM} [A] the electrical current and L_{SM} [H] the electrical inductance.

The electrical torque (T_e) is determined by

$$T_e = K_t.i_{SM} \quad (33),$$

where K_t [Nm/A] is the electrical motor torque constant.

Therefore, supported by the equation of the movement, the mechanical torque (T_{SM}) can be calculated through

$$T_{SM} = T_e - b_{SM}.\dot{\theta}_{SM} - T_{load} \quad (34),$$

In which b_{SM}. [Nms/rad] is the viscous friction coefficient and T_{load} [Nm] the load torque required by the gear transmission.

The angular acceleration ($\ddot{\theta}_{SM}$) in the motor shaft is given by

$$\ddot{\theta}_{SM} = \frac{T_{SM}}{J_{SM}} \quad (35),$$

where J_{SM} [kg.m^2] is the electrical motor moment of inertia.

The adopted parameters for the BLDC motor model are presented in table 4.7.

Table 4.6: Simster electric motor sub-model adopted parameters.

Parameter	Symbol	Value	Unit
Electrical resistance	R_{SM}	R_1	Ohm
Moment of inertia	J_{SM}	J_2	kg.m2
Electrical inductance	L_{SM}	L_1	H
Electrical motor torque constant	K_t	K_2	Nm/A
Back Electromotive Force constant	K_e	K_2	V.s/rad

Source: Author.

5 SIMULATION AND EXPERIMENTAL RESULTS

In this chapter, simulation and experimental tests results are presented and investigated. For the experiments, a test bench composed by the EHA prototype developed by Bosch Rexroth AG, a control module and a computer (Figure 5.1) was operated to perform the main operations of the actuator, such as opening, closing, and the fail-safe functions.

Figure 5.1 – Subsea Valve Actuator prototype and test bench.

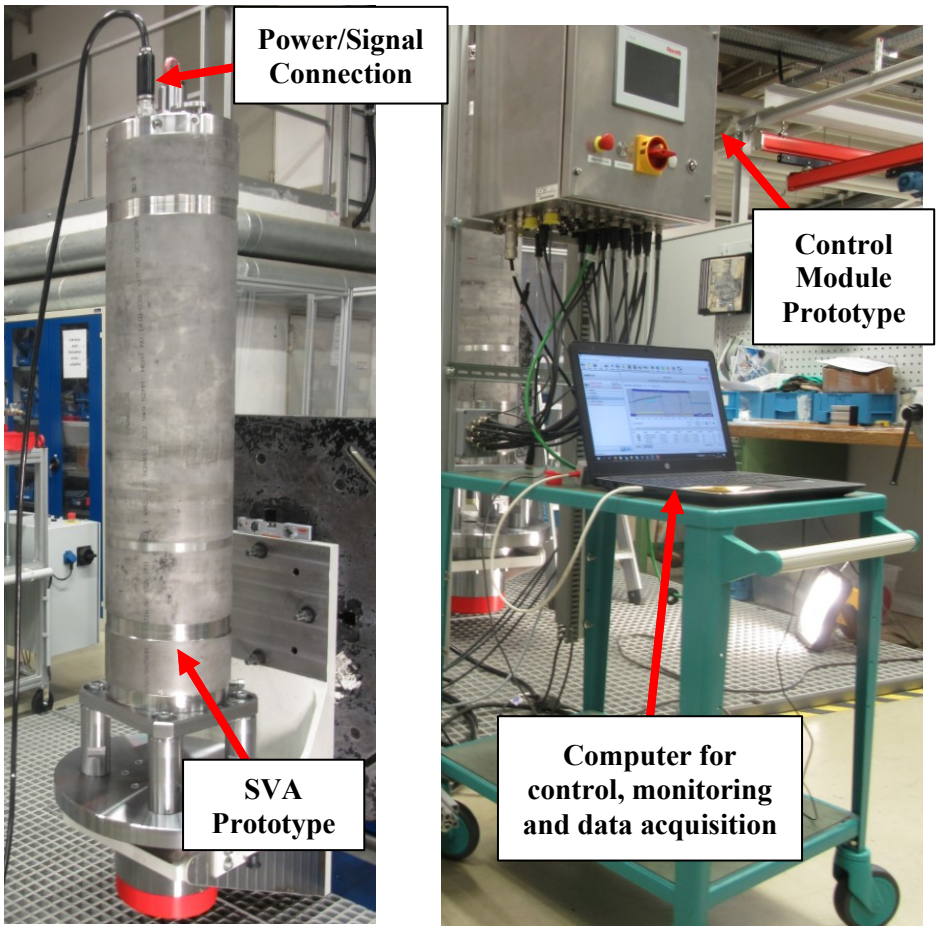

Source: Author.

The parameters experimentally monitored were the pressures in the main cylinder hydraulic chambers, the EHA position (main cylinder position), electric motor angular velocity, and consumed current. Pressure in the spring cylinder chamber C is monitored during most of the experiment by opening one pair of the ON-OFF safety valves as illustrated in Figure 5.2. The color red represents the lines that have the same pressure as chamber C, where during most

of the experiment the pressure losses can be neglected, since there is no flow rate is the ON-OFF safety valves and consequently no pressure drop in the orifice SO.

Figure 5.2 – One pair of safety valves opened during the experiments to allow chamber C pressure monitoring.

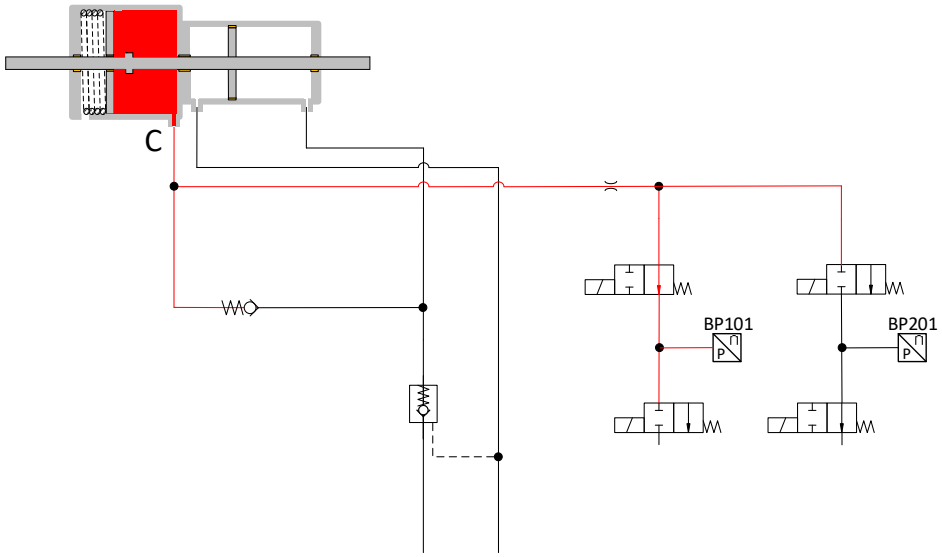

Source: Author

Since, in the first forward movement, the spring cylinder also needs to be moved, this test was performed in two cycles for the sake of observing the system's behavior in both situations (moving while clamping the spring and moving without it). Figure 5.3 illustrates the test routine, in which the system continues the opening and closing movement until it reaches a pre-defined number of cycles. The following subsection presents the experiment and simulation results, in which the data is represented as percentages and/or variables for the protection of the intellectual property, although it is possible to analyze the system behavior by graphic comparisons.

Figure 5.3 - EHA operation test routine.

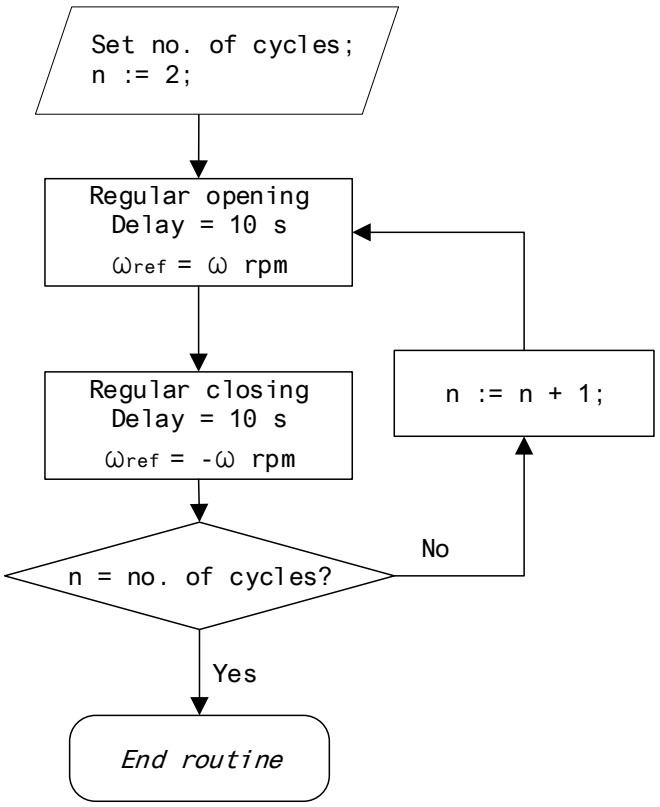

Source: Author.

5.1.1 Position and Pressures Behavior

In Figure 5.4, the position through time result is presented for both simulation and experiment. In the first forward movement, which is the spring clamp operation, the actuator took about 2.75 times the time required to perform the same movement in the second operation. It happens because once there is no load, the pressure required to move the main cylinder is lower than required to clamp the spring cylinder, and consequently both cylinders move together, working as a tandem cylinder, as the pumps flow rate shall provide fluid for both cylinders. On the second forward movement, the spring is already clamped, so the pumps just need to move the main cylinder.

Figure 5.4 – SVA position in the opening and closing functional test and simulation

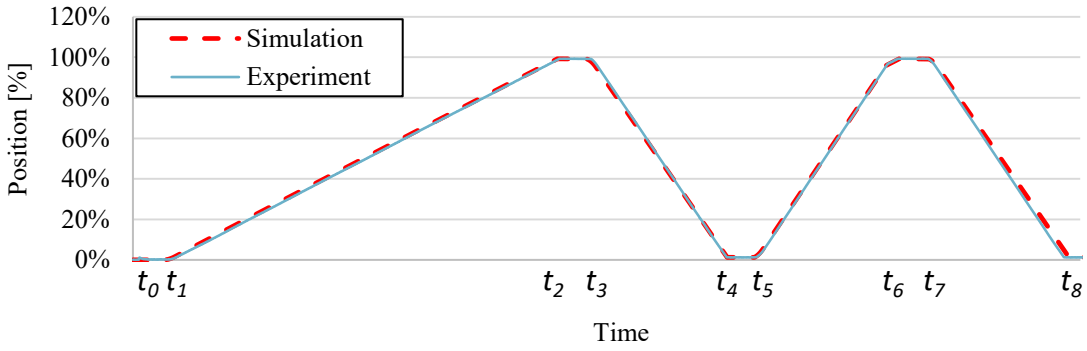

Source: Author.

Since, for this experiment, the SVA position was not controlled but the electric motors angular velocity, the superposition of the simulation and experimental test highlights that the volumetric efficiency of the mathematical model, at this operational condition, is consistent with the prototype results. The pressure in chambers A, B and C, during this operation, can be observed in Figure 5.5.

Figure 5.5 – Pressures at the chambers A, B and C during operation without load.

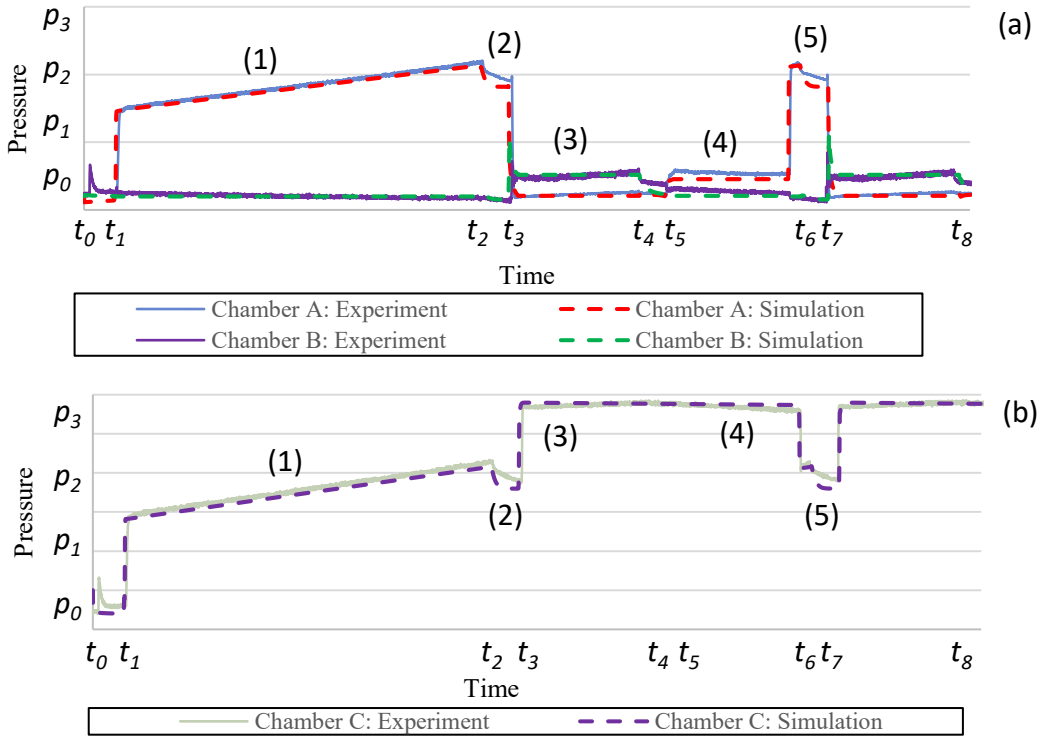

Source: Author.

While moving the spring cylinder (1), both chambers A and C are connected by the check valve CV.SR, then - as represented in Figure 5.5 (a) and (b) - these pressures remains basically the same during the forward movement, with the pressure at chamber A being just a bit higher than chamber C's due to the check valve CV.SR pressure drop.

Once the actuator stops (2), the friction forces decrease and the pressures at chambers A and C reach an equilibrium point.

At the beginning of the returning movement (3), the pressure at chamber C increases to the ratio of the spring compressed force by the spring cylinder area, once the main cylinder rod is disconnected from the spring cylinder piston and it remains clamped by the actions of the check valve CV.SR and the ON-OFF safety valves. During de returning movement (3) and most of the forward movement (4), the pressure differential at the main cylinder is just the required to overcome its friction forces, which in the mathematical model were based on the cylinders experimental data. At the end of the forward movement (5), the main cylinder rod encounters the cylinder spring piston, equalizing chambers A and C pressure again.

5.1.2 Power Consumption

The electric power is expressed by

$$P_e = U_{SM}.i_{SM} \quad (36),$$

where U_{SM} [V] is the electrical voltage and i_{SM} [A] the electrical current. Therefore, it is possible to obtain the system power consumption by monitoring the motor electric current [A] and angular velocity [rad/s] and then substituting Equation 32 into Equation 36, as

$$Pe = i_{SM}.[K_e.\dot{\theta} + R_{SM}.i_{SM} + L_{SM}.\frac{di_{SM}}{dt}] \quad (37).$$

Figure 5.6 presents the electric motors measured angular speed and current and its respective calculated power consumption.

Figure 5.6 – Angular speed, current and power consumption of the electric motors.

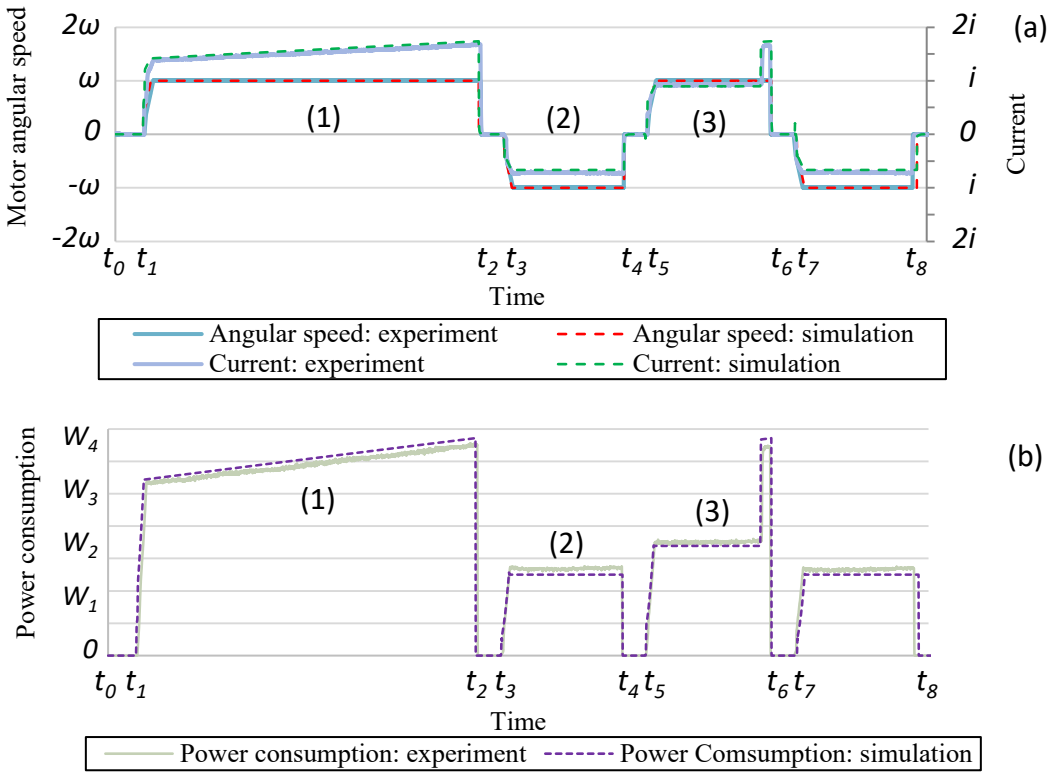

Source: Author.

As illustrated in Figure 5.6 (a), the current in stage (a) increases through time. It happens due to the increase in the spring force while compressing, which causes an increase at the system's pressure – as observed in 5.4 – and consequently in the electric torque.

Figure 5.6 stages (2) and (3) represent the returning and forward movement of the actuator, respectively. It can be seen that the power consumption during the forward movement is higher than during returning. This behavior is due to the pilot check valve PCV.2 pressure drop, which during the return movement (2) is piloted and then represents a smaller pressure drop than during the forward movement (3).

In the final of the forward movement (3), there is a peak in the current and then in power consumption that occurs when the main cylinder rod reaches the spring cylinder's piston.

5.1.3 Fail-Safe Function

On the fail-safe function test, the electric voltage of the electric motors and ON-OFF safety valves solenoids is switched off after the cylinder is in its fully open position, allowing the spring cylinder piston to push the main cylinder rod to its returned position.

During this function, the pressure sensors BP101 and BP201 are connected to the reservoir, and then it was not possible to monitor the pressure at chamber C by any of these sensors. However, the check valve CV.SR – which connects chamber A and C during this operation– allows the analysis of the actuator pressure behavior by the sensor BP001. Figure 5.7 shows the position, velocity, and pressure at chamber A during this operation.

Figure 5.7 – Main cylinder position, velocity and pressure at chamber A during fail safe function.

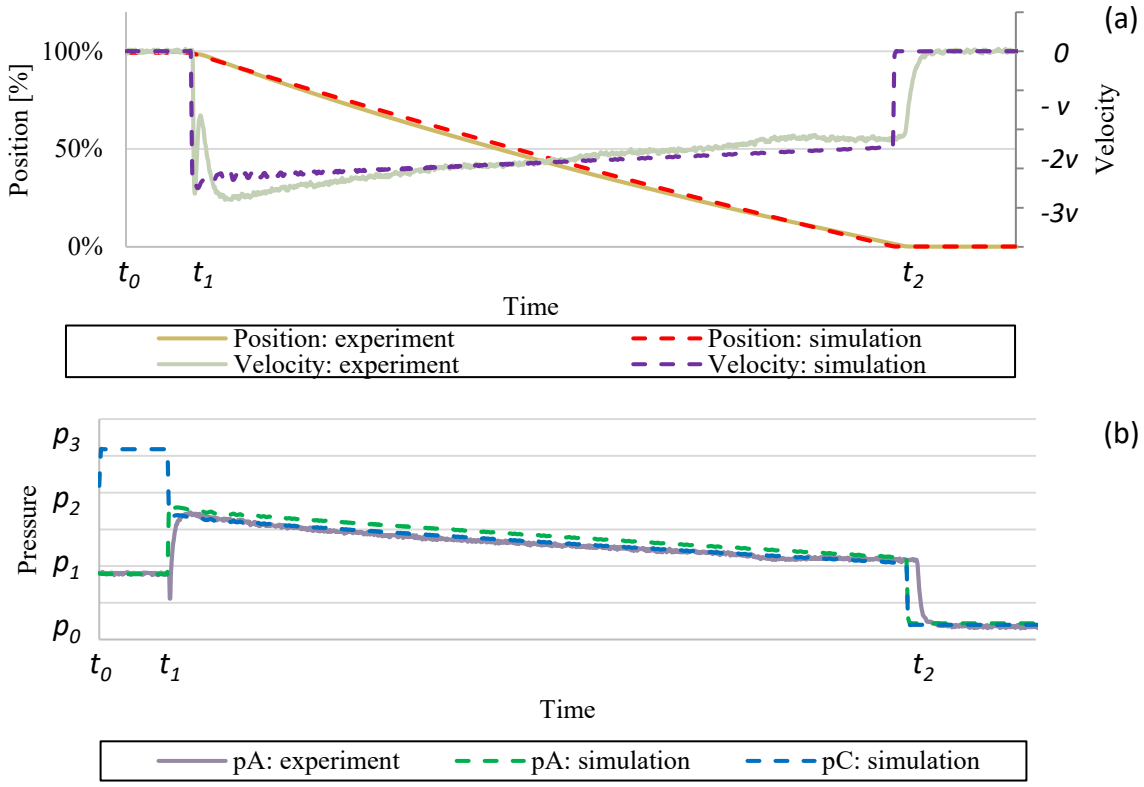

Source: Author.

As illustrated in Figure 5.7 (a), the actuator velocity decreases during the fail-safe function. This behavior can be understood by the velocity dependency in relation to the flow rate at the orifice SO. The orifice SO flow rate is a function of its pressure differential, which

as can be observed in Figure 5.7 (b) decreases during the operation due to the spring decompression. The velocity, then, decreases during the fail-safe function as well.

Through the comparison between experimental and simulation results demonstrated in the prior analyzes, it can be stated that the developed mathematical model has shown a satisfactory closeness to the prototype behavior. In the next subsection, the results of simulations where this validated model was employed in an emulated working environment with a gate valve and hyperbaric external pressure are presented.

5.2 SIMULATION IN EMULATED SUBSEA WORKING ENVIRONMENT

In order to emulate the EHA working force profile, a mathematical model of the gate valve was implemented according to the equations presented in Chapter 4. The constructive and production parameters used to fill this mathematical model are presented in Table 5.1, in which some values are hidden for intellectual property protection.

Table 5.1: Gate valve mathematical model constructive parameters.

Parameter	Symbol	Value	Unit
Seat inner diameter	d_{ID}	52.4x10^{-3}	m
Seat outer diameter	d_{OD}	d_4	m
friction coefficient between the gate valve and its seats	μ	0.2	-
Crack open position	x_{co}	x_2	m
Maximum valve stroke	x_{tot}	x_1	m
Pressure on the surface oil separator	p_{sep}	1x10^{6}	Pa
Specific mass of the production fluid	ρ_{pf}	930	kg/m3
Gravity acceleration	g	9.81	m/s2
Air Gap	AG	30	m
Length of the oil pipe	L	13000	m
Oil pipe diameter	D	52.4x10^{-3}	m
Stem diameter	d_{stem}	d_5	m
Friction force between bonnet seals and stem	F_{seal}	F_6	N

Source: Author.

5.2.1 Standard Operation

In this simulation, a working environment with a water depth of 3000 m and a wellbore pressure of 690 bar [10,000 psi] is emulated to the validated EHA mathematical model on the software Simster. As in the experiment, the EHA is controlled as a discrete system with control commands of stop, open or close as illustrated in Figure 5.8.

Figure 5.8 – Discrete command signal and cylinders position.

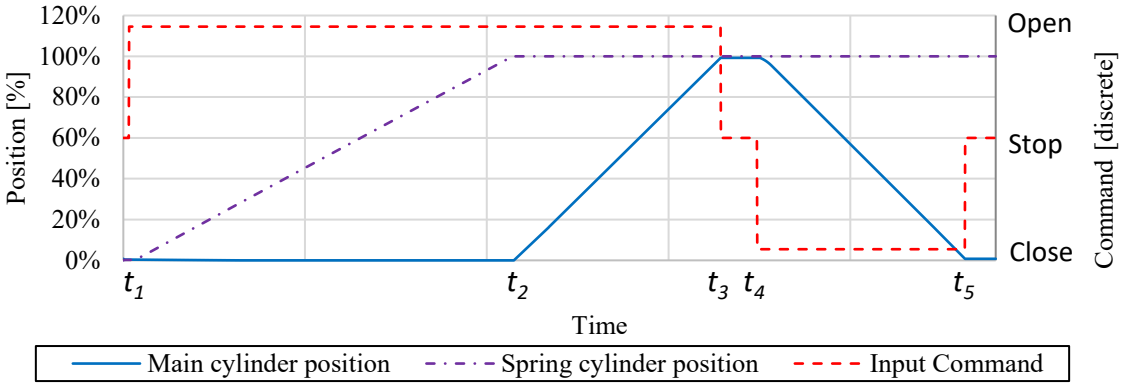

Source: Author

On Figure 5.8, different from Figure 5.4, the spring cylinder moves first than the main cylinder. It occurs because the pressure required to move the spring is smaller than the required to open the gate valve as can be observed in Figure 5.9. The pressure at the reservoir is subtracted from the pressure results for a better understanding.

Figure 5.9 - Cylinders pressure behavior during the gate valve opening movement

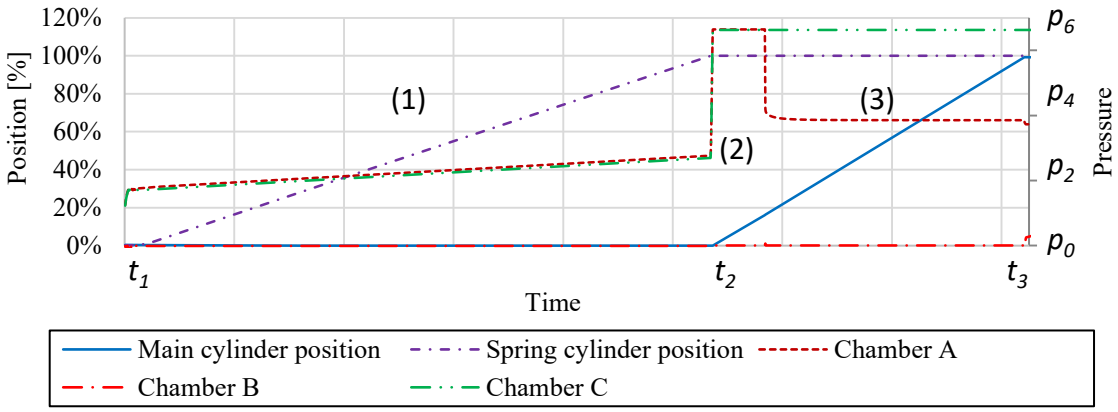

Source: Author

As can be observed in Figure 5.9, during the gate valve opening movement, the pressures at the chambers A and C increase together as the spring cylinder moves forward (1). Once the spring cylinder reaches its final position, the pressure at these chambers increases to the required to overcome the gate valve force (2). After the gate valve opening start, which occurs in x_{co} (see table 5.1), the pressures upstream and downstream of the valve equalize and the force required to move it decreases (3), and the pressure in chamber A decreases proportionally. Due to the check valve CV.SR, which does not allow the flow rate from chamber C to A, the pressure at chamber C remains the highest until the ON-OFF safety valve opening.

Once the clamping of the spring cylinder shall be performed just at the EHA first operation, the next results will not show this operation anymore to focus on the standard operation analyses.

5.2.2 Influence of Water Depth

The water depth influences mainly two of the forces acting on the EHA system, the drag force "F_{drag}" by changing the pressure drop in the gate valve – described in chapter 4.1.4 – and the enclosure force "F_{enc}" – chapter 4.1.1 – by influencing the reservoir compensated pressure. The resultant mechanical force "F_{mec}", which needs to be overcome by the EHA system, is the compound of these two forces with the gate valve stem expulsion force "F_y" and the friction force at the bonnet "F_{seal}" as

$$F_{mec} = F_{drag} + F_{enc} + F_y + F_{seal} \quad (38).$$

The increase at the water depth decreases the "F_{drag}" proportionally and increases the "F_{enc}", so if the wellbore pressure is considered as a constant, the higher is the water depth, the smaller should be the required force to open the gate valve.

ISO 13628-4 (2010) requires that, during valve actuators tests, the valve should be submitted to a pressure differential equal to the wellbore Rated Working Pressure (RWP), which results in the highest drag force and therefore is the most demanding situation for the opening movement.

In order to observe the influence of the water depth in the proposed EHA, simulations at depths of 0, 1000, 2000 and 3000 meters were accomplished. In these simulations, the actuator position was controlled by a proportional integrative (PI) controller to facilitate the comparison of the results. Figure 5.10 shows the resultant mechanical force profile during the EHA stroke and Figure 5.11 the system drive power consumption in all four situations.

Figure 5.10 - EHA mechanical required resultant force in relation to its position and direction of the movement for depths of 0, 1000, 2000 and 3000 meters.

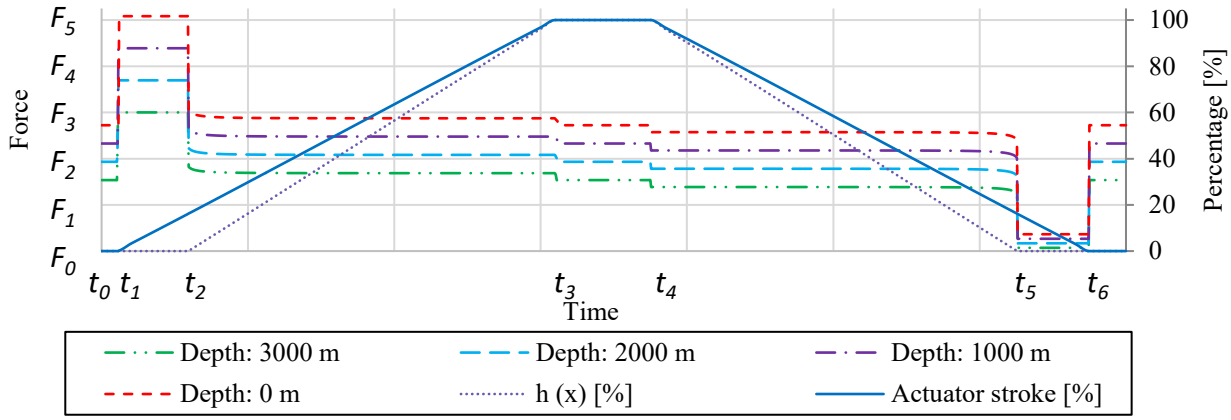

Source: Author

In Figure 5.10, the actuator stroke and valve opening "h(x)" are demonstrated together, so the region where the drag force is in its maximum value, which is the region where the EHA is moving while the valve is closed can be observed in a better way. As mentioned before, the required mechanical force to open the valve is higher as the depth decreases, while the same force helping the closing function during the returning movement is higher as well.

Figure 5.11 - System power consumption at depths of 0, 1000, 2000 and 3000 meters

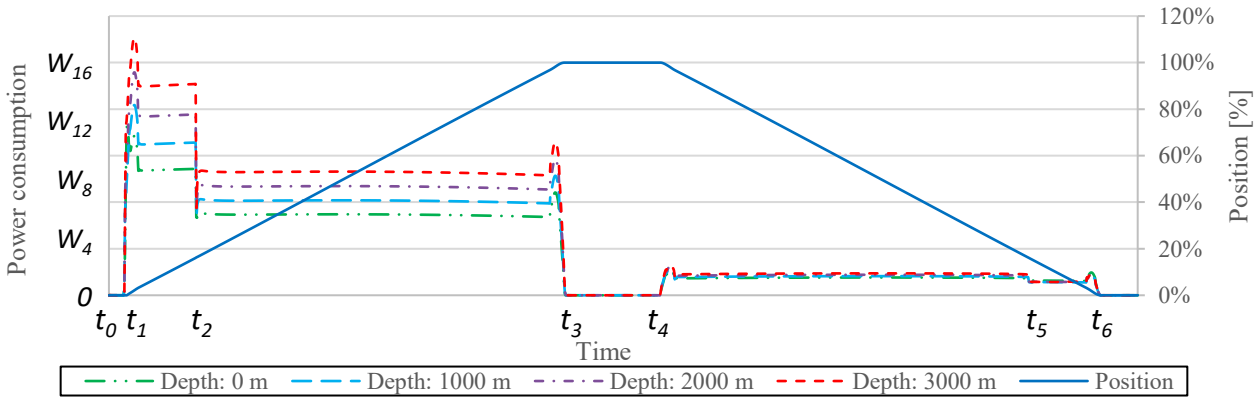

Source: Author

As can be seen in Figure 5.11, the system power consumption in the opening movement increases as the water depth decreases, which can be correlated to Figure 5.10 results. Since the time to open the gate valve remains the same in all four situations, the power should increase proportionally to the force increasing.

Although, in the return movement, the influence of the water depth in the system power consumption is not observed - even with the modification in resultant force helping the closing movement demonstrated in Figure 5.10 – indicating that the system has a power waster during this function. The pilot check valve PCV2, which has the function of guarantee the actuator position when opened, has demonstrated to be this power sink, as illustrated in Figure 5.12.

Figure 5.12 - Power consumption of the pilot operated check valve PCV2 during standard operation for depths of 0, 1000, 2000 and 3000 meters.

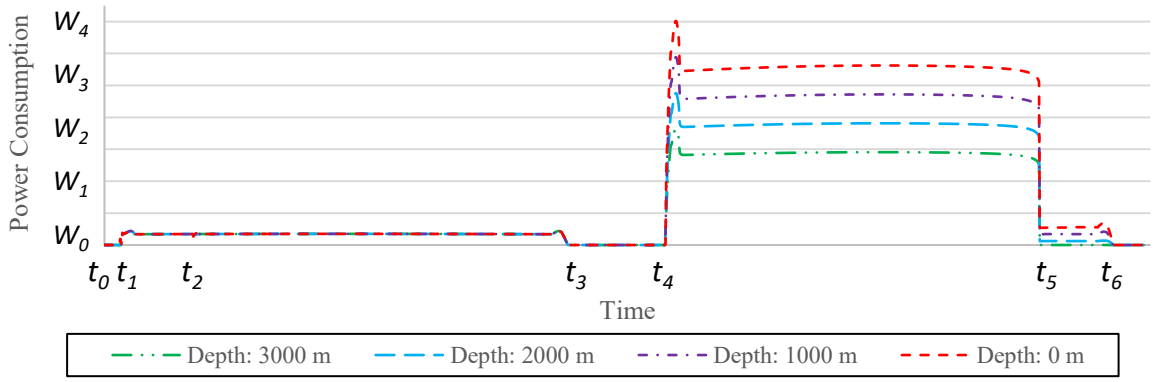

Source: Author.

As presented in Figure 5.12, and correlated with 5.10 and 5.11, during the gate valve closing function, the higher is the force helping the movement the greater is the power dissipation at the pilot operated check valve PCV2.

Costa *et al*. (2015) states that electro-hydrostatic actuators, when working with inline pilot operated check valves alike the studied EHA configuration, in situations where the load force acts in the same direction of the movement, the check valve which is been operated will work as a counterbalance valve, preventing the cylinder from accelerating by the action of the load force. This behavior is observed in the pilot operated check valve PCV2 during the EHA standard returning movement and can be mathematically explained as follow.

According to previously described Equation 19, the minimum pilot pressure required to open the pilot operated check valve is

$$p_{x}{}_{pcv} \geq \left(\frac{p_{Bpcv} - p_{Apcv} + p_{0pcv}}{R_{pcv}} + p_{Apcv}\right) \quad (39).$$

while, on the main cylinder during the returning movement, the forces equilibrium in steady state results in

$$F_{mec} = (p_A - p_B).A_{cyl1} + F_{fric} \quad (40).$$

The main cylinder pressures p_A and p_B correspond respectively to the PCV2 pB_{pcv} and px_{pcv}. Therefore, by isolating px_{pcv} in Equation 40 and substituting in Equation 39, the following is found

$$\left(p_{Bpcv} - p_{Apcv}\right) \geq \frac{R_{pcv}}{R_{pcv} - 1}.\left(\frac{F_{mec} - F_{fric} + \frac{A_{cyl1}.p_{0pcv}}{R_{pcv}}}{A_{cyl1}}\right) \quad (41),$$

where $(p_{Bpcv} - p_{Apcv})$ [Pa], is the pressure drop at the pilot check valve during the returning movement.

As stated in Equation 41, the pressure drop and, as a consequence, the power dissipation at the pilot operated check valve during the gate valve closing movement is dependent of the resultant mechanical force acting on the actuator. An increase at the Pilot area ratio "R_{pcv}" would not have a relevant influence as well, since the current ratio "$\frac{R_{pcv}}{R_{pcv} - 1}$" is already 1.09.

5.2.3 Fail-Safe Function in Critical Scenarios

In agreement with the standard requirements mentioned in Chapter 3 for the gate valve actuator fail-safe function, the four scenarios described in Table 5.2, were emulated during the fail-safe function in the simulations in order to observe the system's ability to overcome the required external forces in all these situations.

Table 5.2: Scenarios to be emulated in the fail-safe function simulations

External pressure: maximum Well bore pressure: maximum	Scenario 1
External pressure: maximum Well bore pressure: atmospheric	Scenario 2
External pressure: atmospheric Well bore pressure: maximum	Scenario 3
External pressure: atmospheric Well bore pressure: atmospheric	Scenario 4

Source: Author.

Scenarios 1 and 2 emulate a water depth of 3000 meters in which in the first one the wellbore pressure is 10.000 psi [690 bar] while in the second there is no wellbore pressure and consequently no pressure inside the gate valve. Although a situation where the valve actuator is at maximum depth and, at the same time, there is no pressure inside the valve as in scenario 2 is unlikely to happen, this standard requirement has the purpose of ensuring that the safe spring has been designed to overcome all external forces without any help of the gate valve expulsion force.

Scenarios 3 and 4 occur at atmospheric external pressure, while the third works with a maximum wellbore pressure and the fourth with no pressure at the well. Figure 5.13 demonstrates the actuator position during all simulated scenarios.

Figure 5.13 - Position curves during the fail-safe function in the four simulated scenarios

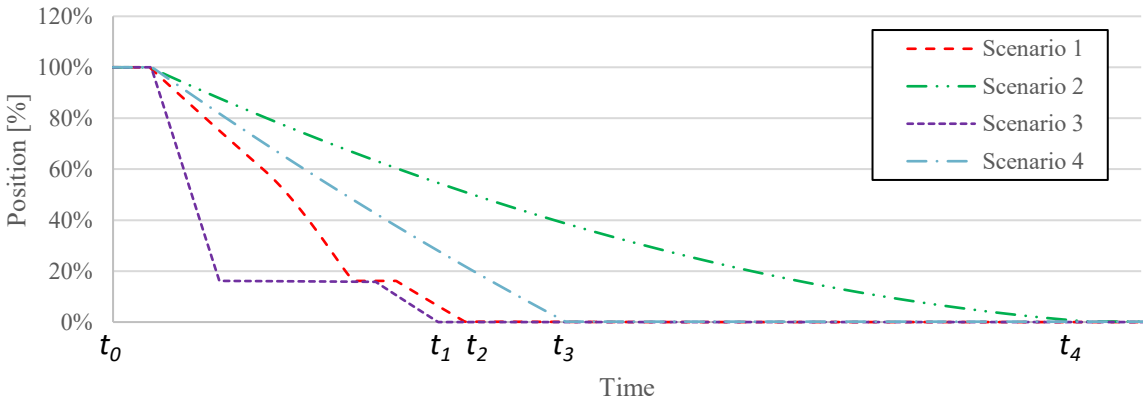

Source: Author

The difference in the curves illustrated in Figure 5.13 is due to the change in the mechanical forces applied to the EHA system during the closing movement. In scenarios 1 and 3, a stop at the closing movement can be observed when the actuator reaches x_{co}. This behavior can be better explained through Figure 5.14 observation.

Figure 5.14 - Scenario 1: EHA mechanical force, main cylinder and spring cylinder positions during fail-safe function.

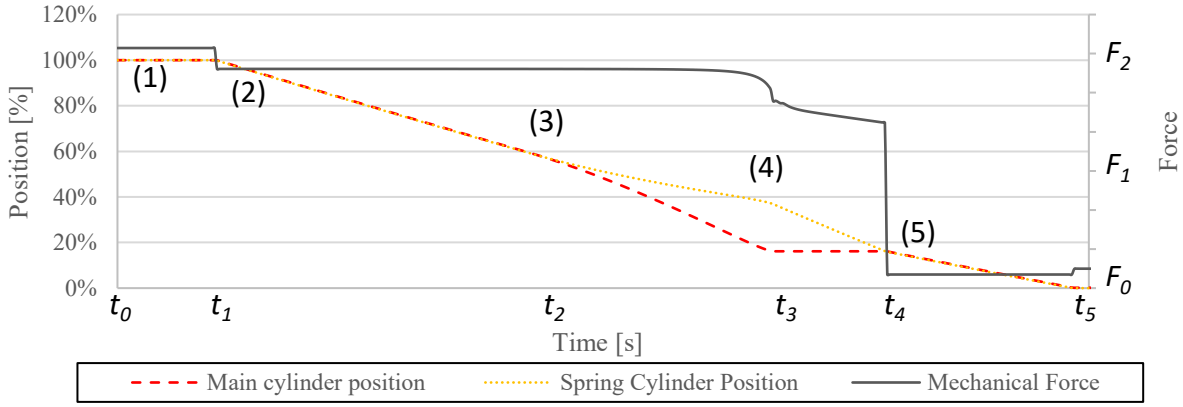

Source: Author.

As illustrated in Figure 5.14 (1), while the EHA is at its rest position the mechanical force "F_{mec}" act in the valve closing direction with a module equal to the gate valve expulsion force "F_y" minus the Enclosure force "F_{enc}". Once the fail-safe function is activated (2) and the EHA starts to move backward, the resultant mechanical force is decreased by the bonnet friction force "F_{seal}". At the point 3, due to the spring force reduction, the main cylinder starts to move faster than the spring cylinder once the spring thrust does not push its piston as much as the mechanical force pushes the main cylinder rod. At the time the valve reaches "x_{co}", the friction force between the gate and its seats "F_{drag}" increases dramatically, reducing the resultant mechanical force, and stops the valve until the spring piston reaches the main cylinder contact again (5) and pushes it to its totally returned position.

Scenario 2 is the one where the EHA took the longest time to totally close the gate valve during the fail-safe function. Its behavior is better explained through Figure 5.15.

Figure 5.15 - Scenario 2: EHA mechanical force, main cylinder and spring cylinder positions during fail-safe function.

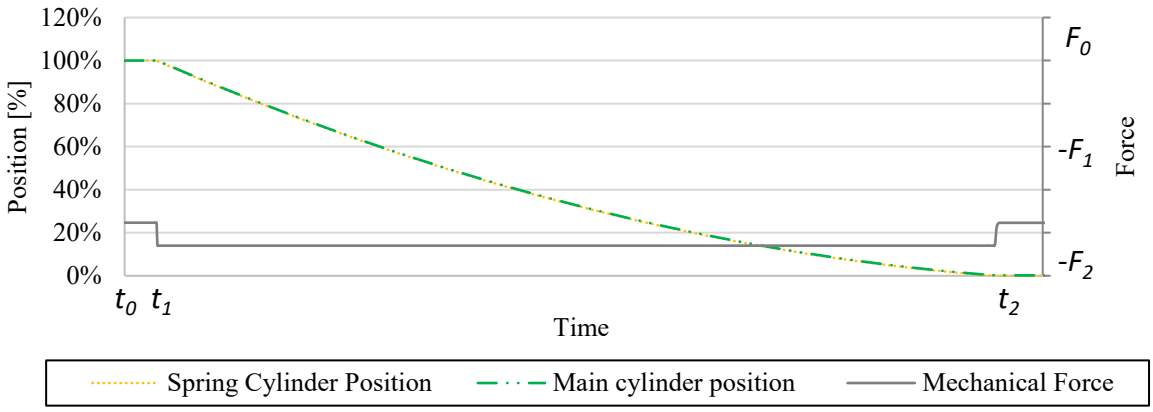

Source: Author.

As there is no pressure inside the gate valve in scenario 2, the resultant mechanical force is the sum of the enclosure force "F_{enc}" and the bonnet friction force "F_{seal}" both opposing to the closing movement culminating in the most demanding scenario for the EHA fail-safe system.

Scenario 3 behavior is similar to scenario 1, but without the influence of the enclosure force "F_{enc}" acting in the opening direction. So in this one, the returning movement is considerably faster. While scenario 4 is nearly the same as the experiment demonstrated in Figure 5.7 with the addition of the "F_{seal}" in the movement opposing direction.

5.2.4 Standard Operation with Power Supply Limitation

The power supply afforded to the valve actuator comes from the Subsea Control Module (SCM), which, as stated in Chapter 2, receives electrical power, communication signals, and hydraulic power supplies from surface control equipment to accomplish its functions, namely valves and chokes actuation and condition monitoring.

During operation, the studied EHA shall be supplied with the adequate electrical power for its drive system, as well as sensors and solenoids of the safety ON-OFF valves. This electrical power supply can be limited depending on the already installed subsea production layout, once in the current electrohydraulic control system the electric power supply is mainly used to open/close the valve actuators directional valves, what does not require a significant amount of power.

As a solution for a possible power supply constraint, the EHA controller can be designed with a power consumption limitation. This control module reads the instantaneous power consumption of the drive system and immediately define a maximum angular velocity set point (ω_{ref_lim}) to the electric motor to work under a pre-defined power consumption limit (Pe_{lim}). The angular velocity limit can be found by rearranging Equation 36 as in

$$\omega_{ref\_lim} = \pm \frac{1}{K_e}.\left[\frac{Pe_{lim}}{i_{SM}} - R_{SM}.i_{SM} - L_{SM}.\frac{di_{SM}}{dt}\right] \quad (42).$$

For the simulation with power consumption control, a scenario with wellbore pressure of 10.000 psi [690 bar] and no water depth was chosen by the reason that it is the most demanding scenario, in terms of energy consumption, for the gate valve opening function as demonstrated in Figure 5.11. The power consumption limit is "W_4", in which the electric motor velocity setpoint has a predefined curve, unless the motor power consumption reaches its maximum value, and then this setpoint decreases to a value inside the maximum power consumption limits according to Equation 42. Figure 5.16 demonstrates the position and mechanical force curve results of the simulation with power limitation control.

Figure 5.16 – EHA position and resultant mechanical force curves with a power limitation of 100 W.

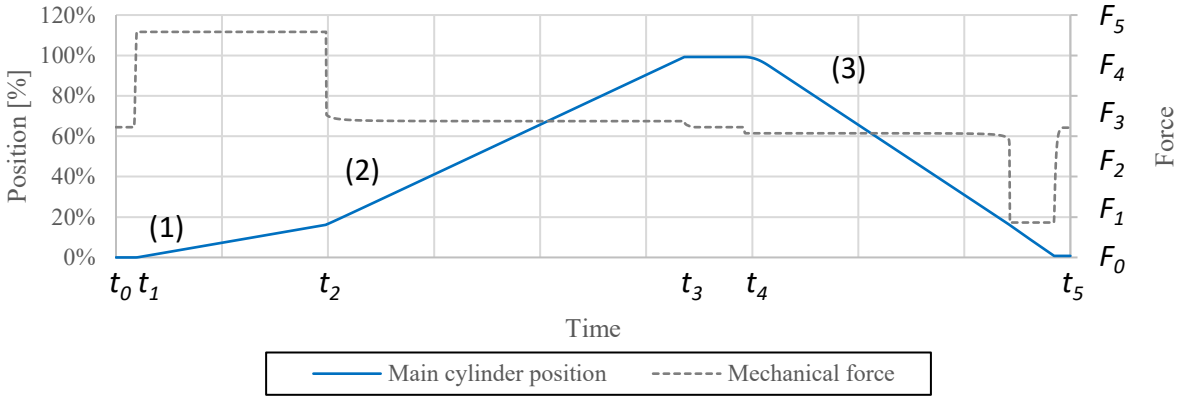

Source: Author

As can be seen in Figure 5.16, in the beginning of the open movement (1), while the gate valve is still closed, the inclination of the EHA position, which means its velocity, is smaller and, once the valve opens and the resultant required mechanical force decreases (2), the velocity increases. In the returning curve (3), there is no influence of the load in the EHA velocity. The mechanical power equation can help the understanding of this behavior, as in

$$P_{mec} = F_{mec} \cdot v \quad (43),$$

where P_{mec} [W] is the mechanical power (it is the EHA power output given to the gate valve), F_{mec} [N] the resultant mechanical force and v [m/s] the EHA velocity.

Thus, once the EHA resultant mechanical force is dependent of external factors, the power limitation controller limits the EHA velocity in order to work beneath the predefined maximum power allowed, as can be also observed in Figure 5.17.

Figure 5.17 – Electric motor power consumption and velocity setpoint curves during the simulation with power limitation.

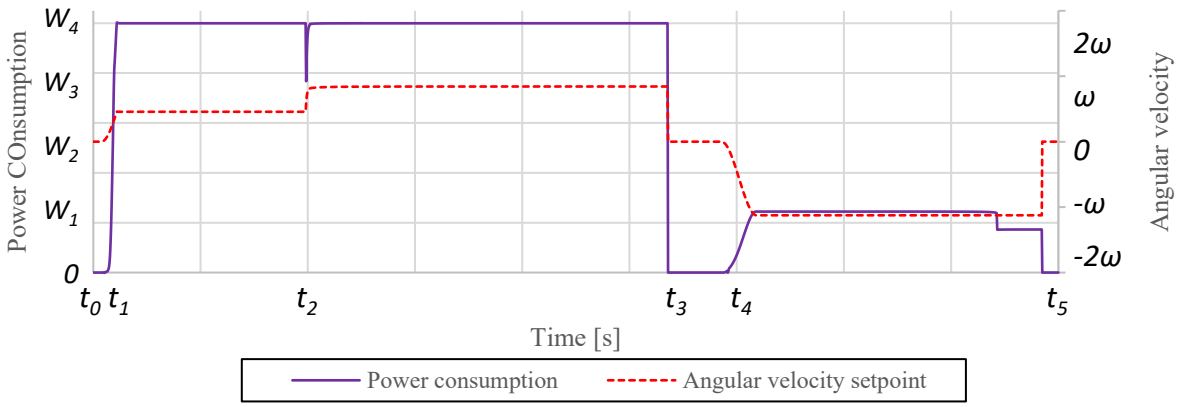

Source: Author.

The electric motor angular velocity setpoint is controlled during all opening movement to guarantee a maximum power consumption of "W_4". At the beginning of the movement, power consumption reached a value of 0.33 % about the predefined power limit. In "t_2", when the gate valve opens and the system resultant mechanical force decreases dramatically, the power consumption decreases 23%, until the control action increases the motor angular velocity to a higher value and, then the power consumption returns to "W_4". During the returning movement, the maximum power consumption was considerably smaller than "W_4", resulting in no action of the power limitation controller.

As demonstrated in Figures 4.13 and 4.14, both the increase at hydraulic pressure and reduction at angular velocity tend to decrease the pumps volumetric and mechanical efficiency, which would bring out a system decline in the resultant efficiency as the EHA mechanical force increases and velocity decreases. This behavior can be measured by the ratio between the system output mechanical power "P_{mec}" and input electrical power "P_e" as demonstrated in Figure 5.18.

Figure 5.18 - EHA efficiency curve during simulation with a power limitation of 100 W.

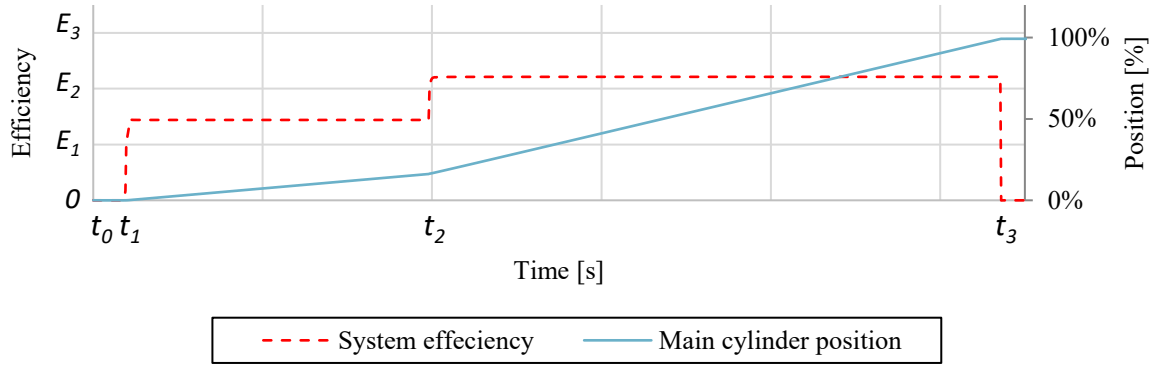

Source: Author.

As can be noticed in Figure 5.18, the system efficiency is considerably different before and after the crack open position "x_{co}", which is according to what was mentioned before about the system efficiency. Therefore, it can be concluded that the reduction at the electric motor angular velocity to control the system power consumption has a cost in terms of global efficiency.

6 CONCLUSIONS

The developed mathematical model has presented an appropriated adherence to the experimental results acquired from the prototype, as volumetric and mechanical efficiencies, power consumption, pressures behavior, and friction forces, allowing the evaluation of the EHA behavior in a simulated working environment. Through these simulations and analyzes, the following conclusions could be reached.

As higher is the water depth, as smaller will be the resultant required force that shall be overcome by the EHA to open the gate, and consequently smaller will be required power by the electric motor to drive the system, what fits with previous researches such as Mashiba (2011), Goularte (2018) and the relevant standards requirements. This behavior is elucidated by the action of the hydrostatic pressure, of both environment and production fluid, which increases with the water depth. On the actuator side, this environmental pressure acts in the stem area producing a force in the opening direction, while on the gate valve side, the production fluid pressure downstream the valve reduces the pressure differential acting at the gate decreasing the resultant friction forces.

The EHA prototype fail-safe system has demonstrated to be capable of totally close the gate valve in all four simulated scenarios, in which, the scenario with no pressure inside the valve and maximum water depth, demonstrated to be the most demanding for the closing spring. In other words, the wellbore pressure helps the closing movement since the gate expulsion force is greater than the friction forces between gate and seats while the external hydrostatic pressure works oppositely, as regards to the fail-safe function.

The pilot operated check valve fulfills its role of maintaining the EHA stopped when the electric motor is at rest, although it works as an energy waster during the gate valve closing operation when the resultant mechanical forces help the returning movement, which is the standard state during closing movements. Increasing the pilot area ratio does not have a significant influence on this behavior. In a study where it is intended to regenerate the energy provided by the valve during the closing movement, the pilot operated check valve utilization should be reviewed.

The power limitation control showed to be a good strategy when it is intended to save power consumption by increasing the time to open the gate valve. Although, as demonstrated in the simulations and can be estimated by the EHA hydraulic pump efficiency maps, the system overall efficiency decreases in smaller velocities. Thus, this power consumption saving to open

the valve would require a resultant amount of energy renouncement. Nonetheless, this reduction at power consumption also affects positively the installation costs reducing the required subsea electrical infrastructure and facilitates the implementation of the studied actuator concept with current subsea electronic modules.

Lastly, this research has presented the strengths and weakness, of the studied prototype for applications in subsea equipment in the investigated scenarios, and not less important, can be used for further studies and analyzes.

6.1 FUTURE RESEARCHES

As a suggestion of future researches to continue the development of the subsea equipment operation system, it can be mentioned:

- Study of the application of EHAs to operate other gate valve diameters and / or different types of valves such as globe, disc or choke valves;
- Perform the EHA tests with a real gate valve in a hyperbaric medium, where the subsea environment can be emulated, and the prototype analyzed experimentally in all scenarios simulated in this research;
- Analyses of the viability of a regenerative design for the EHA system, which could accumulate the energy provided by the valve during its closing function;
- Carry out endurance tests in the prototype and analyze the system's performance as the number of performed cycles increase. ISO 13628-4:2011 requires that, for the validation tests, a valve actuator should be submitted to a minimum number of 600 endurance cycling tests, although it is recommended in the industry a higher number than that. This study would be interesting to estimate the system performance during the years of application.

REFERENCES

ABICHT, D.; HALVORSEN, G.; RAMBERG, R.M. **Subsea All-Electric**. Offshore Technology Conference (OTC), Houston, Texas, USA, 2017.

ALI, S.Z.; SKEELS, H.B.; MONTEMAYOR, B.K. WILLIAMS, M.R. **Subsea Valve Actuator For Ultra Deepwater**. Offshore Technology Conference (OTC), Houston, Texas, USA, 1996.

BAI, Y.; BAI, Q. **Subsea Engineering Handbook**. Burlington, USA: Gulf Professional Publishing - Elsevier, 2010. 911 p. ISBN 978-1-85617-689-7.

BERVEN, J. **Subsea Production Control Systems For All-Electric Xmas Trees**. Master Thesis (Marine and Subsea Technology Master's Degree Programme) - Universitetet i Stavanger, Norway, 2013.

BOSCH REXROTH AG. **Check Valve, Type S**. Germany. 2017. Datasheet.

BOSCH REXROTH AG. **Check Valve, Pilot Operated Type Z2s**. Germany. 2010. Datasheet.

BOSCH REXROTH AG. **Pressure relief valve, direct operated**. Germany. 2014. Datasheet.

BOSCH REXROTH AG. **Subsea Valve Actuator – SVA: An Electro-Mechanical Actuator With Hydrostatic Drive For Subsea Control And Production System.** Germany, 2018.

BOSCH REXROTH US. **Don't guess: Accelerate hydraulic systems prototyping and validation using numerical simulation**. Charlotte, NC, 2014. Available in: https://www.boschrexroth.com/en/us/trends-and-topics/case-studies-tech-papers-and-viewpoints/technical-papers/simulation. Checked in: Oct. 4, 2019.

CHEN, C.; CHI, W.; CHENG, M. **Regenerative Braking Control For Light Electric Vehicles**. International Conference on Power Electronics and Drive Systems (IEEE), Singapore, 2011.

COSTA K. G., SEPEHRI, N. **Hydrostatic Transmissions and Actuators – Operation, Modelling and Applications.** 1st Ed. John Wiley & Sons, Ltd. Chichester, UK. 2015.

EUROPEAN STANDARD EN ISO 10417:2004. **Petroleum And Natural Gas Industries - Subsurface Safety Valve Systems - Design, Installation, Operation And Redress**. Belgium: European Committee for Standardization (CEN), 2004.

EUROPEAN STANDARD EN ISO 10423:2009. **Petroleum And Natural Gas Industries — Drilling And Production Equipment — Wellhead And Christmas Tree Equipment**. Belgium: European Committee for Standardization (CEN), 2009.

EUROPEAN STANDARD EN ISO 13628-4:2010. **Petroleum And Natural Gas Industries - Design And Opera-Tion Of Subsea Production Systems - Part 4: Subsea Wellhead And Tree Equipment**. Belgium: European Committee for Standardization (CEN), 2011.

EUROPEAN STANDARD EN ISO 13628-5:2009. **Petroleum And Natural Gas Industries — Design And Operation Of Subsea Production Systems Part 5: Subsea Umbilicals**. Belgium: European Committee for Standardization (CEN), 2009.

FIKRI, M. **Plugging And Abandoning Subsea Wells Using Light Well Intervention Vessels**. Master Thesis (Faculty of Science and Technology) - University of Stavanger, Norway, 2016.

FISHSAFE. **Subsea Templates And Manifolds**. 2009. Available online at: http://www.fishsafe.eu/en/offshore-structures/subsea-structures/subsea-templates-manifolds.aspx. Checked on: 16 maio 2019.

FRISCHEMEIER, S. **Electrohydrostatic Actuators For Aircraft Primary Flight Control - Types, Modelling And Evaluation**. Fifth Scandinavian International Conference on Fluid Power, Linköping, Sweden, 1997.

FURST, F. L.; DE NEGRI, V.J. **Projeto De Sistemas Hidráulicos De Controle De Posição.** Florianópolis: UFSC, 2002.

GANNON, M. **How Is Electro-Hydrostatic Actuation Technology Improving The Global Aviation Industry**. April 13 of 2017. Available online in:<https://www.mobilehydraulictips.com/electrohydraulic-actuation-technology-improving-global-aviation-industry/. Checked in: May 19 of 2019.

GEßNER, M. **Zuverlässigkeit Eines Elektro-Hydraulischen Kompaktaktuators Für Eine Unterwasseranlage Zur Öl- Und Gasproduktion.** Diploma Thesis, Technische Universität Dresden, Dresden, 2017.

GOULARTE, R. M. **Análise De Desempenho Estático E Dinâmico De Um Atuador Eletro-Hidráulico Para Águas Profundas**. Master Thesis (Graduation Program in Mechanical Engineering) - Federal University of Santa Catarina, Brazil, 2018.

GOULARTE, R.M. SILVA. J.P.D. DE NEGRI, V.J. ORTH, A. **Static And Dynamic Performance Analysis Of An Electro-Hydrostatic System For Ultra-Deep Water**. In: RIO

OIL & GAS, 2018, Rio de Janeiro. IBP1772_18. Available online in: <https://stt.ibp.org.br/eventos/2018/riooil2018/pdfs/Riooil2018_1772_201806151835ibp1772_18_static_.pdf>. Checked in: May 15 2019.

HANSELMAN, D. **Brushless Permanent Magnet Motor Design**. Second Edition. Lebanon, Ohio, USA: Magna Physics Publishing, 2011.

IEA. **World Energy Outlook 2018**: The gold standard of energy analysis. Available in: https://www.iea.org/weo2018/. Checked in: Set. 4th 2019.

KÖRTGEN. A. **Ermittlung Von Anforderungen Und Design Prinzipien Für Drive & Control Systeme In Der Tiefsee-Öl- Und Gasförderung**, Bachelor Thesis, Rheinisch-Westfälische Technische Hochschule, Aachen, 2014.

LANA, E.D. **Avaliação Do Rendimento De Bombas Hidráulicas De Engrenagens Externas Através De Medição De Temperatura**. 2005. Master Thesis (Graduation Program of Mechanical Engineering) - Federal University of Santa Catarina, Florianópolis, SC, Brazil, 2005.

LEDEZMA PÉREZ, J.A. **Controle Robusto De Força Em Atuadores Hidráulicos Aplicando A Teoria De Realimentação Quantitativa**. 2012. Master Thesis (Graduation Program in Mechanical Engineering) - Federal University of Santa Catarina, Brazil, 2012.

MASHIBA, M. H. D. S. **A Influência Dos Parâmetros De Operação E Projeto No Desempenho De Atuação Hidráulica De Válvulas Submarinas Do Tipo Gaveta**. Master Thesis. Graduation Program in Mechanical Engineering - COPPE - Federal University of Rio de Janeiro, Brazil, 2011.

MCKINSEY & COMPANY. **Offshore Drilling Outlook To 2035 Report**. May 2019.

MOOG. **Electrohydraulic valves. A technical look**. MOOG Industrial Controls Division. New York, p. 24. [ca. 2007]. (CDL6566 Rev D 500-170 302).

MORAIS, J.M. **Petróleo Em Águas Profundas : Uma História Tecnológica Da Petrobras Na Exploração E Produção Offshore**. Brasília: Ipea: Petrobras, 2013.

NAVARRO, R. **Performance Of An Electro-Hydrostatic Actuator On The F-18 Systems Research Aircraft**. National Aeronautics and Space Administration, Dryden Flight Research Center, 1997.

NORSOK STANDARD D-010. **Well Integrity In Drilling And Well Operations**. Norwey, 3 ago. 2004. Available online at: https://www.standard.no/pagefiles/1315/d-010r3.pdf. Checked on: 16 maio 2019.

OILFIELD WIKI. **Subsea Control Module (SCM)**. 2017. Available online in: <http://www.oilfieldwiki.com/wiki/Subsea_Control_Module (SCM)>. Checked on: May 17 of 2019.

OILFIELD WIKI. **Subsea Manifold**. 2017. Available online in: < http://www.oilfieldwiki.com/wiki/Subsea_manifold>. Checked on: May 17 of 2019.

OILFIELD WIKI. **Subsea Umbilicals**. 2017. Available online in: < http://www.oilfieldwiki.com/wiki/Subsea_umbilicals>. Checked on: May 17 of 2019.

OLIVEIRA, P. G. O. **Estudo De Confiabilidade De Sistemas De Controle De Dispositivos De Segurança De Sub-Superfície Em Poços De Petróleo**. 2016. Master Thesis in Mechanical Engineering - Federal University of Rio de Janeiro, Rio de Janeiro, 2004.

ORTH, A. **Deep Seas Push Hydraulic-System Boundaries**, Hydraulics & Pneumatics, November, 2014.

ORTH, A.; HENDRIX, G. **An Electro-Mechanical Actuator With Hydrostatic Drive For Subsea Trees To Reduce Capex And Opex With Higher Reliability And Safety Levels**. Offshore Technology Conference (OTC), Houston, Texas, USA, 2018.

ORTH, A. KNOELL, R. KOERTGEN, A. AND SWAGTEN, G. **Elektrohydraulisches System Für Den Einsatz Unter Wasser Und Prozessventil Mit Einem Derartigen Elektrohydraulischen System.** World Intellectual Property Organization, 2016. Patent WO/2016/023712.

PETROBRAS. **Business And Management Plan**. Rio de Janeiro, RJ, Brasil, 2019. Available online at: <http://www.petrobras.com.br/en/about-us/strategic-plan/business-and-management-plan/>. Checked on: May 15 of 2019.

Society of Petroleum Engineers (SPE). **Subsea Wellhead Systems**. 2014. Available online at <http://petrowiki.org/Subsea_wellhead_systems, updated on 5/1/2014>. Checked on: May 15 of 2019.

PLÁCIDO NETO, A. **An Internal Leakage Failure Prognosis System For Electro-Hydrostatic Subsea Valve Actuators**. 2018. Master Thesis (Graduation Program in Control Engineering and Automation) - Federal University of Santa Catarina, Brazil, 2018.

PLÁCIDO NETO, A. **Instrumentation, Electrical Drive Specification And Software Concept For An Electro-Hydrostatic Subsea Valve Actuator**. 2016. Undergraduate Thesis (Course of Control Engineering and Automation) - Federal University of Santa Catarina, Brazil, 2016.

RADUENZ, H. **Experimental And Theoretical Analysis Of A Hydrostatic Transmission For Wind Turbines**. 2018. Master Thesis (Graduation Program of Mechanical Engineering) - Federal University of Santa Catarina, Florianópolis, SC, Brazil, 2018.

SUISSE, B. **Research For Dynamic Seal Friction Modeling In Linear Motion Hydraulic Piston Applications**. 2005. Master Thesis (Master of Science in Mechanical Engineering) - The University of Texas at Arlington, Texas, USA, 2005.

TEXAS INSTRUMENTS. **Sensored 3-phase bldc motor control using msp430**. Dallas, Texas, USA: [s. n.], 2011.

TORBERGSEN, H.B.T. HAGA, H.B. SANGESLAND, S. AADNOY, B.S. SAEBY, J. HOHNSEN, S. RAUSAND, M. LUNDETEIGEN, M.A. **An Introduction To Well Integrity**. 2012. Norwegian University of Science and Technology (NTNU). Available online at: < https://www.norskoljeoggass.no/contentassets/103bce01eb4b445da85ff042df068c7b/introduction-to-well-integrity---04-december-2012.pdf >. Checked on: May 15 of 2019.

VALDIERO, A. C. **Controle De Robôs Hidráulicos Com Compensação De Atrito.** 2005. Doctoral Thesis (Graduation Program in Mechanical Engineering) - Federal Univercity of Santa Catarina, Brazil, 2005.

VON LINSINGEN, I. **Fundamentos de Sistemas Hidráulicos**. 4th Edition. Florianópolis, SC, Brasil: UFSC, 2013. 399 p. ISBN 85-328-00646-8.

VON LINSINGEN, I.; DE NEGRI, V. J. Fundamentals of Hydraulic Systems and Components. In: TOTTEN, G. E. e DE NEGRI, V. J. (Ed.). **Handbook of Hydraulic Fluid Technology**. 2nd ed. Boca Raton, FL: CRC Press, 2011. p.1-52.

WEBER, J. et al. **Novel System Architectures by Individual Drives**. 10th International Fluid Power Conference (10th IFK). Dresden, Germany. 2: 29-62 p. 2016.

YANADA, H.; KHAING, W.H.; TRAN, X.B. **Effect Of Friction Model On Simulation Of Hydraulic Actuator**. The 3rd International Conference on Design Engineering and Science (ICDES), Pilsen, Czech Republic, 2014.

ZALAVADIYA, H. **Energy Efficient System: Design For Underwater Production Plant.** 2018. Master Thesis (Institute of Electrical Power Systems) - University of Duisburg-Essen, Germany, 2018.

APPENDIX A – SIMULATION MODEL OF THE ELECTRO HYDROSTATIC ACTUATOR AND GATE VALVE.

Figure A.1 - EHA mathematical model layout.

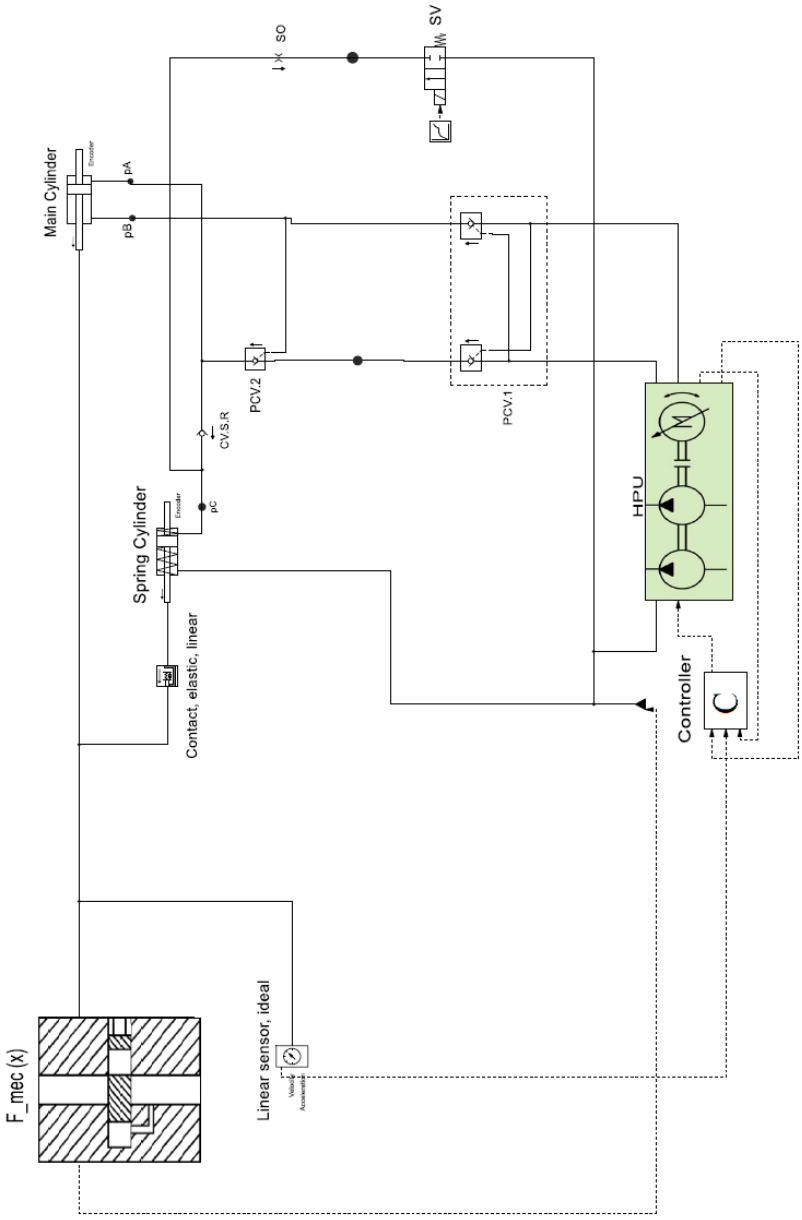

Source: Author.

Figure A. 2 - Hydraulic Power Unit model

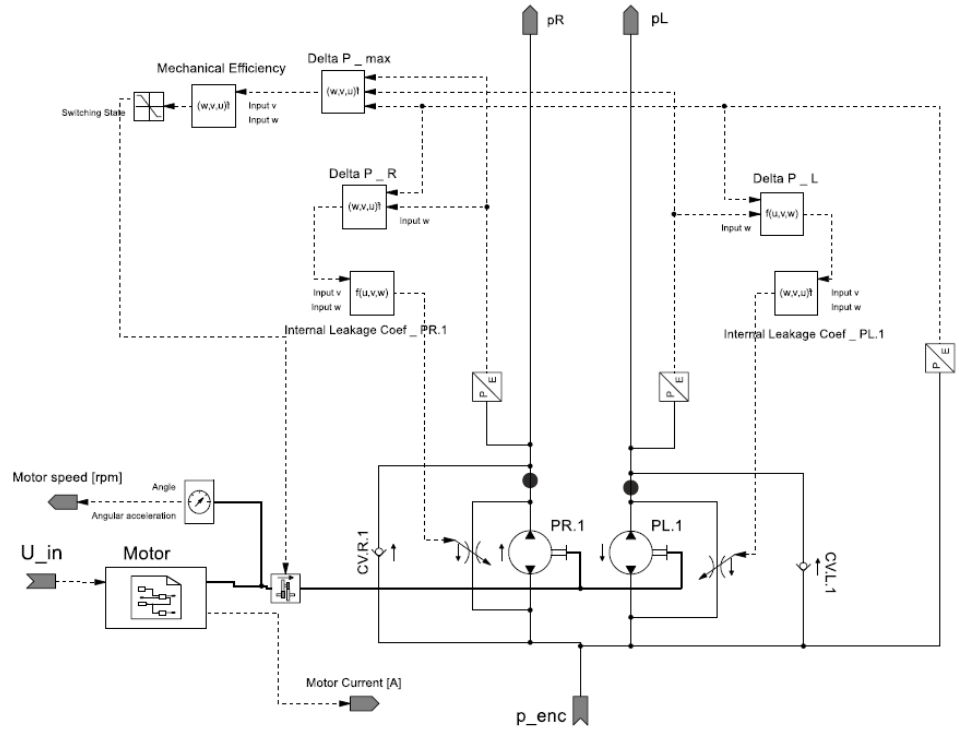

Source: Author.

Figure A. 3 - BLDC motor Simster model

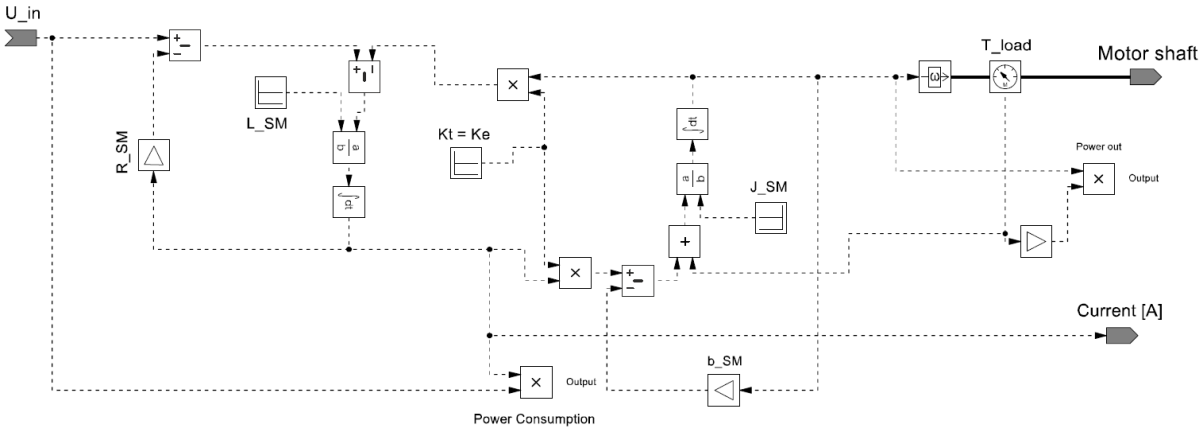

Source: Author

Figure A. 4 - Enclosure pressure, gate valve and mechanical forces summation model.

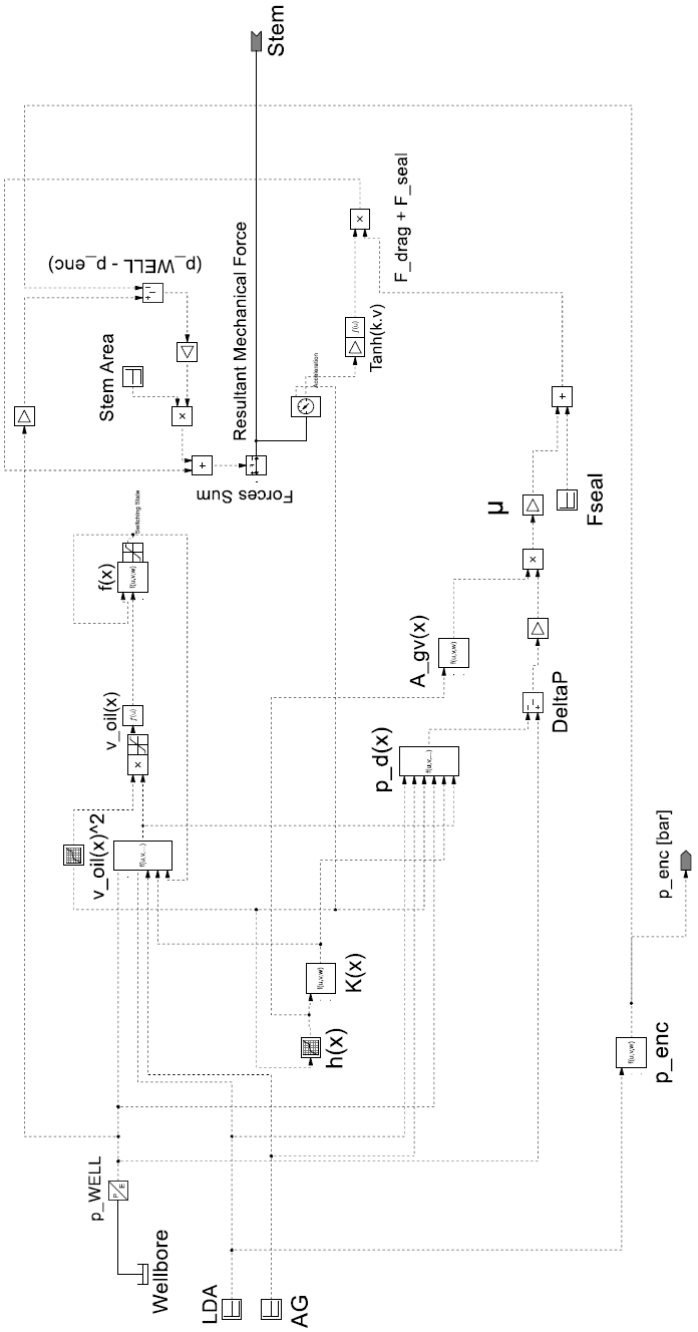

Source: Author.